

Modeling the remnant mass, spin, and recoil from unequal-mass, precessing black-hole binaries: The Intermediate Mass Ratio Regime

Yosef Zlochower and Carlos O. Lousto

*Center for Computational Relativity and Gravitation,
and School of Mathematical Sciences, Rochester Institute of Technology,
85 Lomb Memorial Drive, Rochester, New York 14623*

We revisit the modeling of the properties of the remnant black hole resulting from the merger of a black-hole binary as a function of the parameters of the binary. We provide a set of empirical formulas for the final mass, spin, and recoil velocity of the final black hole as a function of the mass ratio and individual spins of the progenitor. In order to determine the fitting coefficients for these formulas, we perform a set of 128 new numerical evolutions of precessing, unequal-mass black-hole binaries, and fit to the resulting remnant mass, spin, and recoil. In order to reduce the complexity of the analysis, we chose configurations that have one of the black holes spinning, with dimensionless spin $\alpha = 0.8$, at different angles with respect to the orbital angular momentum, and the other nonspinning. In addition to evolving families of binaries with different spin-inclination angles, we also evolved binaries with mass ratios as small as $q = M_1/M_2 = 1/6$. We use the resulting empirical formulas to predict the probabilities of black hole mergers leading to a given recoil velocity, total radiated gravitational energy, and final black hole spin.

PACS numbers: 04.25.dg, 04.30.Db, 04.25.Nx, 04.70.Bw

I. INTRODUCTION

Black holes and black-hole binaries (BHs) are thought to be ubiquitous in nature. Supermassive BHs, which have masses from $\sim 10^6 M_\odot$ to $\sim 10^{10} M_\odot$ (M_\odot is the mass of the sun) are thought to be at the centers of most galaxies with a bulge, while stellar-mass BHs generated in the collapse of massive stars, have masses from $\sim 10M_\odot$ to $\sim 100M_\odot$. There is strong observational evidence for both binaries and solitary black holes from these two populations. More speculative is the intermediate mass BH population, which would have masses from $100M_\odot$ to $\sim 10^6 M_\odot$ (see, e.g., [1]).

In 2005, there was a series of remarkable breakthroughs in numerical relativity (NR) [2–4], that allowed, for the first time, simulations of merging BHs. One of the most remarkable results that came from these simulations is that the merger remnant can recoil at thousands of kilometers per second (see [5–40]).

The first in-depth modeling of the recoil from the merger of nonspinning asymmetric BHs was done in Ref. [14], where it was shown that the maximum recoil is limited to $\approx 175 \text{ km s}^{-1}$. Soon after, other groups showed that the maximum recoil for spinning binaries, where the spins are aligned and antialigned with the angular momentum, is much larger. In Ref. [19] and [24], it was shown that the maximum recoil for an equal mass, spinning binary with one BH spin aligned with the orbital angular momentum and other antialigned is $\sim 475 \text{ km s}^{-1}$. However in Ref. [41] we find that for a mass ratio of $q \approx 0.62$ there is a maximum recoil of $V_{max} \sim 525 \text{ km s}^{-1}$.

The recoils induced by unequal masses and

aligned/antialigned spins is always in the orbital plane of the binary (which, by symmetry, does not precess). In [11], our group performed a set of simulations that showed that the out-of-plane recoil, which is induced by spins lying in the orbital plane, can be much larger. These *superkicks* [10, 11, 13, 15, 27] were found to be up to 4000 km s^{-1} when the spins were exactly in the orbital plane. Originally, it was thought that these in-plane spins maximized the recoil, however, as our group found out in [29–31], due to the hangup and other nonlinear-in-spin effects [42], having partially miss-aligned spins actually leads to a substantially larger recoil (up to 5000 km s^{-1}).

An open question remained, however, of how the recoil behaves as a function of the binary's mass ratio. This problem was first examined in detail in [8], where minimally precessing configurations were examined, and later in [26].

The next major challenge was to distill the results from large numbers of numerical simulations into convenient empirical formulas that map the initial conditions of the binary (individual masses and spins) to the final state of the merged black hole [41, 43–51].

Here we report on an effort to create both a bank of a large number of unequal-mass, precessing BHB simulations and the subsequent modeling of the recoil as a function of the binary's initial configuration. Our goal in this paper is the produce an interpolative formula that is accurate within the mass ratio range $1/6 \lesssim q \leq 1$ and provides a reasonable extrapolative formula down to mass ratios as small as $q = M_1/M_2 = 1/10$, as well as for intrinsic spins $\alpha_i = S_i/M_i^2$ as large as $0.95 - 0.97$ (here S_i is the spin angular momentum of BH i).

In constructing the new formula, we will enforce the

particle limit behavior $v_{\text{rec}} \propto \mathcal{O}(q^2)$, which is the expected behavior provided that the central BH is not spinning too fast (see Refs. [52, 53] for a discussion on resonance recoil which scale as $q^{1.5}$, see also [8, 26] for a discussion on whether or not the recoil should scale generically as $\mathcal{O}(q^2)$).

A note of caution. We will be basing our formulas on runs performed for moderate to high spins $\alpha \lesssim 0.8$. The dynamics of particles in the vicinity of a Kerr BH vary in a non-differentiable way at $\alpha = 1$. Therefore, for extremely high spins, there are likely interesting effects that cannot be elucidated using lower spin simulations. Fortunately, these effects occur at spins higher than what is expected astrophysically. See [54–56] for discussions about these effects.

In addition to modeling the recoil, we also provide new interpolative formulas for the total radiated mass and final remnant spin.

This paper is organized as follows. In Sec. II we summarize the numerical techniques used and describe the configurations we evolve. In Sec. III we review how symmetry arguments can be used to limit the number of terms in an expansion of the recoil and remnant mass and spin, and then explicitly give the form of each expansion term up through fourth-order. In Sec. IV, we provide the procedure used to fit the remnant properties to the parameters of the binary and provide the resulting fitting formulas. In Sec. V, we use these fitting formulas to calculate the statistical probabilities for a given recoil and remnant mass and spin given several plausible distributions for the possible parameters of the binary. Finally, in Sec. VI, we discuss the relevance of our results in the context of galactic and supermassive black-hole evolutions. We also provide an appendix with an extensive list of simulation results that can be used for further modeling.

II. SIMULATIONS AND RESULTS

We evolve the following BHB data sets using the LAZEv [57] implementation of the moving puncture approach [3, 4] with the conformal function $W = \sqrt{\chi} = \exp(-2\phi)$ suggested by Ref. [58]. For the runs presented here, we use centered, eighth-order finite differencing in space [59] and a fourth-order Runge Kutta time integrator. (Note that we do not upwind the advection terms.)

Our code uses the EINSTEINTOOLKIT [60, 61] / CACTUS [62] / CARPET [63] infrastructure. The CARPET mesh refinement driver provides a “moving boxes” style of mesh refinement. In this approach, refined grids of fixed size are arranged about the coordinate centers of both holes. The CARPET code then moves these fine grids about the computational domain by following the trajectories of the two BHs.

We use AHFINDERDIRECT [64] to locate apparent horizons. We measure the magnitude of the horizon spin using the *isolated horizon* (IH) algorithm detailed

in Ref. [65]. Note that once we have the horizon spin, we can calculate the horizon mass via the Christodoulou formula

$$M_H = \sqrt{M_{\text{irr}}^2 + S_H^2/(4M_{\text{irr}}^2)}, \quad (1)$$

where $M_{\text{irr}} = \sqrt{A/(16\pi)}$, A is the surface area of the horizon, and S_H is the spin angular momentum of the BH (in units of M^2). In the tables below, we use the variation in the measured horizon irreducible mass and spin during the simulation as a measure of the error in these quantities. We measure radiated energy, linear momentum, and angular momentum, in terms of the radiative Weyl scalar ψ_4 , using the formulas provided in Refs. [66, 67]. However, rather than using the full ψ_4 , we decompose it into ℓ and m modes and solve for the radiated linear momentum, dropping terms with $\ell \geq 5$ [68]. The formulas in Refs. [66, 67] are valid at $r = \infty$. We extract the radiated energy-momentum at finite radius and extrapolate to $r = \infty$ using both linear and quadratic extrapolations. We use the difference of these two extrapolations as a measure of the error.

Both the variation (with time) of the remnant parameters (as measured using the isolated horizons formalism), and the variation in the extrapolation of the radiation to infinity (as a function of different extraction radii) underestimate the actual errors in the quantity of interest. However, because quantities like the total radiated energy can be obtained from either extrapolations of ψ_4 or, quite independently, from the remnant BHs mass, the difference between these two is a reasonable estimate for the actual error. Furthermore, in [41], the errors associated with finite resolution, finite extraction radii, and using low ℓ modes only were examined in detail. There it was found that for the recoil the errors associated with dropping $\ell \geq 5$, the errors associated with finite extraction radii, and the truncation error were all of a similar size (roughly $5 - 10 \text{ km s}^{-1}$).

We use the TwoPUNCTURES thorn [69] to generate initial puncture data [70] for the BHB simulations described below. These data are characterized by mass parameters $m_{p1/2}$, momenta $\vec{p}_{1/2}$, spins $\vec{S}_{1/2}$, and coordinate locations $\vec{x}_{1/2}$ of each hole. We obtain parameters for the location, momentum, and spin of each BH using the 2.5 PN quasicircular parameters. We normalize our data such that the total Arnowitt-Deser-Misner (ADM) energy is $1M$ and the mass ratio, as measured by the horizons masses on the initial slice, has a given value. Because the BHs absorb energy during the first few M of evolution, the actual mass ratio will be altered. In the fits below, we always use the mass ratio calculated when the BHs have equilibrated.

Our empirical formula will depend on the spins measured with respect to the orbital plane at merger. In Ref [26] we described a procedure for determining an approximate plane. This is based on locating three fiducial points on the BHBs trajectory \vec{r}_+ , \vec{r}_0 , and \vec{r}_- , where \vec{r}_+ is the point where $\ddot{r}(t)$ [$r(t)$ is the orbital separation]

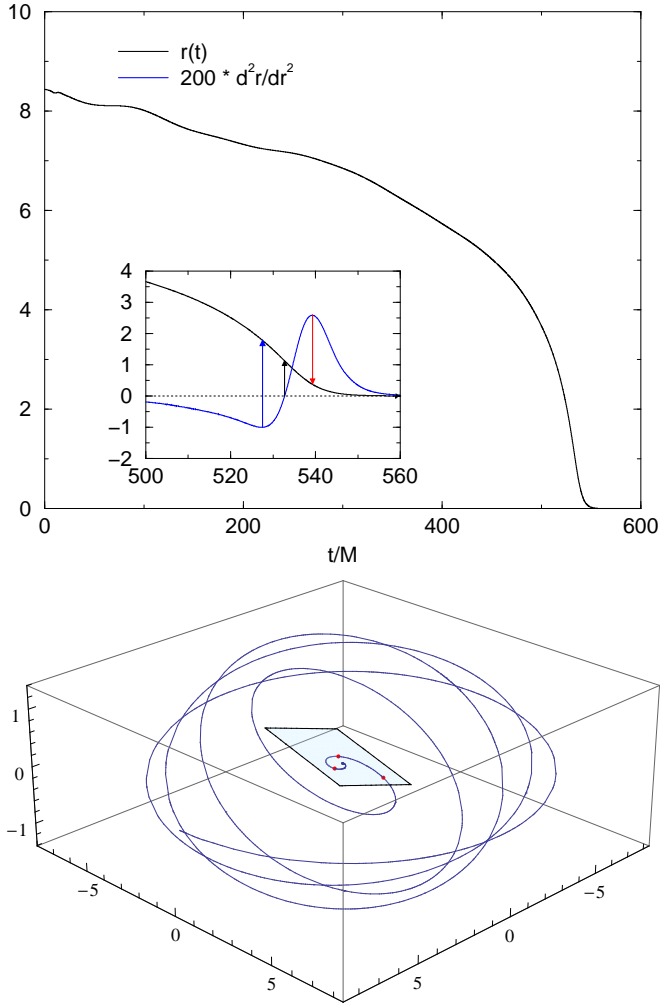


FIG. 1. Finding the orbital plane near merger. The upper plot shows the orbital separation $r(t)$ versus time. The inset shows $r(t)$ near merger and $\dot{r}(t)$ (rescaled by 200 for clarity). The points \vec{r}_+ , \vec{r}_0 , and \vec{r}_- correspond to the times where \dot{r} is maximized, zero, and minimized, respectively (denoted with arrows here). The plot below shows the trajectory, the points \vec{r}_+ , \vec{r}_0 , \vec{r}_- (large red dots) and the “merger” plane.

reaches its maximum, \vec{r}_- is the point where $\ddot{r}(t)$ reaches its minimum, and \vec{r}_0 is the point between the two where $\ddot{r}(t) = 0$. These three points can then be used to define an approximate merger plane (see Fig. 1). We then need to rotate each trajectory such that the infall directions all align (as much as possible). This is accomplished by rotating the system, keeping the merger plane’s orientation fixed, such that the vector $\vec{r}_+ - \vec{r}_0$ is aligned with the y axis. The azimuthal angle φ , described below, is measured in this rotated frame.

A. Configurations

For this exploration of the dependence of the recoil, total radiated energy, and remnant spin on the mass ra-

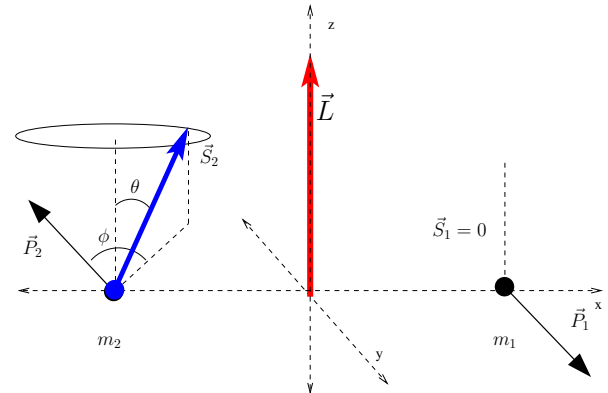


FIG. 2. The NQ configuration. Here one BH is spinning (typically the larger one) and one is nonspinning. Numerical evolutions preserve the NQ configurations approximately.

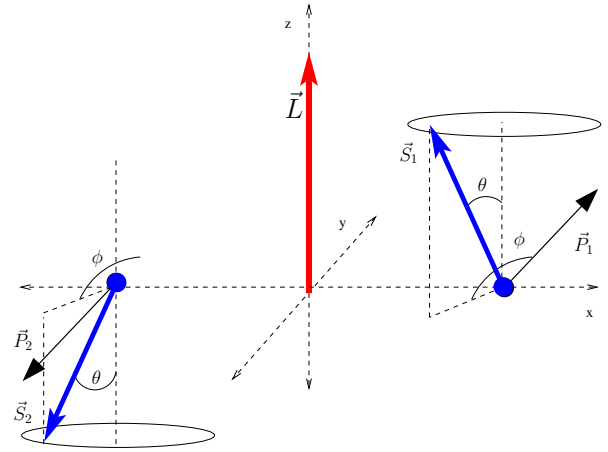


FIG. 3. The K configuration. $S_{1z} = -S_{2z}$, while $S_{1x} = S_{2x}$ and $S_{1y} = S_{2y}$, initially.

tio we will use an extension of the basic N configuration of [30], which we will denote by NQ here. The difference between the N configurations and the new NQ configurations is that the NQ configurations will have non-unit mass ratios. For the N/NQ configuration (see Fig. 2) one BH is spinning and the other nonspinning. By convention, we choose BH2 to be spinning and define the mass ratio q by $q = M_1/M_2$. So $q < 1$ implies that the larger BH is spinning, while $q > 1$ implies that the smaller BH is spinning. The polar orientation of the N/NQ configurations will in general change over the course of the evolution. However, a family of fixed starting polar angle θ and different azimuthal angles ϕ will evolve to a family of configurations at merger with very similar polar orientations. This will be critical to our fitting as we will be examining the maximum recoil over ϕ for a given (ending) polar angle θ and mass ratio q .

We will denote these configurations by NQ $_{xxx}$ TH $_{yyy}$ PH $_{zzz}$, where xxx indicated the mass ratio, yyy indicates the initial polar angle of the spin, and zzz indicated the initial azimuthal orientation of

the spin. We will also reexamine the fitting of the equal-mass N and K configurations of Ref. [30]. Note that while the K configurations start with the two in-plane components of the spins aligned (see Fig. 3), the in-plane components of the two spins rotate with respect to each other.

A detailed list of initial data parameters for the new NQxxxTHyyyPHzzz configurations is given in Table XVIII. The measured radiated mass, angular momentum, and recoil is given in Table XIX. As we saw previously [30, 41, 51], the isolated horizon quantities are more accurate than their radiative counterparts. The two are shown for various configurations in Table XX. The differences between the radiative and isolated horizon measures is a reasonable measure of the true error in the radiative quantities.

Finally, in Table XXI we give the spins near merger and the recoils in a frame adapted to the averaged orbital plane at merger. Results from the K configurations are also reported in these tables.

III. EXPANSIONS FOR UNEQUAL MASS BINARIES

In the sections below we use the following conventions. We denote the horizon mass of the two BHs in a binary by M_1 and M_2 and the total mass by m , where $m = M_1 + M_2$. The symbol M will always denote the unit of mass. We will use \vec{S}_1 and \vec{S}_2 to denote the spins (in units of M^2) of the two BHs. For our expansion formulas, we will use the variables,

$$\delta m = (M_1 - M_2)/m, \quad (2)$$

$$\vec{S} = \vec{S}_1 + \vec{S}_2, \quad (3)$$

$$\vec{\Delta} = m(\vec{S}_2/M_2 - \vec{S}_1/M_1), \quad (4)$$

$$\vec{S}_0 = \vec{S} + (1/2)\delta m \vec{\Delta}, \quad (5)$$

as well as the dimensionless equivalent variables

$$\tilde{\vec{S}} = \vec{S}/m^2, \quad (6)$$

$$\tilde{\vec{\Delta}} = \vec{\Delta}/m^2, \quad (7)$$

$$\tilde{\vec{S}}_0 = \vec{S}_0/m^2. \quad (8)$$

Note that for generic BHs, the component of $\vec{S}_0 = m(\vec{S}_1/M_1 + \vec{S}_2/M_2)$ in the direction of the orbital angular momentum is conserved at low PN order [71] and approximately conserved in full numerical simulations [72].

The set of variables $\{\vec{S}, \vec{\Delta}, \vec{S}_0\}$ is linearly dependent. We will only use the pair of spin variables $(\vec{S}, \vec{\Delta})$ or the pair $(\vec{S}_0, \vec{\Delta})$ in any one fit. Finally, we will decompose vectors in terms of components parallel to the orbital angular momentum, which we will denote with the subscript \parallel , and components in the orbital plane, which we will denote with the subscript \perp .

We have adopted Taylor-like expansion formulas [44] to model the remnant black holes mass and spin [51] and

TABLE I. Symmetry properties of key quantities under parity (P) and exchange of labels (X). Note that \vec{S}_0 has the same symmetries as \vec{S} .

Quantity	P	X
$S_\perp/m^2 = (S_1 + S_2)_\perp/m^2$	–	–
$S_\parallel/m^2 = (S_1 + S_2)_\parallel/m^2$	+	+
$\Delta_\perp/m^2 = (S_2/M_2 - S_1/M_1)_\perp/m$	–	+
$\Delta_\parallel/m^2 = (S_2/M_2 - S_1/M_1)_\parallel/m$	+	–
$\hat{n} = \hat{r}_1 - \hat{r}_2$	+	–
$\delta m = (M_1 - M_2)/m$	+	–
V_\perp	+	–
V_\parallel	–	+
J_\perp/m^2	–	–
J_\parallel/m^2	+	+
M_{rem}/m	+	+

recoil [30]. In the approach above, we considered polynomial formulas in powers of the spin parameters only.

In this paper we generalize the fitting formulas in [30, 51] for unequal, but comparable, mass binaries. To do this, we consider the expansion variable δm to be on the same footing as the spin variables.

A Taylor expansion of a function with v independent variables of a given order of expansion o has n terms, where n is given by [73]

$$n = \frac{(o+v-1)!}{o!(v-1)!}. \quad (9)$$

However, only certain combinations of variables are allowed due to symmetries of both the remnant quantity to be modeled and the binary parameters entering the model. The two key symmetry operations are parity ($x \rightarrow -x, y \rightarrow -y, z \rightarrow -z$) and exchange of labels $1 \leftrightarrow 2$ for the two BHs. These symmetry properties are summarized in Table I.

Our particular expansion functions for the recoil are summarized in Tables II and III. Note that each term in these tables is multiplied by a fitting constant. The total number of terms for the expansion of the recoil, and a comparison to a generic Taylor expansion, is given in Table IV.

Despite the symmetries, which reduce the total number of terms in the two components of the recoil by a factor of ≈ 4 compared to the generic Taylor expansion, there still are many parameters to fit and aliasing can lead to large statistical uncertainty in the values of the fitting constants. To partially overcome this, we use a hierarchical procedure where we fit the full set of coefficients and then reduce the number of fitting constants by setting all constants with large statistical errors in the original fit to zero. The fit is repeated and again the constants with the largest statistical uncertainties are set to zero. This procedure is repeated until the remaining constants have acceptable statistical uncertainties (in practice we demand that the uncertainty in a constant is less than half its absolute value).

TABLE II. Parameter dependence at each order of expansion for the out-of-plane recoil.

Order	Terms in V_{\parallel}
0th	0
1st	Δ_{\perp}
2nd	$\Delta_{\perp}.S_{\parallel} + \Delta_{\parallel}.S_{\perp}$ + $\delta m(S_{\perp})$
3rd	$\Delta_{\parallel}.S_{\perp}.S_{\parallel} + \Delta_{\perp}.S_{\parallel}^2 + \Delta_{\perp}.\Delta_{\parallel}^2 + \Delta_{\perp}^3 + \Delta_{\perp}.S_{\perp}^2$ + $\delta m(\Delta_{\perp}.\Delta_{\parallel} + S_{\perp}.S_{\parallel})$ + $\delta m^2(\Delta_{\perp})$
4th	$S_{\perp}.\Delta_{\parallel}^3 + \Delta_{\perp}.S_{\parallel}^3 + \Delta_{\perp}.S_{\parallel}.\Delta_{\parallel}^2 + S_{\perp}.\Delta_{\perp} .S_{\parallel}^2$ + $\Delta_{\perp}^3.S_{\parallel} + S_{\perp}^3.\Delta_{\parallel} + \Delta_{\perp}^2.S_{\perp}.\Delta_{\parallel} + \Delta_{\perp}.S_{\perp}^2.S_{\parallel}$ + $\delta m(S_{\perp}.\Delta_{\parallel}^2 + S_{\perp}.S_{\parallel}^2 + \Delta_{\perp}.\Delta_{\parallel}.S_{\parallel} + S_{\perp}.\Delta_{\perp}^2 + S_{\perp}^3)$ + $\delta m^2(\Delta_{\perp}.S_{\parallel} + \Delta_{\parallel}.S_{\perp})$ + $\delta m^3(S_{\perp})$

TABLE III. Parameter dependence at each order of expansion for the in-plane recoil.

Order	Terms in V_{\perp}
0th	0
1st	Δ_{\parallel} + δm
2nd	$\Delta_{\parallel}.S_{\parallel} + \Delta_{\perp}.S_{\perp}$ + $\delta m(S_{\parallel})$
3rd	$\Delta_{\perp}.S_{\perp}.S_{\parallel} + \Delta_{\parallel}.S_{\parallel}^2 + \Delta_{\parallel}.\Delta_{\perp}^2 + \Delta_{\parallel}^3 + \Delta_{\parallel}.S_{\perp}^2$ + $\delta m(\Delta_{\parallel}^2 + S_{\parallel}^2 + \Delta_{\perp}^2 + S_{\perp}^2)$ + $\delta m^2(\Delta_{\parallel})$ + δm^3
4th	$S_{\perp}.\Delta_{\perp}^3 + \Delta_{\parallel}.S_{\parallel}^3 + \Delta_{\parallel}.S_{\parallel}.\Delta_{\perp}^2 + S_{\perp}.\Delta_{\perp} .S_{\parallel}^2$ + $\Delta_{\perp}^3.S_{\parallel} + S_{\perp}^3.\Delta_{\perp} + \Delta_{\parallel}^2.S_{\perp}.\Delta_{\perp} + \Delta_{\parallel}.\Delta_{\perp}^2.S_{\parallel}$ + $\delta m(S_{\parallel}.\Delta_{\parallel}^2 + S_{\parallel}.S_{\perp}^2 + \Delta_{\perp}.S_{\perp}.\Delta_{\parallel} + S_{\parallel}.\Delta_{\perp}^2 + S_{\parallel}^3)$ + $\delta m^2(\Delta_{\parallel}.S_{\parallel} + \Delta_{\perp}.S_{\perp})$ + $\delta m^3(S_{\parallel})$

Our particular expansion functions for the remnant spin are summarized in Tables VI and V. Note that each term in these tables is multiplied by a fitting constant. The total number of terms for the expansion of the remnant spin, and a comparison to a generic Taylor expansion, is given in Table VII.

Note that the combined number of terms in the expansions of the two components of \vec{V} and \vec{J} at any given order matches the total number of terms in the Taylor expansion for a scalar function with no symmetries.

The expansion of the radiated mass will have an identical set of terms to the expansion of J_{\parallel} (see Table VIII). We have found that in practice this expansion (up through fourth-order) provides an accurate description

TABLE IV. Number of possible terms at a given order of expansion (with respect to \vec{S} or $\vec{\Delta}$ and δm)

Order	0th	1st	2nd	3rd	4th	5th	6th
V_{\perp}	0	2	3	11	16	36	50
V_{\parallel}	0	1	3	8	16	30	50
Total	0	3	6	19	32	66	100
Taylor	1	5	15	35	70	126	210
Difference	-1	-2	-9	-16	-38	-60	-110

TABLE V. Parameter dependence at each order of expansion for the final spin component perpendicular to the reference \vec{L} direction.

Order	Terms in J_{\perp}
0th	0
1st	S_{\perp}
2nd	$S_{\perp}.S_{\parallel} + \Delta_{\parallel}.\Delta_{\perp}$ + $\delta m(\Delta_{\perp})$
3rd	$\Delta_{\parallel}.\Delta_{\perp}.S_{\parallel} + S_{\perp}.S_{\parallel}^2 + S_{\perp}.\Delta_{\parallel}^2 + S_{\perp}^3 + S_{\perp}.\Delta_{\perp}^2$ + $\delta m(S_{\perp}.\Delta_{\perp} + \Delta_{\perp}.S_{\parallel})$ + $\delta m^2(S_{\perp})$
4th	$\Delta_{\perp}.\Delta_{\perp}^3 + S_{\perp}.S_{\parallel}^3 + S_{\perp}.S_{\parallel}.\Delta_{\parallel}^2 + \Delta_{\perp}.\Delta_{\parallel} .S_{\parallel}^2$ + $S_{\perp}^3.S_{\parallel} + \Delta_{\perp}^3.\Delta_{\parallel} + S_{\perp}^2.\Delta_{\perp}.\Delta_{\parallel} + S_{\perp}.\Delta_{\perp}^2.S_{\parallel}$ + $\delta m(\Delta_{\perp}.\Delta_{\parallel}^2 + \Delta_{\perp}.S_{\parallel}^2 + S_{\perp}.\Delta_{\perp}.\Delta_{\parallel} + \Delta_{\perp}.S_{\perp}^2 + \Delta_{\perp}^3)$ + $\delta m^2(S_{\perp}.S_{\parallel} + \Delta_{\parallel}.\Delta_{\perp})$ + $\delta m^3(\Delta_{\perp})$

TABLE VI. Parameter dependence at each order of expansion for the final spin component along the reference \vec{L} direction and similarly for the remnant mass M_{rem} (or, equivalently, the mass loss of the binary $\delta\mathcal{M}$).

Order	Terms in J_{\parallel} or M_{rem}
0th	$L(S = 0, \delta m = 0)$ or $M(S = 0, \delta m = 0)$
1st	S_{\parallel} + δm
2nd	$\Delta_{\parallel}^2 + S_{\parallel}^2 + \Delta_{\perp}^2 + S_{\perp}^2$ + $\delta m(\Delta_{\parallel})$ + δm^2
3rd	$S_{\parallel}.\Delta_{\parallel}^2 + S_{\parallel}.S_{\perp}^2 + \Delta_{\perp}.S_{\perp}.\Delta_{\parallel} + S_{\parallel}.\Delta_{\perp}^2 + S_{\parallel}^3$ + $\delta m(\Delta_{\parallel}.S_{\parallel} + \Delta_{\perp}.S_{\perp})$ + $\delta m^2(S_{\parallel})$
4th	$\Delta_{\perp}.\Delta_{\parallel}.S_{\perp}.S_{\parallel} + \Delta_{\perp}^4 + \Delta_{\parallel}^4 + S_{\perp}^4 + \Delta_{\perp}^2.\Delta_{\parallel}^2$ + $\Delta_{\perp}^2.S_{\perp}^2 + \Delta_{\perp}^2.S_{\parallel}^2 + \Delta_{\parallel}^2.S_{\perp}^2 + \Delta_{\parallel}^2.S_{\parallel}^2$ + $\delta m(\Delta_{\perp}.S_{\perp}.S_{\parallel} + \Delta_{\parallel}.S_{\parallel}^2 + \Delta_{\parallel}.\Delta_{\perp}^2 + \Delta_{\perp}^3 + \Delta_{\parallel}.S_{\perp}^2)$ + $\delta m^2(\Delta_{\parallel}^2 + S_{\parallel}^2 + \Delta_{\perp}^2 + S_{\perp}^2)$ + $\delta m^3(\Delta_{\parallel})$ + δm^4

TABLE VII. Number of possible terms at a given order of expansion (with respect to \vec{S} or $\vec{\Delta}$ and δm)

Order	0th	1st	2nd	3rd	4th	5th	6th
J_{\perp}	0	1	3	8	16	30	50
J_{\parallel}	1	1	6	8	22	30	60
Total	1	2	9	16	38	60	110
Taylor	1	5	15	35	70	126	210
Difference	0	-3	-6	-19	-32	-66	-100

TABLE VIII. Number of possible terms at a given order of expansion [with respect to \vec{S} or $\vec{\Delta}$ and δm for the final mass (M_{rem})].

Order	0th	1st	2nd	3rd	4th	5th	6th
M_{rem}/m	1	1	6	8	22	30	60
Total	1	1	6	8	22	30	60
Taylor	1	5	15	35	70	126	210
Difference	0	-4	-9	-27	-48	-96	-150

(see [41]) although alternative Padé approximant expressions are also possible as in Ref. [74].

IV. FITS

In this section we fit for the total radiated mass and remnant spin and recoil as a function of the spins of the binary at merger. Our expansion variables, \vec{S} (or \vec{S}_0), $\vec{\Delta}$, and δm are all measured with respect to the *final* orbital plane (see Sec. II and Fig. 1). For consistency with the particle limit, we also include explicit dependence on $\eta = (1 - \delta m^2)/4$.

A. Fitting the Recoil

Before modeling the mass-ratio dependence of the recoil we will reexamine the *cross kick* of Ref. [30]. As we noted there, the recoil should take the form

$$V_{\parallel} = a_0 \vec{\Delta} \cdot \hat{n}_0 + a_1 \vec{\Delta} \cdot \hat{n}_1 (2S_{\parallel}) + \dots + b_0 (2\vec{S}) \cdot \hat{m}_0 \tilde{\Delta}_{\parallel} + b_1 (2\vec{S}) \cdot \hat{m}_1 \tilde{\Delta}_{\parallel} (2S_{\parallel}) + \dots \quad (10)$$

where the unit vectors \hat{n}_i and \hat{m}_i are all in the orbital plane and need not be aligned in any way. As a simplifying assumption, we fit the data assuming all these unit vectors were aligned. While the fit for the N configurations was quite good, we were not able to model the K configurations with the same accuracy. The K configurations started out with nontrivial S_{\perp} and Δ_{\parallel} while having $\Delta_{\perp} = 0$ and $S_{\parallel} = 0$, identically. However, these evolved to configurations with nontrivial Δ_{\perp} . The spin directions and recoils for the K configurations are given in Table XXI.

Here we revisit the fitting of the equal-mass N and K configurations by assuming that $\hat{n}_0 = \hat{n}_1 = \hat{n}_2 \dots$,

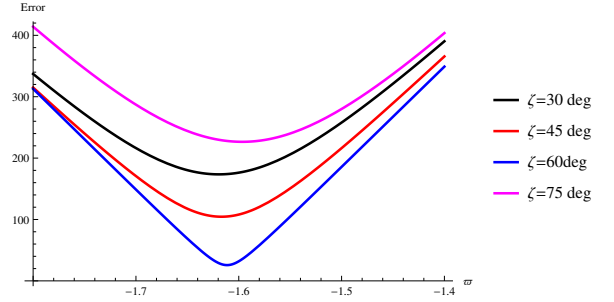


FIG. 4. The RMS error in the prediction of the recoil for the K45 configurations as a function of ϖ (the angle between the unit vector \hat{n}_0 and the x axis of the rotated basis) for several choices of ζ . Note that ϖ is measured in radians.

$\hat{m}_0 = \hat{m}_1 = \hat{m}_2 \dots$, and that \hat{n}_0 and \hat{m}_0 are not aligned. Our procedure is as follows. We assume that the angle between \hat{n}_0 and \hat{m}_0 is some given value, which we will denote by ζ . The expression for the maximum over azimuthal configurations φ of the recoil for the N configurations (equal mass only, see Fig. 2) then takes on the form $V_{\parallel \max}^2 = V_{\text{hang}}^2 + V_{\text{cross}}^2 + 2V_{\text{hang}}V_{\text{cross}} \cos \zeta$, where $V_{\text{hang}} = \tilde{\Delta}_{\perp}(h_1 + h_2(2\tilde{S}_{\parallel}) + h_3(2\tilde{S}_{\parallel})^2 + \dots)$ and $V_{\text{cross}} = (2\tilde{S}_{\perp})\tilde{\Delta}_{\parallel}(\sigma_1 + \sigma_2(2\tilde{S}_{\parallel}) + \sigma_3(2\tilde{S}_{\parallel})^2 + \dots)$. Here $\tilde{\Delta}_{\perp}$ and \tilde{S}_{\perp} are understood to be the magnitudes of the projections of these two vectors in the plane. In practice, we take the coefficients (h_1, h_2, h_3, \dots) from the expression for the *hangup kick* in [29] and only fit to the coefficients (σ_1, σ_2) (we take σ_3 and higher coefficients to be zero).

Once we have σ_1 and σ_2 for a given ζ , we predict the recoil for the K configurations. The prediction takes on the form

$$V_{\parallel} = \vec{\Delta} \cdot \hat{n}_0 (h_1 + h_2(2\tilde{S}_{\parallel}) + h_3(2\tilde{S}_{\parallel})^2 + \dots) + [(\vec{2S}) \cdot \mathbf{R}(\zeta)\hat{n}_0] \tilde{\Delta}_{\parallel} (\sigma_1 + \sigma_2(2\tilde{S}_{\parallel})) \quad (11)$$

where $\hat{m}_0 = \mathbf{R}(\zeta)\hat{n}_0$ is a unit vector in the orbital plane rotated by angle ζ from \hat{n}_0 . The remaining complication arises because we do not know the direction of \hat{n}_0 with respect to the rotated frame where the spins of the K configurations are given. To find this direction, we take $\hat{n}_0 = (\cos \varpi, \sin \varpi)$. The predicted recoil for a given K configuration will then depend on the actual in-plane components of the spins for that configuration and the angle ϖ . We then find the value of ϖ that minimizes the sum

$$\sum_{\varphi \text{configs}} (V_{\text{pred}}(\hat{m}) - V_{\text{meas}})^2.$$

The minimum over ϖ of the sum is itself a function of ζ . Finally, we adjust ζ until we find an absolute minimum. This procedure is illustrated in Fig. 4.

Interestingly, we find that the error is minimized for both the K45 and K22.5 families by a single ζ value of about -59° . For example, the RMS error in the recoil for the K45 configurations assuming that $\hat{n}_0 = \hat{m}_0$ (i.e., $\zeta = 0$) is 275.3 km s^{-1} , while assuming the angle between \hat{n}_0 and \hat{m}_0 is -59° gives an RMS error of 25.2 km s^{-1} with a maximum recoil of $2234 \pm 12 \text{ km s}^{-1}$. Similarly, the RMS error in the prediction for the recoil of the K22.5 configurations is 48.9 km s^{-1} with a maximum recoil of $1731 \pm 25 \text{ km s}^{-1}$ (the RMS errors is 253.4 km s^{-1} if we assume $\hat{n}_0 = \hat{m}_0$).

With this new fitting, the maximum recoil (over azimuthal configurations) for a given polar configuration is given by

$$V_{\parallel}^2 = V_{\text{hang}}^2 + V_{\text{cross}}^2 + 2V_{\text{hang}}V_{\text{cross}} \cos(59\pi/180), \quad (12)$$

where

$$\begin{aligned} V_{\text{hang}} &= \tilde{\Delta}_{\perp} \left(3678 + 2481 \left(2\tilde{S}_{\parallel} \right) \right. \\ &\quad \left. + 1792 \left(2\tilde{S}_{\parallel} \right)^2 + 1507 \left(2\tilde{S}_{\parallel} \right)^3 \right), \end{aligned} \quad (13)$$

$$V_{\text{cross}} = \left(2\tilde{S}_{\perp} \right) \tilde{\Delta}_{\parallel} \left(2160 + 3990 \left(2\tilde{S}_{\parallel} \right) \right). \quad (14)$$

The errors in the last two coefficients are 2160 ± 204 and 3990 ± 680 . If, however, we assume the angle ζ is zero, we get

$$V_{\parallel}^2 = V_{\text{hang}}^2 + V_{\text{cross}}^2 + 2V_{\text{hang}}V_{\text{cross}} \quad (15)$$

where

$$\begin{aligned} V_{\text{hang}} &= \tilde{\Delta}_{\perp} \left(3678 + 2481 \left(2\tilde{S}_{\parallel} \right) \right. \\ &\quad \left. + 1792 \left(2\tilde{S}_{\parallel} \right)^2 + 1507 \left(2\tilde{S}_{\parallel} \right)^3 \right), \end{aligned} \quad (16)$$

$$V_{\text{cross}} = \left(2\tilde{S}_{\perp} \right) \tilde{\Delta}_{\parallel} \left(1200 + 2550 \left(2\tilde{S}_{\parallel} \right) \right). \quad (17)$$

The errors in the last two coefficients are 1200 ± 99 and 2550 ± 340 .

We now move to the more general case of general mass ratios by extending formulas (12)-(17) to include terms proportional to δm .

Simply adding all possible unequal mass corrections to the recoil formula, even at low order, is fraught with difficulty because of the sheer number of terms (and hence the correspondingly large number of runs required). Here we will settle on a compromise formula. One that is *accurate enough* in a given mass ratio range (here $1/8 \lesssim q \leq 1$).

Our procedure is as follows. We fit each family of fixed mass ratio and polar inclination angle to the form

$$V_{\text{kick}} = V_1 \cos(\varphi - \phi_1) + V_3 \cos(3\varphi - 3\phi_3), \quad (18)$$

where V_1 , V_3 , ϕ_1 , and ϕ_3 are fitting coefficients and φ is the angle (at merger) between $\vec{\Delta}_{\perp}$ for a given PHzzz configuration and the corresponding PH0 configuration. Our tests indicate that V_1 can be obtained accurately with six

choices of the initial ϕ_i angles. These fitting parameters for each of the NQ families are given in Table IX.

We then model V_1 as a function of S_{\parallel} , S_{\perp} , Δ_{\parallel} , Δ_{\perp} , and δm using terms up through fourth order in the expansion variables. However, because we only consider contributions linear in $\cos \varphi$, only those terms in Table II that are linear in the perpendicular components of the spins enter the fit. A fit to this reduced form still leads to poor statistics for the fitting constants. We then selectively remove the most poorly fit constants (i.e., set them to zero) and refit. This process is repeated until a satisfactory fit is obtained with the fewest number of free parameters. In particular, we remove only one parameter at a time (always the one with the largest relative uncertainty). We stop removing parameters when all the remaining coefficients have uncertainties that are no larger in magnitude than $1/2$ the value of the coefficient itself. Note that this procedure does not lead to a unique minimal set of expansion terms.

We fit the full set of unequal mass NQ configurations to the two forms V_{x0} and V_{x59} , where

$$\begin{aligned} V_h &= (4\eta)^2 \tilde{\Delta}_{\perp} (3678(1 + c_1 \delta m^2) \\ &\quad + 2481(2\tilde{S}_{\parallel})(1 + c_2 \delta m^2) + 1792(2\tilde{S}_{\parallel})^2 \\ &\quad + 1507(2\tilde{S}_{\parallel})^3 + c_5 \tilde{\Delta}_{\parallel}^2 + \\ &\quad c_7 \tilde{\Delta}_{\parallel}^2 (2\tilde{S}_{\parallel}) + c_9 \delta m \tilde{\Delta}_{\parallel}), \end{aligned} \quad (19)$$

$$\begin{aligned} V_{c0} &= (4\eta)^2 (2\tilde{S}_{\perp}) \tilde{\Delta}_{\parallel} (1200 + c_{12} \delta m^2 \\ &\quad + 2550(2\tilde{S}_{\parallel}) + c_{15} \tilde{\Delta}_{\parallel}^2) \\ &\quad + (2\tilde{S}_{\perp}) [c_{16} \delta m + c_{17} \delta m^3 \\ &\quad + c_{18} \delta m (2\tilde{S}_{\parallel}) + c_{19} \delta m (2\tilde{S}_{\parallel})^2], \end{aligned} \quad (20)$$

$$\begin{aligned} V_{c59} &= (4\eta)^2 (2\tilde{S}_{\perp} \tilde{\Delta}_{\parallel}) (2160 + c_{12} \delta m^2 \\ &\quad + 3990(2\tilde{S}_{\parallel}) + c_{15} \tilde{\Delta}_{\parallel}^2) \\ &\quad + (2\tilde{S}_{\perp}) [c_{16} \delta m + c_{17} \delta m^3 \\ &\quad + c_{18} \delta m (2\tilde{S}_{\parallel}) + c_{19} \delta m (2\tilde{S}_{\parallel})^2], \end{aligned} \quad (21)$$

$$V_{x0} = V_h + V_{c0}, \quad (22)$$

$$V_{x59} = \sqrt{V_h^2 + V_{c59}^2 + 2V_h V_{c59} \cos(59\pi/180)}. \quad (23)$$

Here V_{x0} indicates a fit assuming the *cross kick* and *hangup kick* are aligned and V_{x59} assumes they are misaligned by 59° (note that $4\eta = 1$ for the equal-mass case and that we have assumed a leading η^2 dependence). Finally $x = 4$ indicates a standard fit that includes all terms up through fourth-order, while $x = 4'$ indicates that again all terms up through fourth-order are used but S_0 replaces S in the formula. We report the fitting parameters in Table X, and we show the results of fits in Fig. 5 and Fig. 6. The root-mean-square errors in the fits are: 23 km s^{-1} for V_{459} , 25 km s^{-1} for V_{40} , 20 km s^{-1} for $V_{4'59}$, and 19 km s^{-1} for $V_{4'0}$.

Examining Fig. 5, we can see that quality of the fit changes with mass ratio. Overall, $V_{4'0}$, $V_{4'59}$, and $V_{p'59}$ (discussed below) appear to do best at small mass ratios,

TABLE IX. Fitting parameters for the NQ families of configurations as a function of φ (see text) to the form $V_{\parallel} = V_1 \cos((\varphi - \phi_1)\pi/180) + V_3 \cos(3(\varphi - \phi_3)\pi/180)$. All angles are measured in degrees.

Family	V_1	V_3	ϕ_1	ϕ_3	RMS Err
NQ200TH30	390.27 ± 0.59	11.85 ± 0.57	347.412 ± 0.083	260.87 ± 0.92	0.57
NQ200TH60	643.7 ± 8.5	12.5 ± 8.2	282.30 ± 0.72	320 ± 12	8.24
NQ200TH90	700.6 ± 1.3	2.4 ± 1.3	326.312 ± 0.098	101 ± 10	1.22
NQ200TH135	455.81 ± 0.59	5.60 ± 0.57	145.008 ± 0.070	114.2 ± 2.0	0.57
NQ66TH60	1882 ± 11	24 ± 12	3.93 ± 0.38	0.9 ± 9.3	11.56
NQ50TH30	1313 ± 18	65 ± 16	309.29 ± 0.70	241.8 ± 5.0	16.34
NQ50TH60	1876 ± 22	94 ± 22	170.31 ± 0.65	250.9 ± 4.2	21.03
NQ50TH90	1720.3 ± 7.9	89.3 ± 9.2	29.32 ± 0.30	353.4 ± 1.7	7.13
NQ50TH135	865.2 ± 1.3	28.3 ± 1.2	249.072 ± 0.088	93.23 ± 0.94	1.23
NQ33TH45	1333.5 ± 6.2	114.8 ± 7.0	158.62 ± 0.27	62.73 ± 0.93	5.26
NQ33TH75	1505.4 ± 3.2	62.9 ± 1.7	270.658 ± 0.072	180.4 ± 1.6	1.93
NQ33TH100	1222.0 ± 2.1	50.7 ± 4.8	10.36 ± 0.12	337.41 ± 0.62	1.57
NQ33TH135	632.88 ± 0.21	9.33 ± 0.24	221.306 ± 0.024	72.97 ± 0.47	0.21
NQ25TH30	767.5 ± 2.2	71.9 ± 2.4	88.99 ± 0.19	232.72 ± 0.61	2.13
NQ25TH60	1183.1 ± 2.6	70.4 ± 2.0	94.22 ± 0.11	243.81 ± 0.81	2.90
NQ25TH90	1035.7 ± 1.9	32.1 ± 1.4	97.983 ± 0.052	6.62 ± 0.54	0.56
NQ25TH135	454.58 ± 0.54	5.56 ± 0.75	195.54 ± 0.09	404.4 ± 1.9	0.54
NQ25TH150	277.72 ± 0.91	8.3 ± 1.1	23.19 ± 0.23	130.2 ± 2.2	0.97
NQ16TH45	627.0 ± 5.2	65.6 ± 6.8	124.85 ± 0.27	35.2 ± 1.1	2.37
NQ16TH90	657 ± 10	29.1 ± 3.2	242.871 ± 0.093	149.4 ± 3.7	1.18
NQ16TH115	419.84 ± 0.98	14.59 ± 0.56	192.68 ± 0.19	338.0 ± 1.2	0.38
NQ16TH135	253.4 ± 1.4	6.9 ± 3.1	277.89 ± 0.38	27.0 ± 4.0	0.90
NQ16TH150	154.11 ± 0.10	3.048 ± 0.082	318.774 ± 0.031	87.57 ± 0.60	0.084

at least for the large θ tail. For $q \leq 1/3$, there is a noticeable oscillation in the predicted recoil from V_{459} and V_{40} at large θ . On the other hand, for $q = 2$, V_{40} and V_{459} fit the data best with $V_{4'0}$ and $V_{4'59}$ slightly underestimating the maximum recoil. As shown in Fig. 6, the relative errors in the predicted recoils for all fitting functions are under 10% for all but one configuration (where the error is 15–20%). For $V_{4'59}$ the relative errors are all less than 10%, while the absolute errors are less than 55 km s⁻¹ (less than 40 km s⁻¹ for all but one configuration). Note that at extrapolations down to $q = 1/10$, there is reasonably good agreement between all fitting functions. Based on the relative and absolute errors, the extrapolation to mass ratios as small as $q = 1/10$, and the fact that $S_{0\parallel}$ is approximately conserved in post-Newtonian theory [71] and in full numerical simulations [51, 72], we conclude that $V_{4'59}$ has the best overall performance.

Note that while $S_{0\parallel}$ is conserved, the other quantities entering $V_{4'59}$ are not. Thus $V_{4'59}$ is still a function of the binary's parameters near merger and not at infinite

separation.

Motivated by the success of $V_{4'59}$ in modeling the recoil, we also reexamined the Padé approximation for the *hangup kick* kick formula we proposed in [29]. The Padé approximation has the form

$$V_{\text{hang(pade)}} = \tilde{\Delta}_{\perp} 3684.73 \left(\frac{1 + 0.0705104(2\tilde{S}_{\parallel})}{1 - 0.623831(2\tilde{S}_{\parallel})} \right), \quad (24)$$

which has pole when $\tilde{S}_{\parallel} \approx 0.8015$. This pole can only be reached for mass ratios smaller than $q = 1/8$. However, by replacing S_{\parallel} with $S_{0\parallel}$ in Eq. (24), there is no pole for any physically allowed values for the spins. We were thus able to fit (V_1) the recoil to the form

$$V_{p'59} = \sqrt{V_h^2 + V_k^2 + 2V_h V_k \cos(59\pi/180)}, \quad (25)$$

where

$$V_h = (4\eta)^2 \tilde{\Delta}_{\perp} \left[3684.73 \left(\frac{1 + c_1 \delta m^2 + 0.0705104(2\tilde{S}_{0\parallel})(1 + c_2 \delta m^2)}{1 - 0.623831(2\tilde{S}_{0\parallel})} \right) + c_5 \tilde{\Delta}_{\parallel}^2 + c_7 \Delta_{\parallel}^2 (2\tilde{S}_{0\parallel}) \right] + (4\eta)^2 (c_9 \delta m \tilde{\Delta}_{\perp} \tilde{\Delta}_{\parallel}) \quad (26)$$

$$V_k = (4\eta)^2 \tilde{\Delta}_{\parallel} (2\tilde{S}_{0\perp}) (2090 + c_{12} \delta m^2 + 4150(2\tilde{S}_{0\parallel}) + c_8 (2\tilde{S}_{0\parallel})^2 + c_{15} \tilde{\Delta}_{\parallel}^2) + (4\eta)^2 (2\tilde{S}_{0\perp}) (c_{16} \delta m + c_{17} \delta m^3 + c_{18} \delta m (2\tilde{S}_{0\parallel}) + c_{19} \delta m (2\tilde{S}_{0\parallel})^2). \quad (27)$$

TABLE X. Fitting coefficients in Eqs. (19)-(23) and Eqs. (25)-(27) for the remnant recoil velocity in. All coefficients not given here were set to zero.

V_{40}			
c_1	-0.747 ± 0.065	c_8	-1490 ± 520
c_{16}	-480 ± 90	c_{12}	-1670 ± 780
c_{19}	2430 ± 250		
V_{459}			
c_1	-0.757 ± 0.069	c_8	-2100 ± 720
c_{19}	4200 ± 360	c_{16}	-880 ± 140
$V_{4'0}$			
c_1	-0.612 ± 0.044	c_2	-1.13 ± 0.37
c_{18}	-3430 ± 500	c_{16}	-640 ± 80
$V_{4'59}$			
c_1	-0.673 ± 0.051	c_{12}	-6300 ± 1750
c_{18}	-5580 ± 1000	c_{16}	-1130 ± 160
$V_{p'59}$			
c_1	-0.677 ± 0.046	c_9	-2540 ± 250
		c_{16}	-1280 ± 130

The coefficients 2090 ± 210 and 4150 ± 690 in Eq. (27) were obtained by fitting to the equal-mass N configurations assuming an angle of -59° between the cross and hangup components. The remaining nonzero components are given in Table X (we compare the predictions for the statistical distributions of recoil velocities for $V_{p'59}$ to $V_{4'59}$ in Table XVII).

In the previous discussion we ignored the in-plane component to the recoil. The reason is, there is significant contamination from the out-of-plane component (e.g., by a small misidentification of the orientation of the orbital plane) which leads to an in-plane component that is highly dependent on the procedure used to identify the plane. We *avoid* this issue by modeling the in-plane recoil using only the nonprecessing results of [41]. The relative error in doing so can be large (for the in-plane component). However, as this error is large when the out-of-plane component is much larger than the in-plane component, and because the two components add in quadrature, the net error in the magnitude of the recoil is less than 10% for all but 3 configurations (where the absolute error is $< 100 \text{ km s}^{-1}$). In Table XI, we show the maximum recoil for a given family and the RMS and maximum errors in our prediction of the total recoil and the out-of-plane component of the recoil. Interestingly, the dominant error in the total recoil is generally associated with the out-of-plane component.

Finally, we note that while the out-of-plane recoil is the dominant component, it is important (e.g., for modeling electromagnetic counterparts to BH mergers) to determine the direction of the recoil with respect to the orbital plane (more specifically, the orbital plane when the binary decoupled from any surrounding disk). As shown in Fig. 7, for the NQ configurations, the distribution of recoil angles is quite broad for smaller re-

TABLE XI. The maximum net recoil measured for each family of NQ configurations and the RMS and maximum errors in the predictions of the total recoil (center columns) and the out-of-plane component of the recoil (right columns) for each family.

Family	V_{\max}	RMS	MAX	RMS	MAX
NQ200TH30	434	9	10	4	6
NQ200TH60	660	16	21	10	13
NQ200TH90	714	15	26	7	11
NQ200TH135	467	11	14	5	7
NQ66TH60	1920	27	50	32	44
NQ50TH30	1237	70	114	68	109
NQ50TH60	1812	87	123	72	94
NQ50TH90	1752	81	104	41	52
NQ50TH135	926	57	66	18	25
NQ33TH45	1386	40	53	25	31
NQ33TH75	1424	82	127	58	78
NQ33TH100	1288	97	118	27	31
NQ33TH135	731	56	71	14	18
NQ25TH30	820	9	14	8	12
NQ25TH60	1231	66	91	37	61
NQ25TH90	1087	64	93	30	37
NQ25TH135	569	65	72	7	11
NQ25TH150	409	38	41	6	9
NQ16TH45	681	22	32	9	14
NQ16TH90	551	75	90	18	27
NQ16TH115	527	34	69	27	37
NQ16TH135	361	52	77	8	11
NQ16TH150	262	22	26	23	36

coil velocities ($< 700 \text{ km s}^{-1}$) but is narrow for large recoils ($> 1000 \text{ km s}^{-1}$). There are substantial recoils ($> 1000 \text{ km s}^{-1}$) for inclinations as small as 40° .

B. Fitting the radiated energy and remnant spin

The total mass loss of the binary from its complete inspiral (starting at infinite separation) is given by

$$\delta\mathcal{M} = \frac{M_1^\infty + M_2^\infty - M_{\text{rem}}}{M_1^\infty + M_2^\infty}, \quad (28)$$

where M_1^∞ and M_2^∞ are the initial masses of the two BHs (i.e., at infinite separations) and M_{rem} is the remnant mass. Since the BH horizon is essentially constant during the inspiral, we get a very good approximation to $\delta\mathcal{M}$ using

$$\delta\mathcal{M} \approx \frac{M_1 + M_2 - M_{\text{rem}}}{M_1 + M_2}, \quad (29)$$

where M_1 and M_2 are the horizon masses of the two BHs in the binary as measured after the initial burst of radiation.

For each family of NQ configurations with fixed q and θ , we fit $\delta\mathcal{M}$ to the form

$$\delta\mathcal{M} = E_c + E_\phi \cos(2\varphi - 2\phi_2^m), \quad (30)$$

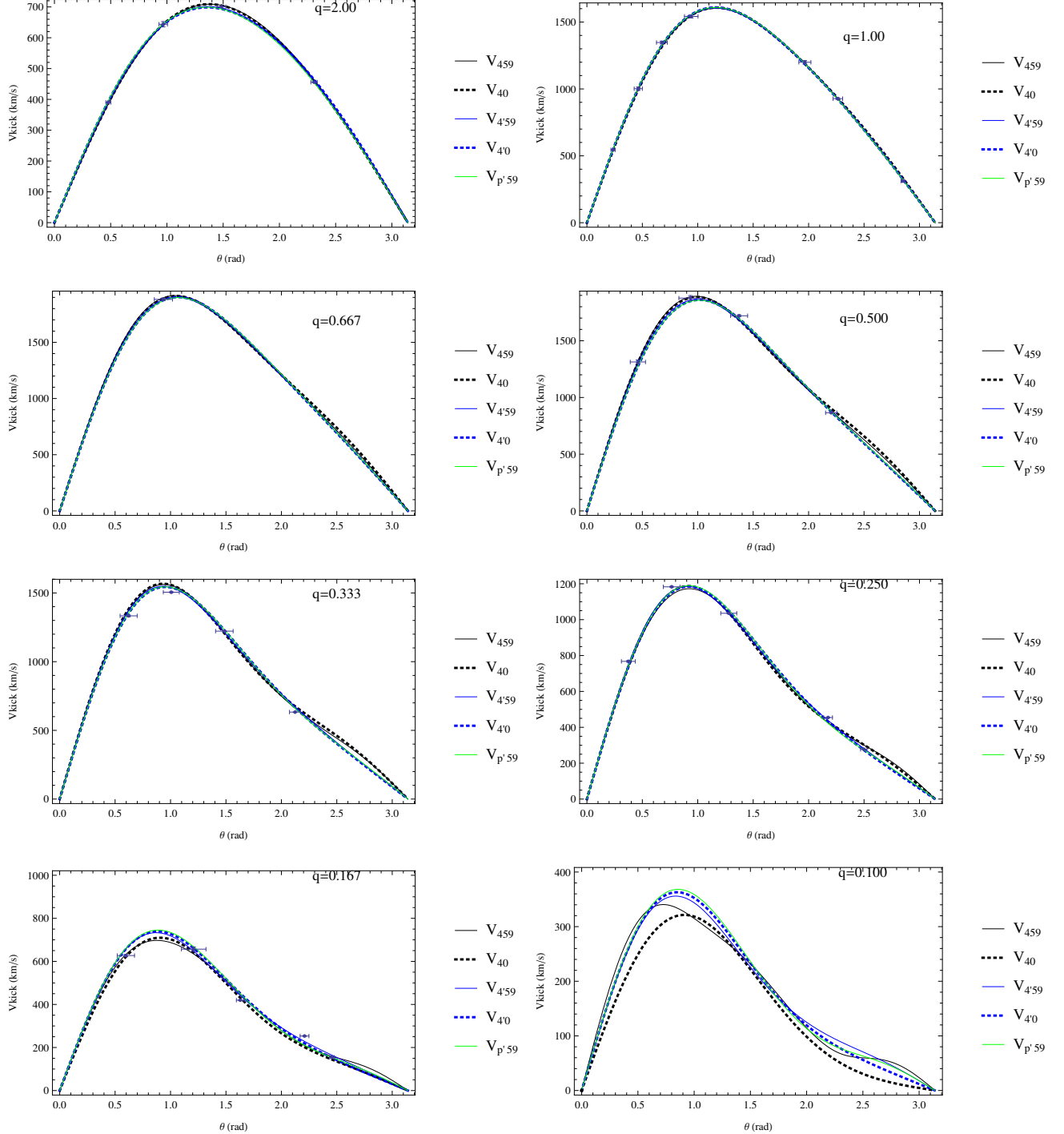


FIG. 5. Plots of the fitted V_1 versus inclination angle θ and q for the NQ configurations. Each data point represents the maximum of V_1 over a family of azimuthal configurations with the same inclination angle and mass ratio. The last plot shows an extrapolation to $q = 1/10$.

where E_c , E_ϕ , and ϕ_2^m are fitting constants. We also fit the square of the dimensionless remnant spin α^2 to the form,

$$\alpha^2 = A_c + A_\phi \cos(2\varphi - 2\phi_2^a), \quad (31)$$

where A_c , A_ϕ , and ϕ_2^a are fitting constants. The results are given in Table XII. Note that E_c and A_c dominate the expressions for the mass loss and remnant spin. Note also that in Tables XII and XX there are missing entries. These missing entries are due to missing remnant horizon

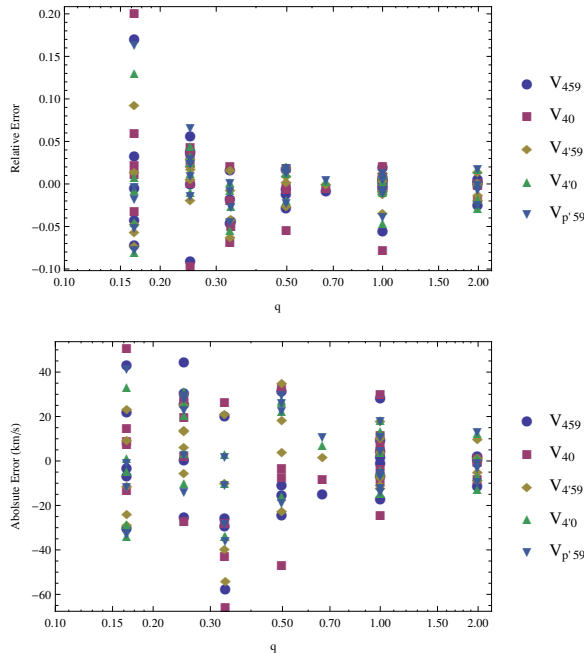


FIG. 6. The relative errors (residuals) in the fit of V_ϕ versus q . Note that there are multiple data points for each q .

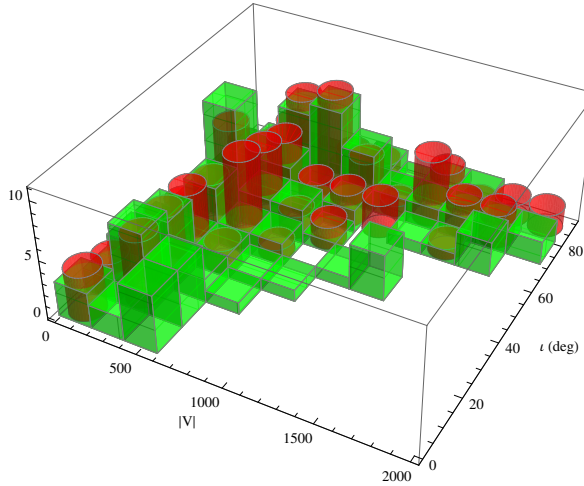


FIG. 7. The distribution of recoils for the NQ configurations. The green boxes indicate the recoil angle as measured with respect to the initial orbital plane while the red cylinders indicate the recoil angle is measured with respect to the orbital plane at merger. Here i is the inclination angle of the recoil with respect to the orbital plane in units of degrees and the recoil is measured in units of km s^{-1} .

mass and spin data.

To fit E_c as a function of q and θ , we start by refitting the configurations of Healy *et al.* [41] (all these configurations were nonprecessing). We need to refit the results there because our fitting formulas are different. There the fits were to the remnant mass and here we are fitting to the mass loss.

As in [41], we keep terms up through fourth-order in the spins and δm , and enforce the particle limit. Our fitting function for E_c is given by

$$\begin{aligned} E_c^{\parallel} = & (4\eta)^2 \left(E_{\text{HU}} + k_{2a}\delta m \tilde{\Delta}_{\parallel} + (0.000743)\tilde{\Delta}_{\parallel}^2 + k_{2d}\delta m^2 \right. \\ & + k_{3a}\delta m \tilde{\Delta}_{\parallel} \tilde{S}_{\parallel} + k_{3b}\tilde{S}_{\parallel} \tilde{\Delta}_{\parallel}^2 + k_{3d}\delta m^2 \tilde{S}_{\parallel} \\ & + k_{4a}\delta m \tilde{\Delta}_{\parallel} \tilde{S}_{\parallel}^2 + k_{4b}\delta m \tilde{\Delta}_{\parallel}^3 + (0.000124)\tilde{\Delta}_{\parallel}^4 + k_{4e}\tilde{\Delta}_{\parallel}^2 \tilde{S}_{\parallel} \\ & \left. + k_{4f}\delta m^4 + k_{4g}\delta m^3 \tilde{\Delta}_{\parallel} \right) + \delta m^6 \eta (1 - E_{\text{isco}}), \end{aligned} \quad (32)$$

where E_{HU} is given by [74]

$$E_{\text{HU}} = 0.0025829 - \frac{0.0773079}{2\tilde{S}_{0\parallel} - 1.693959}, \quad (33)$$

E_c^{\parallel} denotes that spins are aligned or antialigned with the orbital angular momentum, and E_{isco} is the energy of the innermost stable circular orbit (ISCO). For the fits here and below we approximate E_{isco} by the ISCO energy of a particle on an equatorial geodesic on a Kerr background with spin parameter $\alpha = \tilde{S}_{\parallel}$. Note that we define E_{HU} using the \tilde{S}_0 variable. This is due to the fact that E_{HU} would have a pole at small mass ratios if we defined it using \tilde{S} . In the equal-mass limit, both definitions are equivalent.

As in our fits to the recoil, we successively remove the most uncertain of the fitting coefficients. Our final fitting parameters are summarized in Table XIII. We then fit E_c from each family of the NQ configurations to

$$\begin{aligned} E_c = & E_c^{\parallel} + (4\eta)^2 \left(|\tilde{S}_{\perp}|^2 (e_1 + e_2 \tilde{S}_{\parallel} + e_3 \tilde{S}_{\parallel}^2) \right. \\ & + |\tilde{\Delta}_{\perp}|^2 (\epsilon_1 + \epsilon_2 \tilde{S}_{\parallel} + \epsilon_3 \tilde{S}_{\parallel}^2) + \delta m^2 |\tilde{S}_{\perp}|^2 (E_A + \tilde{S}_{\parallel} E_B) \\ & + \delta m^2 |\tilde{\Delta}_{\perp}|^2 (E_D + \tilde{S}_{\parallel} E_E) + E_F \delta m |\tilde{\Delta}_{\perp}| |\tilde{S}_{\perp}| \\ & \left. + E_G \tilde{\Delta}_{\parallel}^2 |\tilde{\Delta}_{\perp}|^2 + E_H \tilde{\Delta}_{\parallel}^2 |\tilde{S}_{\perp}|^2 \right), \end{aligned} \quad (34)$$

where E_c^{\parallel} is given by Eq. (32), and the constants e_1 , e_2 , e_3 , ϵ_1 , ϵ_2 , and ϵ_3 were determined in [51] (note that the constants e_1, \dots here are denoted by e'_1, \dots in [51]). For the convenience of the reader, those constants are also given in Table XIII. The remaining terms in Eq. (34) were chosen by adding even powers in δm to terms present in the equal-mass case. In addition, we found that term odd in δm (E_F) was needed in order to fit the $q = 2$ family.

Unlike in the equations for the recoil in the preceding section [e.g., Eqs. (19)-(23) and Eqs. (25)-(27)], here S_{\perp} and Δ_{\perp} arise from the magnitudes of the in-plane components of these two vectors rather than dot products with unit vectors in the plane. We therefore use the notation $|S_{\perp}|$, etc., to distinguish between these types of terms and those in for the recoil. This distinction will be important when generalizing to arbitrary binaries.

When fitting the remaining constants in Eq. (34) we take all previously fitted constants as exact (i.e., we do not include the uncertainties in these constants in subsequent fits). Once again, we successively remove the least

TABLE XII. Fitting parameters for the NQ families of configurations as a function of φ (see text) to the form $\delta\mathcal{M}_{\parallel} = E_c + E_{\phi} \cos(2(\varphi - \phi_2^m)\pi/180)$ and $\alpha_{\text{rem}}^2 = A_c + A_{\phi} \cos(2(\varphi - \phi_2^{\alpha})\pi/180)$. All angles are measured in degrees.

Family	$100E_c$	$100E_{\phi}$	ϕ_2^m	A_c	$100A_{\phi}$	ϕ_2^{α}
NQ200TH30	4.28514 ± 0.00080	0.0183 ± 0.0014	3.30 ± 2.42	0.441972 ± 0.000001	-0.028 ± 0.001	-6.8 ± 1.2
NQ200TH60	4.13687 ± 0.00032	-0.02329 ± 0.00045	24.79 ± 0.56	0.42292 ± 0.00001	0.1154 ± 0.0018	12.87 ± 0.46
NQ200TH90	3.92326 ± 0.00052	0.03107 ± 0.00070	-24.66 ± 0.69	0.394768 ± 0.000002	$-0.1160 \pm .0002$	-35.87 ± 0.07
NQ200TH135						
NQ66TH60	5.5982 ± 0.0025	0.12438 ± 0.0035	12.62 ± 0.79	0.6244 ± 0.0001	-0.421 ± 0.013	11.43 ± 0.91
NQ50TH30	5.9302 ± 0.0029	0.0602 ± 0.0040	4.3 ± 2.0	0.7215 ± 0.0001	-0.1674 ± 0.0074	-12.1 ± 1.4
NQ50TH60	5.1623 ± 0.0065	0.1290 ± 0.0092	0.0 ± 2.0	0.63855 ± 0.00036	-0.386 ± 0.050	-5.5 ± 3.7
NQ50TH90	4.2528 ± 0.0084	0.108 ± 0.011	35.9 ± 4.4	0.49782 ± 0.00021	-0.578 ± 0.027	38.9 ± 1.5
NQ50TH135	3.20389 ± 0.00085	-0.0344 ± 0.0012	-11.92 ± 0.94	0.24812 ± 0.00013	0.247 ± 0.018	-17.0 ± 2.0
NQ33TH45	4.5458 ± 0.0083	0.099 ± 0.011	-4.7 ± 3.1	0.69928 ± 0.00010	-0.286 ± 0.014	-5.9 ± 1.4
NQ33TH75	3.6795 ± 0.0030	-0.1241 ± 0.0040	29.57 ± 0.91	0.56914 ± 0.00057	0.506 ± 0.071	18.5 ± 4.4
NQ33TH100	3.0122 ± 0.0038	0.0936 ± 0.0056	33.5 ± 1.5	0.41316 ± 0.00044	-0.554 ± 0.065	32.9 ± 2.9
NQ33TH135	2.33489 ± 0.00050	-0.03034 ± 0.00069	32.55 ± 0.62	0.179672 ± 0.000078	0.230 ± 0.011	-35.0 ± 1.3
NQ25TH30	4.02044 ± 0.00024	-0.04259 ± 0.00025	33.52 ± 0.24	0.735887 ± 0.000061	0.1853 ± 0.0089	-0.3 ± 1.1
NQ25TH60	3.346 ± 0.013	-0.1059 ± 0.0048	16.2 ± 6.4	0.64155 ± 0.00036	0.40 ± 0.20	12 ± 45
NQ25TH90	2.5618 ± 0.0021	-0.0845 ± 0.0019	27.97 ± 0.92	0.47050 ± 0.00088	0.449 ± 0.081	23.4 ± 7.3
NQ25TH135	1.7785 ± 0.00052	0.02772 ± 0.00070	38.53 ± 0.76	0.157916 ± 0.000096	-0.178 ± 0.012	34.0 ± 2.2
NQ25TH150	1.64828 ± 0.00057	-0.01193 ± 0.00078	135.02 ± 0.19	0.074246 ± 0.000057	-0.0702 ± 0.0078	38.3 ± 3.3
NQ16TH45	2.5836 ± 0.0057	0.065 ± 0.011	-36.9 ± 3.3	0.6870 ± 0.0011	-0.11 ± 0.24	33 ± 16
NQ16TH90						
NQ16TH115	1.36377 ± 0.00094	0.0411 ± 0.0010	40.60 ± 0.90	0.30713 ± 0.00033	-0.208 ± 0.023	30.3 ± 7.1
NQ16TH135						
NQ16TH150	1.06412 ± 0.00037	0.00893 ± 0.00052	-11.3 ± 1.6	0.093108 ± 0.000065	-0.0483 ± 0.0091	-27.8 ± 5.2

TABLE XIII. Fitting coefficients in Eqs. (32) and (34). A prime ($'$) indicates that the variable S was replaced by S_0 in the fitting formula (except in E_{isco} , which always takes \tilde{S}_{\parallel} as its arguments). All coefficients not given here were set to zero identically. Note that the equal-mass terms $e_1, e_2, e_3, \epsilon_1, \epsilon_2$, and ϵ_3 are unaffected by the change from S to S_0 .

k_{2a}	-0.024 ± 0.003	k_{3a}	-0.055 ± 0.003	k_{3d}	-0.019 ± 0.009
k_{4a}	-0.119 ± 0.029	k_{4b}	0.005 ± 0.004	k_{4f}	0.035 ± 0.005
k_{4g}	0.022 ± 0.016	E_B	0.59 ± 0.31	E_E	-0.51 ± 0.20
E_F	0.056 ± 0.004	E_G	-0.073 ± 0.016	e_1	0.0356 ± 0.0025
e_2	0.096 ± 0.012	e_3	0.122 ± 0.067	ϵ_1	0.0043 ± 0.0012
ϵ_2	0.0050 ± 0.0021	ϵ_3	-0.009 ± 0.026		
k'_{2a}	-0.017 ± 0.003	k'_{3a}	-0.091 ± 0.008	k'_{4a}	-0.146 ± 0.022
k'_{4b}	-0.01 ± 0.005	k'_{4f}	0.037 ± 0.007	E'_A	-0.075 ± 0.001
E'_B	-0.29 ± 0.14	E'_D	-0.019 ± 0.006	E'_H	-0.244 ± 0.063
e'_1	0.0356 ± 0.0025	e'_2	0.096 ± 0.012	e'_3	0.122 ± 0.067
ϵ'_1	0.0043 ± 0.0012	ϵ'_2	0.0050 ± 0.0021	ϵ'_3	-0.009 ± 0.026

certain of the new fitting constants. The final fitting parameters are given in Table XIII. In the table, we report on fits using our standard choice of variables $\{\vec{S}, \vec{\Delta}, \delta m\}$ and the alternative choice $\{\vec{S}_0, \vec{\Delta}, \delta m\}$. In both cases, E_{isco} is calculated using \vec{S} , and E_{HU} is calculated using \vec{S}_0 .

The following section corrects an error in the published version of the manuscript. We use a very similar procedure for fitting A_c . Here, we have several choices for how we incorporate previous results. First, we can start with the form of Healy *et al.* [41] for the remnant spin for the

aligned case and add non-aligned corrections. Alternatively, we may start with alternate forms of the aligned spin remnant spin function.

The form of the Healy *et al.* spin is

$$\begin{aligned} \alpha_{\text{align}} = & (4\eta)^2 \left\{ L_0 + L_1 \tilde{S}_{\parallel} + \right. \\ & L_{2a} \tilde{\Delta}_{\parallel} \delta m + L_{2b} \tilde{S}_{\parallel}^2 + L_{2c} \tilde{\Delta}_{\parallel}^2 + L_{2d} \delta m^2 + \\ & L_{3a} \tilde{\Delta}_{\parallel} \tilde{S}_{\parallel} \delta m + L_{3b} \tilde{S}_{\parallel} \tilde{\Delta}_{\parallel}^2 + L_{3c} \tilde{S}_{\parallel}^3 + \\ & L_{3d} \tilde{S}_{\parallel} \delta m^2 + L_{4a} \tilde{\Delta}_{\parallel} \tilde{S}_{\parallel}^2 \delta m + L_{4b} \tilde{\Delta}_{\parallel}^3 \delta m + \\ & L_{4c} \tilde{\Delta}_{\parallel}^4 + L_{4d} \tilde{S}_{\parallel}^4 + L_{4e} \tilde{\Delta}_{\parallel}^2 \tilde{S}_{\parallel}^2 + \\ & L_{4f} \delta m^4 + L_{4g} \tilde{\Delta}_{\parallel} \delta m^3 + \\ & \left. L_{4h} \tilde{\Delta}_{\parallel}^2 \delta m^2 + L_{4i} \tilde{S}_{\parallel}^2 \delta m^2 \right\} + \\ & \tilde{S}_{\parallel} (1 + 8\eta) \delta m^4 + \eta L_{\text{isco}} \delta m^6, \end{aligned} \quad (35)$$

where the values of these coefficients are reproduced in Table XIV, and the last line in Eq. (35) is due to the particle limit and

$$\begin{aligned} L_{\text{isco}} &= \frac{2}{\sqrt{3} r_{\text{isco}}} \left(3\sqrt{r_{\text{isco}}} - 2\tilde{S}_{\parallel} \right), \\ r_{\text{isco}} &= 3 + Z_2 - \text{SIGN}(\tilde{S}_{\parallel}) \sqrt{(3 - Z_1)(3 + Z_1 + 2Z_2)}, \\ Z_1 &= 1 + (1 - \tilde{S}_{\parallel}^2)^{1/3} ((1 + \tilde{S}_{\parallel})^{1/3} + (1 - \tilde{S}_{\parallel})^{1/3}), \\ Z_2 &= \sqrt{3\tilde{S}_{\parallel}^2 + Z_1^2}. \end{aligned}$$

We will also consider replacing \vec{S} with $\vec{S}_0 = \vec{S} + 1/2\delta m \vec{\Delta}$ and using Hemberger *et al.*'s [74] coefficients for some of

the terms in Eq. (35).

The fitting formula for the generic case is

$$\begin{aligned} A_c = A_c^{\parallel} + (4\eta)^2 & \left(|\tilde{S}_{\perp}|^2(a_1 + a_2\tilde{S}_{\parallel} + a_3\tilde{S}_{\parallel}^2) + |\tilde{\Delta}_{\perp}|^2(\zeta_1 + \zeta_2\tilde{S}_{\parallel} + \zeta_3\tilde{S}_{\parallel}^2) + \delta m^2|\tilde{S}_{\perp}|^2(A_A + \tilde{S}_{\parallel}A_B) \right. \\ & + \delta m^2|\tilde{\Delta}_{\perp}|^2(A_D + \tilde{S}_{\parallel}A_E) + A_F\delta m|\tilde{\Delta}_{\perp}||\tilde{S}_{\perp}| + A_G\tilde{\Delta}_{\parallel}^2|\tilde{\Delta}_{\perp}|^2 + A_H\tilde{\Delta}_{\parallel}^2|\tilde{S}_{\perp}|^2 \Big) + \\ & \delta m^6(1 + 12\eta)S_{\perp}^2, \end{aligned} \quad (36)$$

where $A_c^{\parallel} \equiv \alpha_{\text{align}}^2$ and the last line in Eq. (36) is due to the particle limit.

TABLE XIV. Coefficients in Eq. (35) for the A_c fit. These are from Healy *et al.* and reproduced here for reference.

L0	0.686710	L1	0.613247
L2a	-0.145427	L2b	-0.115689
L2c	-0.005254	L2d	0.801838
L3a	-0.073839	L3b	0.004759
L3c	-0.078377	L3d	1.585809
L4a	-0.003050	L4b	-0.002968
L4c	0.004364	L4d	-0.047204
L4e	-0.053099	L4f	0.953458
L4g	-0.067998	L4h	0.001629
L4i	-0.066693		

Here we consider three alternatives denoted by A_c , A'_c , and A_{alt} . The A_c fit is obtained by using the Healy *et al.* parameters as given there (reproduced here in Table XIV) for Eq. (35) and then fitting the remaining coefficients in Eq. (36). For the A'_c fit, we replace \vec{S} by \vec{S}_0 for all terms in both Eq. (35) and Eq. (36), except for terms associated with the particle limit (last line in Eq. (35) and Eq. (36)). To do this, we need to refit the Healy *et al.* data to the new form of Eq. (35). In addition, we also used the Hemberger *et al.* choices for some of the parameters (see Table XV). A_{alt} is like A'_c except we do not replace S by S_0 (but do refit the Healy *et al.* data). The fitting coefficients are given in Tables XV and XVI. Relative RMS errors are 0.020, 0.024, 0.005. Absolute RMS errors are 0.0029, 0.0027, 0.0009.

Overall the fits for the radiated energy $\delta\mathcal{M}$ are accurate to within 3% (that is a 3% error in the radiated mass, not a 3% error in the remnant mass) and the fits for the square of remnant spin are accurate to within 10%. There is no clear advantage here for using \vec{S}_0 or \vec{S} as the expansion variable.

V. STATISTICAL ANALYSIS

Now that we have empirical formulas for the recoil velocity of the remnant BH that are shown to be accurate at least for moderate spins and mass ratios, we can begin to model the distributions of astrophysical recoils. Our formulas are based on the spin-magnitudes and di-

TABLE XV. Coefficients in Eq. (35). Left values are for A'_c and right for A_{alt} . The coefficients below the line are common to both and are derived from Hemberger *et al.*. All unspecified coefficients are zero.

$L2a$	-0.517 ± 0.01	$L2a$	-0.148 ± 0.007
$L2d$	0.81 ± 0.017	$L2c$	-0.003 ± 0.001
$L3d$	1.587 ± 0.061	$L2d$	0.814 ± 0.008
$L4f$	0.692 ± 0.054	$L3a$	-0.099 ± 0.043
$L4g$	1.003 ± 0.081	$L3d$	1.615 ± 0.01
		$L4b$	-0.013 ± 0.011
		$L4e$	-0.077 ± 0.058
		$L4f$	0.832 ± 0.05
		$L4i$	-0.093 ± 0.067
$L0$	0.686403		
$L1$	0.613203		
$L2b$	-0.107373		
$L3c$	-0.0784152		
$L4d$	-0.079896		

TABLE XVI. Coefficients in Eq. (36) for A_c (top), A'_c (middle), A_{at} (bottom). Coefficients common to all are listed below the double line.

A_A	3.008 ± 0.862	A_B	-7.334 ± 4.39
A_D	-2.011 ± 0.552	A_E	5.1 ± 2.816
A_G	-2.804 ± 0.864	A_H	5.143 ± 1.539
A_A	2.189 ± 0.025	A_D	0.547 ± 0.099
A_A	3.402 ± 0.859	A_B	-4.571 ± 4.373
A_D	-2.216 ± 0.55	A_E	3.713 ± 2.805
A_G	-3.099 ± 0.86	A_H	5.999 ± 1.534
a_1	0.8401 ± 0.0061	a_2	-0.328 ± 0.029
a_3	-0.61 ± 0.16	ζ_1	-0.0209 ± 0.0070
ζ_2	-0.038 ± 0.012	ζ_3	0.04 ± 0.16

rection measured during the final plunge. We will thus be using several assumptions to tie the statistical distributions of spins for distant binaries to the statistical distributions of spins near merger. Our primary assumption will be that the distribution of inclination angles at merger is the same as the distribution of inclination angles for distant binaries (note, this is an assumption

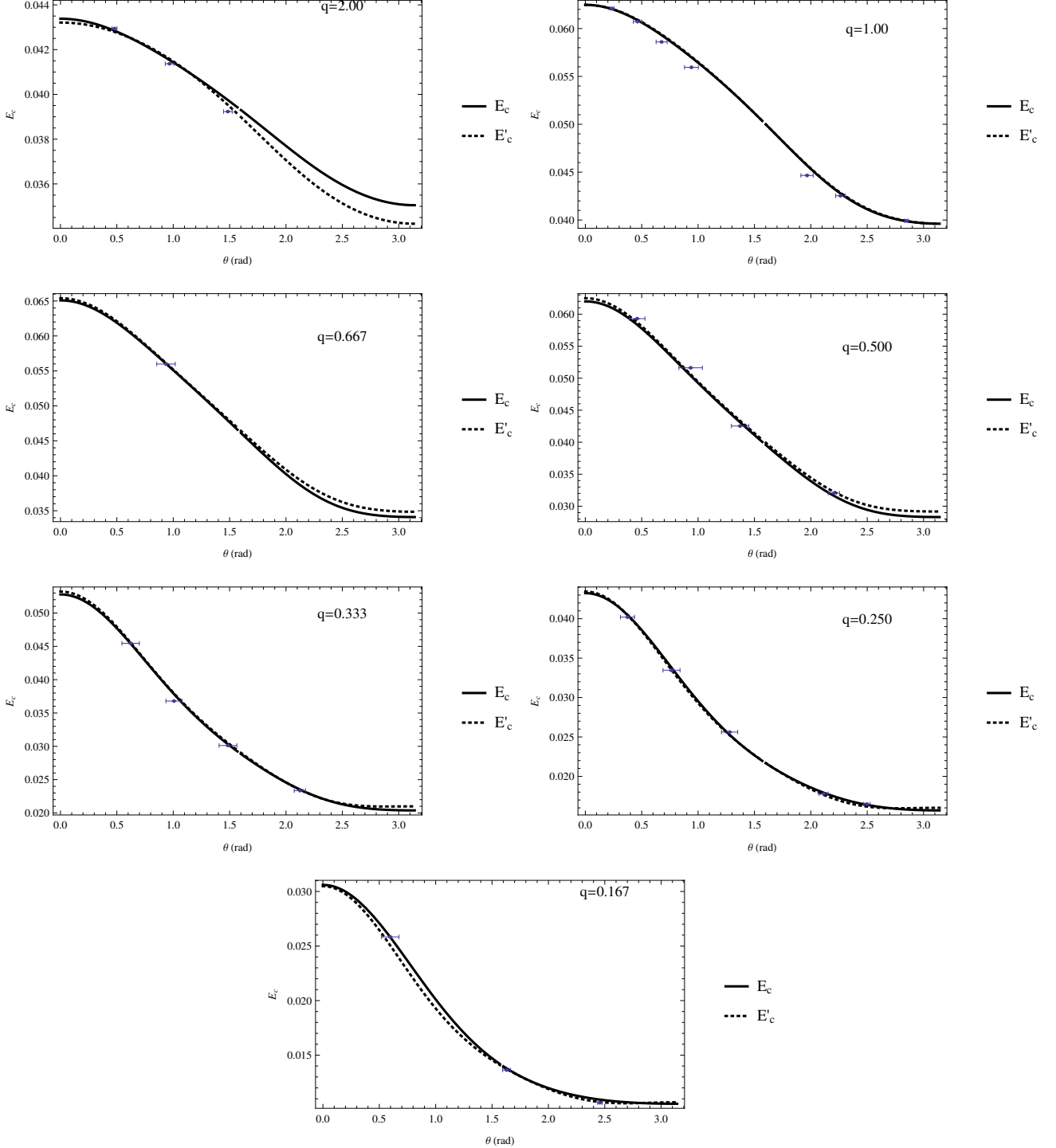


FIG. 8. Plots of the fitted E_c versus inclination angle θ and q for the NQ configurations. Each data point represents the value of E_c for a family of azimuthal configurations with the same inclination angle and mass ratio. Note $\delta M \approx E_c$, and that a prime denotes that \vec{S}_0 was used in the fits, rather than \vec{S} .

on distributions, we are not assuming that a given binary's spin-inclination angle will not change). We expect that for distant binaries the azimuthal orientations of the spins are uniformly distributed. However, post-

Newtonian spin resonances can align or antialign the two spins in the binary azimuthally [75–77]. To account for this, we will consider three azimuthal distributions, spins aligned azimuthally, spins antialigned azimuthally, and

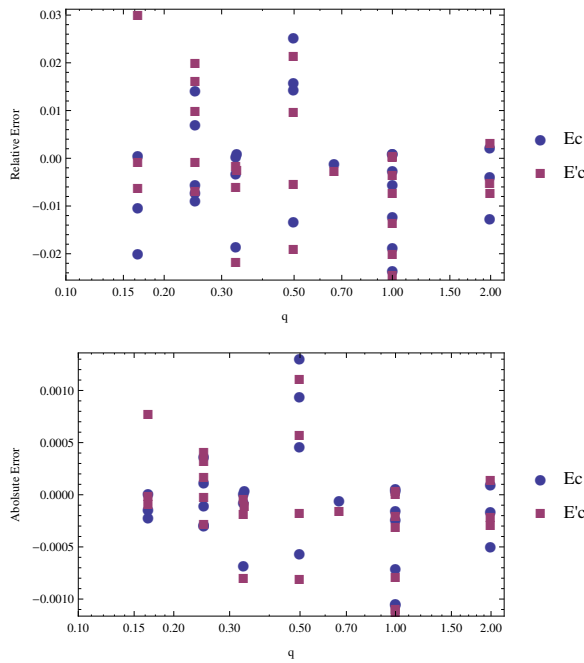


FIG. 9. The relative errors (residuals) in the fit of E_c as a function of the binary’s parameters. Note that there are multiple data points for each q , and that a prime denotes that \tilde{S}_0 was used in the fits, rather than \tilde{S} .

random azimuthal alignments.

To this end, we consider binaries with spin magnitudes α_1 and α_2 given by the hot and cold accretion models

(i.e., wet accretion) described in Ref. [31], and the “dry” merger model described in Ref. [78]. The distributions are given by $P(\alpha) \propto (1-\alpha)^{(b-1)}\alpha^{(a-1)}$, where $a = 3.212$, $b = 1.563$; $a = 5.935$, $b = 1.856$; and $a = 10.5868$, $b = 4.66884$, for hot, cold, and dry mergers, respectively.

For the directions of the spins \hat{S}_1 and \hat{S}_2 , we use the distributions $P(\theta) \propto (1-\theta)^{(b-1)}\theta^{(a-1)}$, there θ is measured in radians and $a = 2.018$, $b = 5.244$ and $a = 2.544$, $b = 19.527$ for hot and cold accretion, respectively. For dry mergers, we choose a distribution uniform in $\cos \theta$. Note that the distributions for θ assume $0 \leq \theta \leq 1$. The probabilities for $\theta > 1$ are taken to be identically zero.

In addition, we use a mass ratio distribution motivated by cosmological simulations $P(q) \propto q^{-0.3}(1-q)$, as given in Ref. [79–81]. Note that our formulas are constructed so that the same recoil / remnant properties are given when the labels of the two BHs are interchanged ($1 \leftrightarrow 2$). Hence we need to only consider $0 \leq q \leq 1$.

We performed the statistical analysis itself by analyzing the recoil, radiated mass, and remnant spin from 10^9 randomly chosen configurations consistent with the above distributions for the parameters of the binary. Note that we did not make any assumptions about correlations between these parameters (with the exception of the above mentioned azimuthal distributions).

The total radiated energy and final remnant spin for a generic BHB is given by Eqs. (32)–(36) directly. The total recoil, however, is given by $V_{\text{rec}}^2 = V_{\parallel}^2 + V_{\perp}^2$, where V_{\parallel} is given by one of (for the sake of brevity, we only give the explicit formulas for $V_{4'59}$ and $V_{p'59}$)

$$V_{\parallel 4'59} = (4\eta^2) \left[\vec{\Delta} \cdot \hat{n}_0 (3678. - 2475\delta m^2 + 4962.\tilde{S}_{0\parallel} + 7170.\tilde{S}_{0\parallel}^2 + 12050.\tilde{S}_{0\parallel}^3) \right. \\ \left. + \tilde{S}_0 \cdot \hat{m}_{59} \left(\tilde{\Delta}_{\parallel} \left[4315. - 1262\delta m^2 + 15970\tilde{S}_{0\parallel} \right] - 2256\delta m - 2231\delta m\tilde{S}_{0\parallel} \right) \right], \quad (37)$$

$$V_{\parallel p'59} = (4\eta^2) \left[\vec{\Delta} \cdot \hat{n}_0 \left(\frac{3685(1 - 0.6766\delta m^2 + 0.1410\tilde{S}_{0\parallel})}{1 - 1.248\tilde{S}_{0\parallel}} - 2537\tilde{\Delta}_{\parallel}\delta m \right) \right. \\ \left. + \tilde{S}_0 \cdot \hat{m}_{59} \left(\Delta_{\parallel} \left[4180 + 1660\tilde{S}_{0\parallel} \right] - 2565\delta m \right) \right], \quad (38)$$

and V_{\perp}^2 is given by

$$V_{\perp}^2 = (4\eta)^4 \left(2.106 \times 10^5 \tilde{\Delta}_{\parallel}^2 + 4.967 \times 10^5 \tilde{\Delta}_{\parallel} \delta m - 2.116 \times 10^5 \tilde{\Delta}_{\parallel}^3 \delta m - 5.037 \times 10^5 \tilde{\Delta}_{\parallel}^2 \delta m^2 \right. \\ \left. - 1.269 \times 10^5 \tilde{\Delta}_{\parallel} \delta m^3 - 3.384 \times 10^5 \tilde{\Delta}_{\parallel}^2 \tilde{S}_{0\parallel} - 6.440 \times 10^5 \delta m^2 \tilde{S}_{0\parallel} + 2.138 \times 10^6 \tilde{\Delta}_{\parallel}^2 \tilde{S}_{0\parallel}^2 \right. \\ \left. - 4.905 \times 10^6 \tilde{\Delta}_{\parallel} \delta m \tilde{S}_{0\parallel}^2 - 1.100 \times 10^6 \delta m^2 \tilde{S}_{0\parallel}^2 - 1.024 \times 10^7 \tilde{\Delta}_{\parallel}^2 \tilde{S}_{0\parallel}^3 \right) + \left[1.2 \times 10^4 \eta^2 \delta m (1 - 0.93\eta) \right]^2. \quad (39)$$

In Eqs.(37) and (38) there are two unspecified unit vectors \hat{n}_0 and \hat{m}_{59} . As explained in Sec. IV A, \hat{n}_0 is a

unit vector in the final orbital plane and \hat{m}_{59} is another unit vector in this plane rotated by -59° with respect

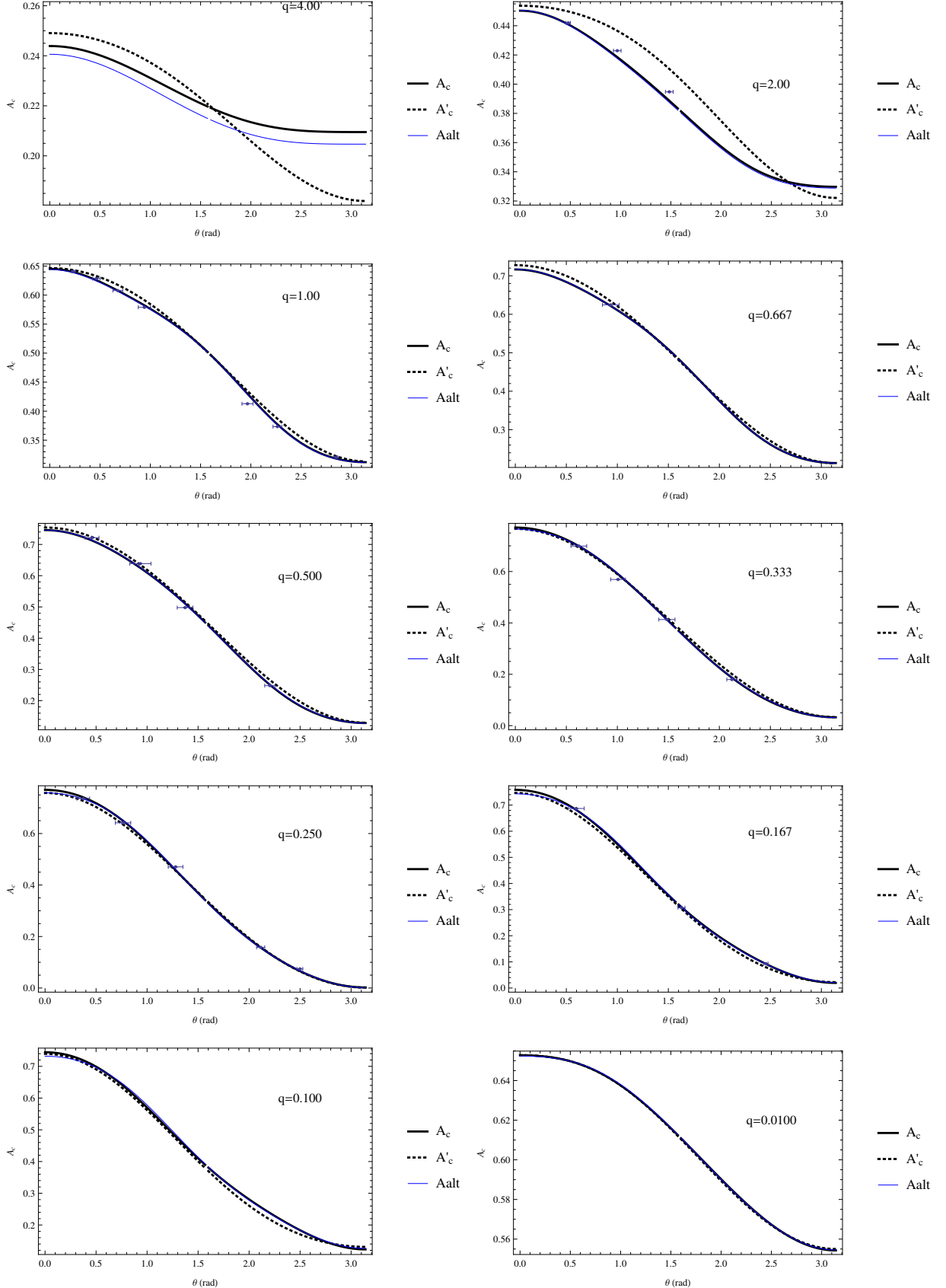


FIG. 10. Plots of the fitted A_c versus inclination angle θ and q for the NQ configurations. Each data point represents the value of A_c for a family of azimuthal configurations with the same inclination angle and mass ratio. Note that $\alpha \approx \sqrt{A_c}$ and that a prime denotes that \vec{S}_0 was used in the fits, rather than \vec{S} .

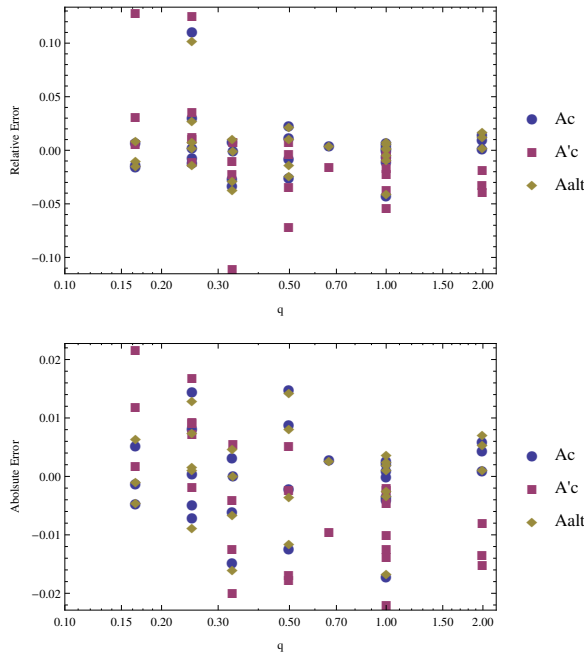


FIG. 11. The relative errors (residuals) in the fit of A_c as a function of the binary's parameters. Note that there are multiple data points for each q and a prime denotes that \vec{S}_0 was used in the fits, rather than \vec{S} .

to \hat{n}_0 . The direction of \hat{n}_0 is unknown (we only know that it must lie in the final orbital plane). From a practical point of view, this means that if we choose azimuthal distributions that are uniform with respect to some external reference frame, then the choice of \hat{n}_0 will not affect the resulting distributions of recoils. In practice we take $\hat{n}_0 = (1, 0, 0)$ and $\hat{m}_{59} = (\cos 59^\circ, -\sin 59^\circ, 0)$. Finally, Eq. (39) was obtained by fitting the square of the recoil for the nonprecessing runs in [41]. This formula has the advantage that there is no explicit dependence on the angle ξ , but does have the drawback that it can predict negative values for V_\perp^2 . This can only happen when V_\perp^2 is small and we therefore take $V_\perp^2 = 0$ in these cases.

Figure 12 shows the resulting probabilities for a given recoil v or larger (i.e., an integrated probability). Perhaps not too surprisingly, the *dry* distribution with antialigned spins (azimuthally) give the largest probabilities for high recoils. We summarize the probabilities for very high recoils in Table XVII. Assuming the most pessimistic distribution (cold accretion, azimuthal alignment), there is a 2×10^{-7} chance of a supermassive BH recoiling at 2000 km s^{-1} . For dry mergers with azimuthal alignment, on the other hand, the probability would be 142 times larger (for dry mergers with random alignment the probability would be 47 000 times larger).

In Figs. 15, we compare the new predicted distributions with the *hangup kick* and *cross kick* predictions. Note that if we assume random azimuthal alignment, the predictions of $V_{4'59}$ match very closely to the *hangup kick* predictions. Interestingly, while the *cross kick* and

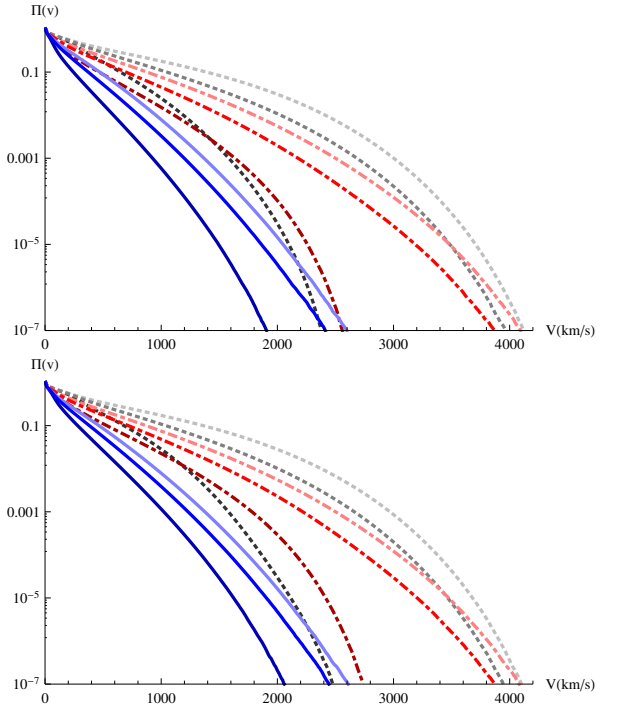


FIG. 12. The integrated probability $\Pi(v)$ for the remnant to recoil at speed v or higher (in km s^{-1}). The blue (solid) curves are for cold accretion models, the red (dot-dashed) curves are for hot accretion models, and gray (dotted) curves are for dry mergers. Within a given color/line style (blue, red, gray), the dark shade indicates that the spins were aligned azimuthally, the light shade indicates that the spins were antialigned azimuthally, and the intermediate shade indicates random azimuthal alignment. The top plot shows the probabilities when modeling the recoil with V_{459} and the lower panel shows the probabilities when modeling the recoil with $V_{4'59}$.

hangup kick predictions were based on simple ansätze for how the equal-mass contributions to the recoil generalize, the predictions are not too different (within a factor of 2) from the results obtained by our new fitting to unequal-mass configurations. This gives some assurance that further modifications to the empirical formula for the recoil will give incremental improvements in accuracy.

In Figs. 13 and 14, we show the probability distributions for a binary losing $\delta\mathcal{M}$ of its total mass to gravitational radiation [i.e., $P(\delta\mathcal{M})$] and the probability that the remnant will have a spin α [i.e., $P(\alpha)$]. Unlike in the previous figures, here we show the raw probabilities rather than the integrated ones. The probability distribution $P(\delta\mathcal{M})$ has three distinct regions: a large peak centered at $\delta\mathcal{M} = 0$, which is produced by the small mass ratio binaries, a plateau where the distribution is almost constant, and decaying tail at *high* energies. The plateau ends at $\delta\mathcal{M} \approx 4\%$ for dry mergers, $\delta\mathcal{M} \approx 7\%$ for hot accretion, and $\delta\mathcal{M} \approx 8\%$ for cold accretion. The plateau extends to the highest energies for the cold accretion model, indicating that such binaries will, on average, be the loudest gravitational wave sources.

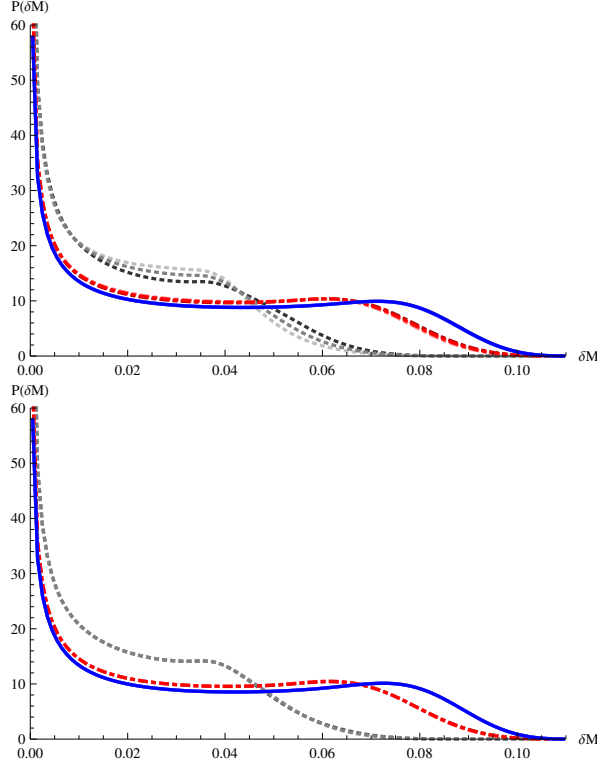


FIG. 13. The probability (nonintegrated) for a mass loss of $\delta\mathcal{M}$. The blue (solid) curves are for cold accretion models, the red (dot-dashed) curves are for hot accretion models, and gray (dotted) curves are for dry mergers. Within a given color/line style (blue, red, gray), the dark shade indicates that the spins were aligned azimuthally, the light shade indicates that the spins were antialigned azimuthally, and the intermediate shade indicates random azimuthal alignment. The upper panel displays probabilities when the radiated energy is modeled in terms of the spin variable \tilde{S} and the lower panel when the variable is chosen to be \tilde{S}_0 .

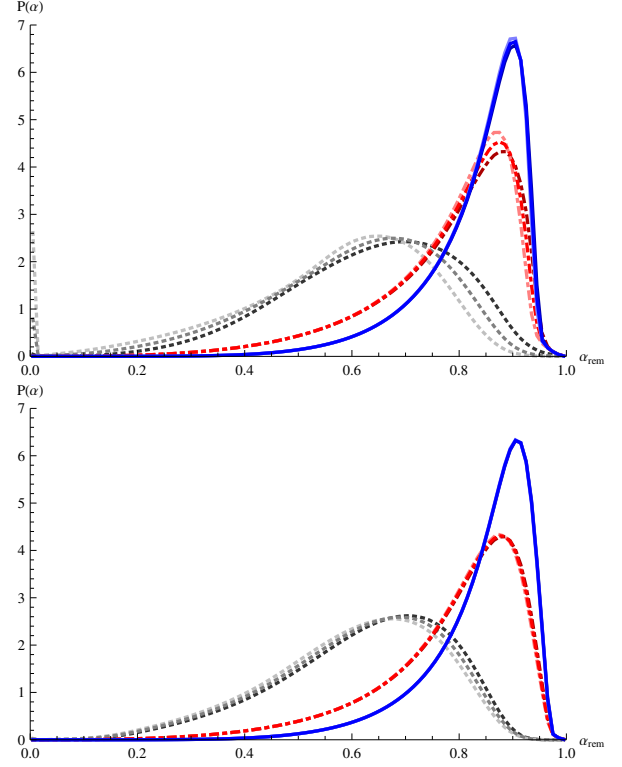


FIG. 14. The probability (nonintegrated) for a remnant spin α . The blue (solid) curves are for cold accretion models, the red (dot-dashed) curves are for hot accretion models, and gray (dotted) curves are for dry mergers. Within a given color/line style (blue, red, gray), the dark shade indicates that the spins were aligned azimuthally, the light shade indicates that the spins were antialigned azimuthally, and the intermediate shade indicates random azimuthal alignment. The upper panel displays probabilities when the final remnant spin magnitude is modeled in terms of the total spin variable \tilde{S} and the lower panel when the variable is chosen to be \tilde{S}_0 .

TABLE XVII. The probability in units of percent of a recoil v or larger assuming the Hot, Cold, and Dry merger models and assuming the spins are antialigned (AA) azimuthally, aligned (A) azimuthally, or randomly distributed (R) azimuthally. In all cases the recoil was calculated using $V_{4'59}$ for the number outside the parenthesis and using $V_{p'59}$ for the number inside the parenthesis.

Model	$\Pi(1000 \text{ km s}^{-1})$	$\Pi(2000 \text{ km s}^{-1})$	$\Pi(3000 \text{ km s}^{-1})$
Hot A	2.292 (2.280)	0.30 (0.029)	0(0)
Hot R	4.884 (4.721)	0.233 (0.229)	0.003 (0.003)
Hot AA	7.568 (7.220)	0.563 (0.550)	0.012 (0.014)
Cold A	0.120 (0.126)	$2 \cdot 10^{-5}$ ($3 \cdot 10^{-5}$)	0(0)
Cold R	0.398 (0.418)	$5 \cdot 10^{-4}$ ($7 \cdot 10^{-4}$)	$0(2 \cdot 10^{-7})$
Cold AA	0.814 (0.846)	0.002 (0.003)	$1 \cdot 10^{-7}$ ($6 \cdot 10^{-7}$)
Dry A	2.900 (3.216)	0.003 (0.003)	0(0)
Dry R	10.932 (11.006)	1.033 (1.009)	0.020 (0.019)
Dry AA	17.404 (17.327)	2.849 (2.759)	0.088 (0.082)

This long plateau in the radiated energy distribution is related to the probability that merger remnant will have high spin, which in turn is related to the probability that the binary will have a large net spin in the direction of the orbital angular momentum. As shown in Fig. 14, the probability distribution for the remnant spin magnitude for dry mergers is very broad and peaks at $\alpha \approx 0.7$, with very low probabilities for high spins. The hot and cold accretion models lead to much narrower peaks centered at higher spins (near $\alpha \approx 0.9$ for cold accretion). Both these models have the spins of the two BHs strongly aligned with the orbital angular momentum. This leads to both large radiated energies and large remnant spins [31].

The fact that black holes merging in an accretion dominated environment have a non-negligible probability of radiating up to 8–9% of their total mass make them more *visible* for gravitational wave detectors than binary black holes merging in a relatively dry scenario. In particular, according to Fig. 13 wet mergers produce nearly double the radiation of dry mergers (and hence roughly 1.4 times

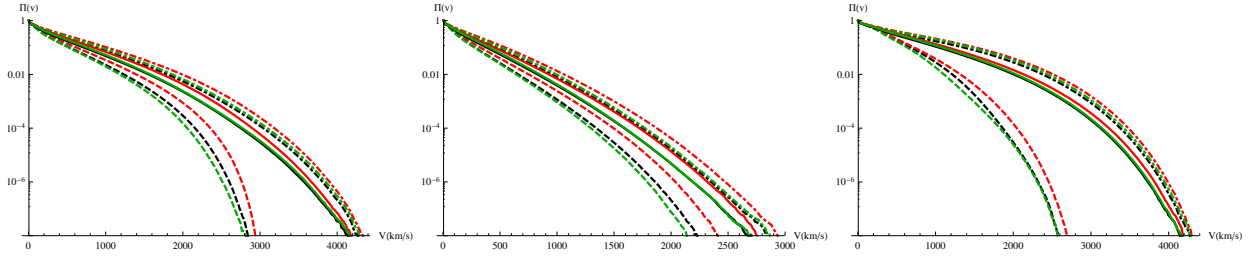


FIG. 15. The integrated probability $\Pi(v)$ for the remnant to recoil at speed v or higher (in km s^{-1}) as predicted using $V_{p'59}$ (black curves), the older *cross kick* formula (red curves), and the original *hangup kick* formula (green curves). The plot on the left shows the results for hot accretion, the plot in the center shows the results for cold accretion, and the plot on the right shows the results for dry mergers. In each plot, solid curves are for random azimuthal alignment, dashed curves are for azimuthal alignment, and dot-dashed curves are for antiazimuthal alignment.

the gravitational wave strain), which means that merging BHs from accretion dominated systems are detectable in a volume 2.8 times larger than for dry mergers [82–85].

VI. DISCUSSION

In this paper we revisited the question of generating empirical formulas describing the remnant mass, spin, and recoil from the mergers of black-hole binaries. We extended the formulas of Refs. [30, 51] to include explicit mass difference dependence.

Our final formula for the recoil along the orbital angular momentum at merger is given by Eqs. (19)–(23) with fitting coefficients provided in Table X. While we provide several alternatives of fitting to study the robustness of the empirical formula, our results favor formulas $V_{4'59}$ and $V_{p'59}$.

While Fig. 5 provides an overview of the quality of the fittings for the recoil velocities from our simulations in the range of $1/6 \leq q \leq 2$, Fig. 6 gives a more quantitative measure of the absolute and relative errors of the fits. We observe that all but one point lies within a relative error of 12% (which translates to an absolute error bound of within 60 km s^{-1}). These errors should be acceptable for most astrophysical applications, and in particular to estimate the probability of observing recoiling black holes near active galactic nuclei with peculiar features such as displaced narrow and wide spectral lines, displaced luminosity centers, etc. (see [86, 87] for a review). An important factor to consider is also the lifetime of accretion disks carried by recoiling black holes [88, 89], as they can only be observed for a few million years and at distances from the center of the colliding galaxies that depend strongly on the angle of the recoil with respect to the final orbital plane. Importantly, large recoil velocities are strongly beamed along the orbital angular momentum (see Figs. 11–14 of Ref. [31] and Fig. 7 here).

We also provide fitting formulas adapted to include the unequal mass parameter δm for the total radiated gravitational energy of the binary. The leading terms of the radiated energy are given by expression (34), with fitting

coefficients given in Table XIII. Figure 8 shows the actual fitting curves for the alternative variables based on \vec{S} or \vec{S}_0 , which provides a measure of the errors in truncating the fitting formula. Figure 9 shows the residuals of such fits (the error is within 3% of the total radiated energy).

The final spin magnitude of the remnant black hole can also be fitted with our new approach. The leading term of the final spin (actually α^2) is given by expression (36), with fitting coefficients given in Tables XIV–XVI. Figure 10 shows the actual fitting of the curves for the alternative variables based on \vec{S} or \vec{S}_0 , which provides a measure of the errors in truncating the fitting formula. Figure 11 shows the residuals of such fittings. The relative errors (except for one point) are within 10% for the square of the spin. Regarding the final spin direction, as reported in the last two columns of Table XX, we observe that the net deviation of the total angular momentum with respect to its initial orientation is always small (within a few degrees) for comparable mass ratios (within 1:2). This deviation increases, reaching up to 20 degrees, with smaller mass ratios and spins pointing in the opposite direction to the orbital angular momentum, in agreement with the studies in Refs. [51, 72].

We note that our modeling is based on configurations with one BH spinning and the other nonspinning extrapolated to both BHs spinning. In the small-mass-ratio regime, where the spin of the lighter component will have a relatively small effect, this extrapolation should be accurate. However, when the spins of both BHs are dynamically important, we can foresee two main sources of error. First \vec{S} and $\vec{\Delta}$ will not be aligned, which means that our formulas should depend on the azimuthal orientations of \vec{S}_\perp and $\vec{\Delta}_\perp$ independently. Second, the magnitude of \vec{S} and $\vec{\Delta}$ can be effectively double the magnitudes achievable with the NQ configurations (but only in the similar mass regime). We partially addressed the first source of error when we refit the K configurations. Our new model is based on the terms $\Delta_\perp = \vec{\Delta} \cdot \hat{n}_0$ and $S_\perp = \vec{S} \cdot \hat{m}_0$ where \hat{n}_0 and \hat{m}_0 are rotated with respect to each other by 59° , which we found to be the correct azimuthal dependence of the recoil for K configurations. And while this modification allowed for an accurate mod-

eling of the K configurations, it had a negligible effect on the statistical distribution of recoils. We thus have good evidence that this first source of error is acceptable for statistical studies. The second source of error is potentially more problematic because we use terms up to fourth-order in the spin (and hence errors can increase by a factor of 16). Fortunately, these terms tend to be largest for the equal-mass configurations that we previously studied and used to construct our empirical formulas.

Padé approximants give an alternative to the Taylor-like expansions to fit the remnant recoil. We first used a Padé approximation when modeling the “hangup-recoil” configurations of Ref. [29, 31]. There our goal was to resum the S_{\parallel} dependence (which proved to be a very slowly converging series). Here, in the unequal mass context, we use the more appropriate variable $\tilde{S}_0 \cdot \hat{L}$. This variable has the advantage of being “essentially” conserved [71] during evolution thus allowing us to relate the parameters of the binary at large separations with the parameters around merger. The Padé expansion has also been used in Ref. [74] to better fit the energy radiated (or final mass) of equal-mass, (anti)aligned spins of merging binaries.

One clear avenue for improvement of our modeling concerns the fact that we base our formulas on the spin orientations near merger, rather than at large separations. Such a program would implicitly entail modeling the precession of the spins and orbital plane from the distant PN regime down to merger. The use of $S_{0\parallel}$ in our modeling is a step in this direction and the work of Ref [90] to find other constants of the motion and of Ref [91] to model the precession may prove to be useful.

One can foresee a further decomposition of the modeling of the recoil into three distinct characteristic regimes: the inspiral (where most of the recoil is represented by an almost self-canceling wobbling of the center of mass with the orbital period), the merger, where most of the anisotropic radiation of linear momentum takes place, and the ringdown of the final, highly distorted, black holes which gives rise to the antikick phenomenon [34].

While we have included in the modeling the particle limit through the ISCO energy and angular momentum and the η^2 leading dependence of the recoil, a set of simulations in the region around mass ratios $q = 1/10$ would be beneficial to improve the accuracy of the interpolation fits. Another area of improvement would be to use near maximally spinning black holes, i.e. intrinsic spins above $\alpha = 0.99$. This is particularly interesting for the modeling of the recoil since it has been pointed out in [52, 53] that resonance effects in the for small-mass ratio

spirals around a highly-spinning primary can lead to mass ratio dependences in the recoil that scale as $\sim \eta^{1.5}$ rather than η^2 .

Finally, we note that as seen in Fig. 15, our new formula for the recoil is consistent (within a factor of 2) with our older formulas, which were based on ansätze on how the equal-mass contributions to the recoil generalize. This gives some assurance that further modifications to the empirical formula for the recoil will give incremental improvements in accuracy.

In conclusion, we provided a set of formulas that describe the final state of the mergers of black hole binaries within reasonable errors for astrophysical applications and tested in the comparable mass ratio regime of $1/6 \leq q \leq 6$ and spins $S_i/M_i^2 \leq 0.8$ with reasonable extrapolation properties.

ACKNOWLEDGMENTS

We thank the referee for their careful review and for the many helpful suggestions on how we could improve the paper. The authors gratefully acknowledge the NSF for financial support from Grants PHY-1305730, PHY-1212426, PHY-1229173, AST-1028087, PHY-0969855, OCI-0832606, and DRL-1136221. Computational resources were provided by XSEDE allocation TG-PHY060027N, and by NewHorizons and BlueSky Clusters at Rochester Institute of Technology, which were supported by NSF grant No. PHY-0722703, DMS-0820923, AST-1028087, and PHY-1229173.

Appendix A: Data from the full numerical evolution

In this appendix we provide detailed data for the 126 new BHB configurations studied here. Our configurations have one BH spinning (generally the larger one, except for the $q = 2$ configurations) and the other non-spinning. The initial data parameters are given in Table XVIII. The radiated angular momentum, mass, and recoil (all in the original frame) are given in Table XIX. In Table XX we compare the radiated mass and angular momentum as measured by the isolated horizons formalism to the radiated mass and angular momentum as measured directly from ψ_4 . The difference between the two measures provides an error estimate for the ψ_4 -based measure of these quantities. The missing entries in these tables are due to missing horizon data for certain configurations. Finally, in Table XXI, we give the BH spins and remnant recoil in the rotated frame of the final plunge.

TABLE XVIII: Initial data parameters. In all cases the puncture masses were chosen such that the total ADM mass of the binary was $1.0 \pm 10^{-6}M$. Here the punctures are located at $(x_{1,2}, 0, 0)$ with momenta $\pm(0, p, 0)$ and spins $\vec{S}_2 = (S_x, S_y, S_z)$ [note that $\vec{S}_1 = 0$ for all configurations]. For the NQ200 configurations $\vec{P}_1 = -(0, p, 0)$, for all other configurations $\vec{P}_1 = (0, p, 0)$. In all cases, $\vec{P}_2 = -\vec{P}_1$. The approximate initial eccentricities e_i , eccentricities measured over the last orbit e_f , and the number of orbits N , are also given.

CONF	m_{p1}/M	m_{p2}/M	x_1/M	x_2/M	p/M	S_x/M^2	S_y/M^2	S_z/M^2	M_{H1}	M_{H2}	$N^{e_i}_{e_f}$
NQ200TH30PH0	0.657661	0.202748	-2.771460	5.527396	0.097847	0.000000	0.045426	0.078681	0.672522	0.338027	$5^{0.02}_{0.005}$
	PH30	0.657672	0.202779	-2.771460	5.527396	0.097847	-0.022713	0.039340	0.078681	0.672533	0.338026
	PH60	0.657694	0.202838	-2.771460	5.527396	0.097847	-0.039340	0.022713	0.078681	0.672554	0.338021
	PH90	0.657706	0.202865	-2.771460	5.527396	0.097847	-0.045426	0.000000	0.078681	0.672564	0.338016
	PH120	0.657695	0.202837	-2.771460	5.527396	0.097847	-0.039340	-0.022713	0.078681	0.672552	0.338018
	PH150	0.657672	0.202780	-2.771460	5.527396	0.097847	-0.022713	-0.039340	0.078681	0.672531	0.338024
NQ200TH60PH0	0.657769	0.202707	-2.891856	5.572900	0.096793	0.000000	0.078662	0.045416	0.672365	0.338011	$4^{0.02}_{0.005}$
	PH30	0.657803	0.202792	-2.891856	5.572900	0.096793	-0.039331	0.068123	0.045416	0.672400	0.338009
	PH60	0.657869	0.202965	-2.891856	5.572900	0.096793	-0.068123	0.039331	0.045416	0.672461	0.337993
	PH90	0.657905	0.203045	-2.891856	5.572900	0.096793	-0.078662	0.000000	0.045416	0.672491	0.337976
	PH120	0.657871	0.202961	-2.891856	5.572900	0.096793	-0.068123	-0.039331	0.045416	0.672456	0.337987
	PH150	0.657803	0.202793	-2.891856	5.572900	0.096793	-0.039331	-0.068123	0.045416	0.672393	0.337999
NQ200TH90PH0	0.659633	0.204521	-3.585439	7.192939	0.082538	0.000000	0.090460	0.000000	0.671069	0.337321	$7.5^{0.02}_{0.003}$
	PH30	0.659666	0.204614	-3.585439	7.192939	0.082538	-0.045230	0.078341	0.000000	0.671103	0.337320
	PH60	0.659730	0.204803	-3.585439	7.192939	0.082538	-0.078341	0.045230	0.000000	0.671162	0.337307
	PH90	0.659766	0.204889	-3.585439	7.192939	0.082538	-0.090460	0.000000	0.000000	0.671192	0.337291
	PH120	0.659731	0.204801	-3.585439	7.192939	0.082538	-0.078341	-0.045230	0.000000	0.671158	0.337299
	PH150	0.659665	0.204615	-3.585439	7.192939	0.082538	-0.045230	-0.078341	0.000000	0.671096	0.337310
NQ200TH135PH0	0.659637	0.203763	-3.597259	7.249463	0.083015	0.000000	0.063950	-0.064273	0.671041	0.337289	$6.5^{0.02}_{0.005}$
	PH30	0.659653	0.203811	-3.597259	7.249463	0.083015	-0.031975	0.055382	-0.064273	0.671058	0.337288
	PH60	0.659688	0.203903	-3.597259	7.249463	0.083015	-0.055382	0.031975	-0.064273	0.671090	0.337281
	PH90	0.659706	0.203945	-3.597259	7.249463	0.083015	-0.063950	0.000000	-0.064273	0.671104	0.337274
	PH120	0.659687	0.203905	-3.597259	7.249463	0.083015	-0.055382	-0.031975	-0.064273	0.671085	0.337279
	PH150	0.659653	0.203812	-3.597259	7.249463	0.083015	-0.031975	-0.055382	-0.064273	0.671054	0.337286
NQ66TH60PH0	0.386665	0.370633	5.121102	-3.323698	0.103661	0.000000	0.255407	0.147459	0.403229	0.607961	$4.5^{0.02}_{0.003}$
	PH30	0.386678	0.370705	5.121102	-3.323698	0.103661	-0.127703	0.221189	0.147459	0.403241	0.607968
	PH60	0.386702	0.370854	5.121102	-3.323698	0.103661	-0.221189	0.127703	0.147459	0.403262	0.607967
	PH90	0.386714	0.370929	5.121102	-3.323698	0.103661	-0.255407	0.000000	0.147459	0.403272	0.607959
	PH120	0.386702	0.370854	5.121102	-3.323698	0.103661	-0.221189	-0.127703	0.147459	0.403261	0.607952
	PH150	0.386678	0.370705	5.121102	-3.323698	0.103661	-0.127703	-0.221189	0.147459	0.403240	0.607953
NQ50TH30PH0	0.320153	0.413088	5.635539	-2.699285	0.094907	0.000000	0.181834	0.314946	0.335733	0.674862	$5.5^{0.02}_{0.004}$
	PH30	0.320156	0.413103	5.635539	-2.699285	0.094907	-0.090917	0.157473	0.314946	0.335735	0.674864
	PH60	0.320161	0.413137	5.635539	-2.699285	0.094907	-0.157473	0.090917	0.314946	0.335739	0.674863
	PH90	0.320164	0.413152	5.635539	-2.699285	0.094907	-0.181834	0.000000	0.314946	0.335741	0.674858
	PH120	0.320161	0.413137	5.635539	-2.699285	0.094907	-0.157473	-0.090917	0.314946	0.335739	0.674857
	PH150	0.320156	0.413103	5.635539	-2.699285	0.094907	-0.090917	-0.157473	0.314946	0.335735	0.674859
NQ50TH60PH0	0.320095	0.412854	5.661860	-2.756275	0.095914	0.000000	0.314772	0.181734	0.335621	0.674669	$5.5^{0.02}_{0.004}$
	PH30	0.320102	0.412905	5.661860	-2.756275	0.095914	-0.157386	0.272600	0.181734	0.335626	0.674674
	PH60	0.320117	0.413015	5.661860	-2.756275	0.095914	-0.272600	0.157386	0.181734	0.335637	0.674670
	PH90	0.320125	0.413067	5.661860	-2.756275	0.095914	-0.314772	0.000000	0.181734	0.335643	0.674660
	PH120	0.320117	0.413016	5.661860	-2.756275	0.095914	-0.272600	-0.157386	0.181734	0.335636	0.674655
	PH150	0.320102	0.412906	5.661860	-2.756275	0.095914	-0.157386	-0.272600	0.181734	0.335626	0.674658
NQ50TH90PH0	0.321251	0.413415	6.294671	-3.135128	0.090701	0.000000	0.362558	0.000000	0.335224	0.673868	$5.5^{0.02}_{0.005}$
	PH30	0.321259	0.413489	6.294671	-3.135128	0.090701	-0.181279	0.313984	0.000000	0.335231	0.673875
	PH60	0.321278	0.413635	6.294671	-3.135128	0.090701	-0.313984	0.181279	0.000000	0.335245	0.673875
	PH90	0.321287	0.413706	6.294671	-3.135128	0.090701	-0.362558	0.000000	0.000000	0.335253	0.673865

Continued on next page

TABLE XVIII – continued from previous page

CONF	m_{p1}/M	m_{p2}/M	x_1/M	x_2/M	p/M	S_x/M^2	S_y/M^2	S_z/M^2	M_{H1}	M_{H2}	$N_{ef}^{e_i}$	
PH120	0.321278	0.413634	6.294671	-3.135128	0.090701	-0.313984	-0.181279	0.000000	0.335245	0.673858		
PH150	0.321259	0.413489	6.294671	-3.135128	0.090701	-0.181279	-0.313984	0.000000	0.335230	0.673859		
NQ50TH135PH0	0.322668	0.412356	7.247496	-3.648883	0.083814	0.000000	0.255728	-0.257019	0.334841	0.673107	$5.5^{0.02}_{0.004}$	
	PH30	0.322671	0.412394	7.247496	-3.648883	0.083814	-0.127864	0.221467	-0.257019	0.334843	0.673112	
	PH60	0.322680	0.412461	7.247496	-3.648883	0.083814	-0.221467	0.127864	-0.257019	0.334851	0.673113	
	PH90	0.322685	0.412492	7.247496	-3.648883	0.083814	-0.255728	0.000000	-0.257019	0.334856	0.673109	
	PH120	0.322680	0.412461	7.247496	-3.648883	0.083814	-0.221467	-0.127864	-0.257019	0.334851	0.673107	
	PH150	0.322671	0.412394	7.247496	-3.648883	0.083814	-0.127864	-0.221467	-0.257019	0.334843	0.673106	
NQ33TH45PH0	0.238240	0.465805	6.488977	-2.115092	0.078787	0.000000	0.324038	0.324038	0.251143	0.757233	$7^{0.02}_{0.005}$	
	PH30	0.238242	0.465823	6.488977	-2.115092	0.078787	-0.162019	0.280625	0.324038	0.251143	0.757235	
	PH60	0.238246	0.465856	6.488977	-2.115092	0.078787	-0.280625	0.162019	0.324038	0.251145	0.757229	
	PH90	0.238248	0.465872	6.488977	-2.115092	0.078787	-0.324038	0.000000	0.324038	0.251146	0.757220	
	PH120	0.238246	0.465856	6.488977	-2.115092	0.078787	-0.280625	-0.162019	0.324038	0.251145	0.757219	
	PH150	0.238242	0.465823	6.488977	-2.115092	0.078787	-0.162019	-0.280625	0.324038	0.251144	0.757225	
NQ33TH75PH0	0.238466	0.465801	6.706603	-2.208784	0.078621	0.000000	0.442251	0.118501	0.251030	0.756911	$6^{0.02}_{0.005}$	
	PH30	0.238470	0.465836	6.706603	-2.208784	0.078621	-0.221125	0.383000	0.118501	0.251032	0.756915	
	PH60	0.238478	0.465903	6.706603	-2.208784	0.078621	-0.383000	0.221125	0.118501	0.251036	0.756905	
	PH90	0.238483	0.465935	6.706603	-2.208784	0.078621	-0.442251	0.000000	0.118501	0.251038	0.756891	
	PH120	0.238479	0.465902	6.706603	-2.208784	0.078621	-0.383000	-0.221125	0.118501	0.251036	0.756888	
	PH150	0.238470	0.465836	6.706603	-2.208784	0.078621	-0.221125	-0.383000	0.118501	0.251032	0.756899	
NQ33TH100PH0	0.238700	0.465917	6.922442	-2.301121	0.078312	0.000000	0.450542	-0.079443	0.250941	0.756638	$5^{0.02}_{0.005}$	
	PH30	0.238704	0.465955	6.922442	-2.301121	0.078312	-0.225271	0.390181	-0.079443	0.250943	0.756643	
	PH60	0.238712	0.466029	6.922442	-2.301121	0.078312	-0.390181	0.225271	-0.079443	0.250948	0.756635	
	PH90	0.238717	0.466068	6.922442	-2.301121	0.078312	-0.450542	0.000000	-0.079443	0.250950	0.756623	
	PH120	0.238712	0.466030	6.922442	-2.301121	0.078312	-0.390181	-0.225271	-0.079443	0.250947	0.756620	
	PH150	0.238704	0.465954	6.922442	-2.301121	0.078312	-0.225271	-0.390181	-0.079443	0.250943	0.756627	
NQ33TH135PH0	0.238673	0.466056	6.984499	-2.346910	0.079538	0.000000	0.323321	-0.323321	0.250893	0.756475	$3.5^{0.02}_{0.005}$	
	PH30	0.238675	0.466077	6.984499	-2.346910	0.079538	-0.161661	0.280004	-0.323321	0.250897	0.756477	
	PH60	0.238680	0.466120	6.984499	-2.346910	0.079538	-0.280004	0.161661	-0.323321	0.250899	0.756474	
	PH90	0.238682	0.466141	6.984499	-2.346910	0.079538	-0.323321	0.000000	-0.323321	0.250900	0.756468	
	PH120	0.238680	0.466119	6.984499	-2.346910	0.079538	-0.280004	-0.161661	-0.323321	0.250899	0.756466	
	PH150	0.238675	0.466077	6.984499	-2.346910	0.079538	-0.161661	-0.280004	-0.323321	0.250897	0.756470	
NQ25TH30PH0	0.189189	0.497251	6.646760	-1.592485	0.068115	0.000000	0.260215	0.450706	0.200676	0.806742	$7^{0.02}_{0.004}$	
	PH30	0.189189	0.497253	6.646760	-1.592485	0.068115	-0.130108	0.225353	0.450706	0.200676	0.806743	
	PH60	0.189190	0.497257	6.646760	-1.592485	0.068115	-0.225353	0.130108	0.450706	0.200675	0.806739	
	PH90	0.189191	0.497258	6.646760	-1.592485	0.068115	-0.260215	0.000000	0.450706	0.200675	0.806733	
	PH120	0.189190	0.497256	6.646760	-1.592485	0.068115	-0.225353	-0.130108	0.450706	0.200676	0.806735	
	PH150	0.189189	0.497253	6.646760	-1.592485	0.068115	-0.130108	-0.225353	0.450706	0.200676	0.806740	
NQ25TH60PH0	0.189172	0.497121	6.707817	-1.630201	0.069087	0.000000	0.450479	0.260084	0.200625	0.806549	$7^{0.02}_{0.004}$	
	PH30	0.189174	0.497128	6.707817	-1.630201	0.069087	-0.225240	0.390126	0.260084	0.200625	0.806551	
	PH60	0.189178	0.497141	6.707817	-1.630201	0.069087	-0.390126	0.225240	0.260084	0.200625	0.806536	
	PH90	0.189178	0.497155	6.707817	-1.630201	0.069087	-0.450479	0.000000	0.260084	0.200623	0.806524	
	PH120	0.189176	0.497148	6.707817	-1.630201	0.069087	-0.390126	-0.225240	0.260084	0.200623	0.806526	
	PH135	0.189174	0.497141	6.707817	-1.630201	0.069087	-0.318537	-0.318537	0.260084	0.200623	0.806533	
NQ25TH90PH0	0.189174	0.497128	6.707817	-1.630201	0.069087	-0.225240	-0.390126	0.260084	0.200625	0.806539		
	PH150	0.189174	0.497129	6.707817	-1.630201	0.069087	-0.116593	-0.435129	0.260084	0.200623	0.806549	
	PH165	0.189171	0.497129	6.707817	-1.630201	0.069087	-0.116593	-0.435129	0.260084	0.200623	0.806549	
	PH120	0.189172	0.497128	6.707817	-1.630201	0.069087	-0.116593	-0.435129	0.260084	0.200623	0.806549	
	PH135	0.189174	0.497141	6.707817	-1.630201	0.069087	-0.318537	-0.318537	0.260084	0.200623	0.806533	

Continued on next page

TABLE XVIII – continued from previous page

CONF	m_{p1}/M	m_{p2}/M	x_1/M	x_2/M	p/M	S_x/M^2	S_y/M^2	S_z/M^2	M_{H1}	M_{H2}	$N_{ef}^{e_i}$
NQ25TH135PH0	0.189675	0.497432	7.279719	–1.834398	0.069249	0.000000	0.367050	–0.367050	0.200442	0.805802	$3.5^{0.02}_{0.004}$
	PH30	0.189677	0.497441	7.279719	–1.834398	0.069249	–0.183525	0.317875	–0.367050	0.200442	0.805802
	PH60	0.189679	0.497462	7.279719	–1.834398	0.069249	–0.317875	0.183525	–0.367050	0.200443	0.805796
	PH90	0.189681	0.497470	7.279719	–1.834398	0.069249	–0.367050	0.000000	–0.367050	0.200443	0.805789
	PH120	0.189679	0.497461	7.279719	–1.834398	0.069249	–0.317875	–0.183525	–0.367050	0.200443	0.805791
	PH150	0.189677	0.497441	7.279719	–1.834398	0.069249	–0.183525	–0.317875	–0.367050	0.200443	0.805798
NQ25TH150PH0	0.191547	0.498278	8.969521	–2.262266	0.059615	0.000000	0.259019	–0.448634	0.200253	0.805027	$6.5^{0.013}_{0.003}$
	PH30	0.191547	0.498284	8.969521	–2.262266	0.059615	–0.129509	0.224317	–0.448634	0.200254	0.805029
	PH60	0.191548	0.498295	8.969521	–2.262266	0.059615	–0.224317	0.129509	–0.448634	0.200254	0.805029
	PH90	0.191549	0.498300	8.969521	–2.262266	0.059615	–0.259019	0.000000	–0.448634	0.200254	0.805027
	PH120	0.191548	0.498295	8.969521	–2.262266	0.059615	–0.224317	–0.129509	–0.448634	0.200254	0.805027
	PH150	0.191547	0.498284	8.969521	–2.262266	0.059615	–0.129509	–0.224317	–0.448634	0.200254	0.805027
NQ16TH45PH0	0.133879	0.532969	6.876253	–1.109823	0.053722	0.000000	0.420852	0.420852	0.143033	0.862491	$9^{0.02}_{0.006}$
	PH30	0.133879	0.532961	6.876253	–1.109823	0.053722	–0.210426	0.364468	0.420852	0.143032	0.862491
	PH60	0.133881	0.532945	6.876253	–1.109823	0.053722	–0.364468	0.210426	0.420852	0.143031	0.862478
	PH90	0.133882	0.532938	6.876253	–1.109823	0.053722	–0.420852	0.000000	0.420852	0.143030	0.862470
	PH120	0.133881	0.532944	6.876253	–1.109823	0.053722	–0.364468	–0.210426	0.420852	0.143031	0.862469
	PH150	0.133879	0.532961	6.876253	–1.109823	0.053722	–0.210426	–0.364468	0.420852	0.143032	0.862482
NQ16TH90PH0	0.134416	0.533165	7.501062	–1.237255	0.052689	0.000000	0.594371	0.000000	0.142945	0.861982	$6.5^{0.025}_{0.004}$
	PH30	0.134417	0.533158	7.501062	–1.237255	0.052689	–0.297185	0.514740	0.000000	0.142944	0.861977
	PH60	0.134420	0.533145	7.501062	–1.237255	0.052689	–0.514740	0.297185	0.000000	0.142943	0.861956
	PH90	0.134422	0.533138	7.501062	–1.237255	0.052689	–0.594371	0.000000	0.000000	0.142943	0.861940
	PH120	0.134420	0.533145	7.501062	–1.237255	0.052689	–0.514740	–0.297185	0.000000	0.142943	0.861944
	PH150	0.134417	0.533158	7.501062	–1.237255	0.052689	–0.297185	–0.514740	0.000000	0.142945	0.861966
NQ16TH115PH0	0.134769	0.533355	7.930790	–1.322498	0.051705	0.000000	0.538296	–0.251012	0.142901	0.861704	$5.5^{0.015}_{0.004}$
	PH30	0.134770	0.533355	7.930790	–1.322498	0.051705	–0.269148	0.466178	–0.251012	0.142900	0.861701
	PH60	0.134771	0.533353	7.930790	–1.322498	0.051705	–0.466178	0.269148	–0.251012	0.142899	0.861688
	PH90	0.134773	0.533350	7.930790	–1.322498	0.051705	–0.538296	0.000000	–0.251012	0.142899	0.861677
	PH120	0.134771	0.533353	7.930790	–1.322498	0.051705	–0.466178	–0.269148	–0.251012	0.142899	0.861681
	PH150	0.134770	0.533355	7.930790	–1.322498	0.051705	–0.269148	–0.466178	–0.251012	0.142900	0.861694
NQ16TH135PH0	0.134575	0.533333	7.795857	–1.308997	0.053162	0.000000	0.419958	–0.419958	0.142900	0.861696	$3.5^{0.01}_{0.005}$
	PH30	0.134576	0.533331	7.795857	–1.308997	0.053162	–0.209979	0.363694	–0.419958	0.142900	0.861688
	PH60	0.134577	0.533330	7.795857	–1.308997	0.053162	–0.363694	0.209979	–0.419958	0.142899	0.861676
	PH90	0.134578	0.533329	7.795857	–1.308997	0.053162	–0.419958	0.000000	–0.419958	0.142899	0.861667
	PH120	0.134577	0.533330	7.795857	–1.308997	0.053162	–0.363694	–0.209979	–0.419958	0.142900	0.861676
	PH150	0.134576	0.533331	7.795857	–1.308997	0.053162	–0.209979	–0.363694	–0.419958	0.142900	0.861684
NQ16TH150PH0	0.134938	0.533515	8.192215	–1.380000	0.051564	0.000000	0.296825	–0.514116	0.142874	0.861508	$3.5^{0.01}_{0.006}$
	PH30	0.134938	0.533517	8.192215	–1.380000	0.051564	–0.148412	0.257058	–0.514116	0.142873	0.861508
	PH60	0.134938	0.533517	8.192215	–1.380000	0.051564	–0.257058	0.148412	–0.514116	0.142873	0.861504
	PH90	0.134939	0.533518	8.192215	–1.380000	0.051564	–0.296825	0.000000	–0.514116	0.142873	0.861501
	PH120	0.134938	0.533517	8.192215	–1.380000	0.051564	–0.257058	–0.148412	–0.514116	0.142873	0.861503
	PH150	0.134938	0.533517	8.192215	–1.380000	0.051564	–0.148412	–0.257058	–0.514116	0.142873	0.861506

TABLE XIX: Radiated mass, angular momentum, and the remnant recoil (in original frame) as calculated from ψ_4 . Errors quoted are from differences between two extrapolations to $r = \infty$. See Table XX for more accurate measurement of the error.

CONF	δM_{rad}	δJ_x	δJ_y	δJ_z	V_x	V_y	V_z
NQ200TH30PH0	0.0323 ± 0.0001	-0.0011 ± 0.0002	0.0129 ± 0.0002	0.2709 ± 0.0027	-63 ± 2	-178 ± 2	390 ± 2
	0.0323 ± 0.0001	-0.0073 ± 0.0001	0.0105 ± 0.0002	0.2707 ± 0.0027	-64 ± 2	-184 ± 2	309 ± 2
	0.0322 ± 0.0001	-0.0116 ± 0.0001	0.0053 ± 0.0001	0.2704 ± 0.0027	-55 ± 2	-190 ± 2	152 ± 2
	0.0322 ± 0.0001	-0.0128 ± 0.0002	-0.0013 ± 0.0000	0.2703 ± 0.0027	-47 ± 2	-189 ± 2	-46 ± 2

Continued on next page

TABLE XIX – continued from previous page

CONF	δM_{rad}	δJ_x	δJ_y	δJ_z	V_x	V_y	V_z
PH120	0.0322 ± 0.0001	-0.0105 ± 0.0002	-0.0076 ± 0.0000	0.2704 ± 0.0027	-47 ± 2	-183 ± 2	-238 ± 2
PH150	0.0323 ± 0.0001	-0.0055 ± 0.0002	-0.0118 ± 0.0002	0.2707 ± 0.0027	-54 ± 2	-177 ± 2	-365 ± 2
NQ200TH60PH0	0.0303 ± 0.0001	-0.0046 ± 0.0021	0.0250 ± 0.0028	0.2516 ± 0.0017	-145 ± 26	83 ± 8	131 ± 4
PH30	0.0302 ± 0.0001	-0.0130 ± 0.0011	0.0151 ± 0.0045	0.2490 ± 0.0014	-132 ± 20	67 ± 8	-191 ± 6
PH60	0.0303 ± 0.0001	-0.0187 ± 0.0031	0.0011 ± 0.0106	0.2481 ± 0.0036	-121 ± 18	51 ± 2	-420 ± 6
PH90	0.0305 ± 0.0001	-0.0210 ± 0.0024	-0.0113 ± 0.0114	0.2486 ± 0.0041	-124 ± 12	61 ± 2	-593 ± 6
PH120	0.0306 ± 0.0001	-0.0164 ± 0.0026	-0.0216 ± 0.0103	0.2529 ± 0.0005	-134 ± 20	88 ± 2	-640 ± 6
PH150	0.0305 ± 0.0001	-0.0071 ± 0.0025	-0.0273 ± 0.0079	0.2539 ± 0.0032	-141 ± 32	97 ± 2	-455 ± 2
NQ200TH90PH0	0.0308 ± 0.0001	0.0053 ± 0.0002	0.0281 ± 0.0009	0.3083 ± 0.0071	136 ± 2	-46 ± 2	586 ± 4
PH30	0.0304 ± 0.0001	-0.0092 ± 0.0003	0.0265 ± 0.0009	0.3063 ± 0.0071	84 ± 2	-88 ± 2	199 ± 2
PH60	0.0303 ± 0.0001	-0.0212 ± 0.0007	0.0185 ± 0.0006	0.3065 ± 0.0072	108 ± 2	-83 ± 2	-4 ± 2
PH90	0.0303 ± 0.0001	-0.0275 ± 0.0009	0.0054 ± 0.0002	0.3072 ± 0.0072	139 ± 2	-85 ± 2	-266 ± 4
PH120	0.0306 ± 0.0002	-0.0265 ± 0.0009	-0.0093 ± 0.0002	0.3084 ± 0.0072	169 ± 2	-86 ± 2	-566 ± 4
PH150	0.0308 ± 0.0002	-0.0184 ± 0.0006	-0.0217 ± 0.0006	0.3093 ± 0.0072	177 ± 2	-52 ± 2	-690 ± 4
NQ200TH135PH0	0.0279 ± 0.0001	0.0007 ± 0.0002	0.0176 ± 0.0006	0.2855 ± 0.0067	67 ± 2	72 ± 2	-374 ± 2
PH30	0.0278 ± 0.0001	-0.0082 ± 0.0001	0.0156 ± 0.0006	0.2851 ± 0.0068	69 ± 2	78 ± 2	-195 ± 2
PH60	0.0278 ± 0.0001	-0.0148 ± 0.0007	0.0094 ± 0.0004	0.2829 ± 0.0058	65 ± 6	89 ± 2	21 ± 2
PH90	0.0278 ± 0.0001	-0.0174 ± 0.0007	0.0008 ± 0.0003	0.2853 ± 0.0068	52 ± 2	95 ± 2	214 ± 2
PH120	0.0279 ± 0.0001	-0.0154 ± 0.0007	-0.0081 ± 0.0001	0.2858 ± 0.0068	53 ± 2	88 ± 2	401 ± 4
PH150	0.0280 ± 0.0001	-0.0093 ± 0.0005	-0.0149 ± 0.0004	0.2859 ± 0.0067	61 ± 2	75 ± 2	457 ± 4
NQ66TH60PH0	0.0449 ± 0.0001	-0.0050 ± 0.0008	0.0982 ± 0.0090	0.3173 ± 0.0024	-167 ± 8	319 ± 12	1886 ± 10
PH30	0.0448 ± 0.0001	-0.0522 ± 0.0058	0.0709 ± 0.0063	0.3173 ± 0.0015	-269 ± 10	158 ± 12	1736 ± 8
PH60	0.0443 ± 0.0001	-0.0832 ± 0.0063	0.0343 ± 0.0088	0.3148 ± 0.0028	-231 ± 8	-9 ± 10	1407 ± 4
PH90	0.0433 ± 0.0000	-0.0949 ± 0.0089	-0.0133 ± 0.0114	0.3103 ± 0.0042	-61 ± 4	-76 ± 8	739 ± 4
PH120	0.0427 ± 0.0000	-0.0811 ± 0.0088	-0.0621 ± 0.0164	0.3075 ± 0.0051	109 ± 4	68 ± 10	-398 ± 4
PH150	0.0438 ± 0.0000	-0.0436 ± 0.0041	-0.0938 ± 0.0158	0.3111 ± 0.0057	41 ± 6	301 ± 14	-1481 ± 8
NQ50TH30PH0	0.0476 ± 0.0003	-0.0009 ± 0.0060	0.0556 ± 0.0093	0.3434 ± 0.0126	36 ± 6	94 ± 22	1225 ± 14
PH30	0.0473 ± 0.0002	-0.0285 ± 0.0007	0.0474 ± 0.0038	0.3420 ± 0.0109	-8 ± 8	61 ± 22	904 ± 12
PH60	0.0468 ± 0.0003	-0.0483 ± 0.0037	0.0261 ± 0.0009	0.3405 ± 0.0102	-3 ± 8	12 ± 20	425 ± 8
PH90	0.0465 ± 0.0002	-0.0544 ± 0.0059	-0.0018 ± 0.0063	0.3397 ± 0.0098	45 ± 4	-12 ± 20	-173 ± 2
PH120	0.0468 ± 0.0002	-0.0465 ± 0.0074	-0.0290 ± 0.0107	0.3408 ± 0.0102	95 ± 4	18 ± 20	-816 ± 6
PH150	0.0474 ± 0.0002	-0.0265 ± 0.0084	-0.0486 ± 0.0125	0.3429 ± 0.0110	89 ± 6	73 ± 18	-1232 ± 10
NQ50TH60PH0	0.0411 ± 0.0002	0.0105 ± 0.0134	0.0996 ± 0.0015	0.2854 ± 0.0007	141 ± 2	-339 ± 2	-1775 ± 10
PH30	0.0405 ± 0.0002	-0.0534 ± 0.0024	0.0856 ± 0.0011	0.2814 ± 0.0007	197 ± 6	-133 ± 6	-1401 ± 10
PH60	0.0399 ± 0.0002	-0.0823 ± 0.0069	0.0539 ± 0.0081	0.2803 ± 0.0003	147 ± 2	12 ± 6	-1046 ± 4
PH90	0.0390 ± 0.0002	-0.1033 ± 0.0026	0.0014 ± 0.0062	0.2760 ± 0.0022	-35 ± 2	38 ± 4	-378 ± 2
PH120	0.0389 ± 0.0002	-0.0972 ± 0.0131	-0.0476 ± 0.0075	0.2764 ± 0.0019	-201 ± 8	-180 ± 4	803 ± 8
PH150	0.0406 ± 0.0002	-0.0594 ± 0.0115	-0.0869 ± 0.0031	0.2830 ± 0.0012	-77 ± 2	-421 ± 6	1739 ± 8
NQ50TH90PH0	0.0339 ± 0.0002	0.0026 ± 0.0010	0.1356 ± 0.0014	0.2412 ± 0.0044	-219 ± 4	600 ± 8	1465 ± 6
PH30	0.0343 ± 0.0002	-0.0658 ± 0.0002	0.1186 ± 0.0019	0.2437 ± 0.0046	-544 ± 6	380 ± 6	1615 ± 6
PH60	0.0343 ± 0.0002	-0.1167 ± 0.0007	0.0692 ± 0.0017	0.2448 ± 0.0046	-647 ± 8	36 ± 4	1628 ± 6
PH90	0.0343 ± 0.0002	-0.1348 ± 0.0014	0.0013 ± 0.0012	0.2450 ± 0.0047	-486 ± 8	-307 ± 2	1548 ± 6
PH120	0.0330 ± 0.0002	-0.1152 ± 0.0017	-0.0645 ± 0.0002	0.2389 ± 0.0046	28 ± 4	-269 ± 4	780 ± 6
PH150	0.0324 ± 0.0002	-0.0686 ± 0.0015	-0.1143 ± 0.0007	0.2355 ± 0.0044	198 ± 2	331 ± 4	-657 ± 2
NQ50TH135PH0	0.0233 ± 0.0001	0.0393 ± 0.0025	0.1014 ± 0.0161	0.2060 ± 0.0091	-181 ± 22	26 ± 12	-384 ± 6
PH30	0.0235 ± 0.0001	-0.0121 ± 0.0179	0.1130 ± 0.0087	0.2026 ± 0.0264	14 ± 20	-124 ± 4	-646 ± 4
PH60	0.0237 ± 0.0001	-0.0569 ± 0.0522	0.0985 ± 0.0178	0.2067 ± 0.0057	206 ± 8	-61 ± 18	-780 ± 2
PH90	0.0239 ± 0.0001	-0.0856 ± 0.0763	0.0533 ± 0.0240	0.2111 ± 0.0026	302 ± 8	181 ± 12	-856 ± 4
PH120	0.0239 ± 0.0001	-0.0914 ± 0.0687	-0.0066 ± 0.0270	0.2128 ± 0.0062	130 ± 18	453 ± 14	-688 ± 4
PH150	0.0234 ± 0.0001	-0.0753 ± 0.0354	-0.0620 ± 0.0248	0.2094 ± 0.0011	-174 ± 22	358 ± 12	-140 ± 6
NQ33TH45PH0	0.0370 ± 0.0004	-0.0045 ± 0.0009	0.0831 ± 0.0011	0.2665 ± 0.0040	-112 ± 8	-307 ± 10	-1347 ± 2
PH30	0.0368 ± 0.0004	-0.0454 ± 0.0001	0.0696 ± 0.0015	0.2657 ± 0.0041	26 ± 2	-285 ± 12	-1144 ± 4

Continued on next page

TABLE XIX – continued from previous page

CONF	δM_{rad}	δJ_x	δJ_y	δJ_z	V_x	V_y	V_z
PH60	0.0365 ± 0.0004	-0.0740 ± 0.0007	0.0371 ± 0.0013	0.2651 ± 0.0041	128 ± 4	-210 ± 10	-955 ± 4
PH90	0.0359 ± 0.0003	-0.0822 ± 0.0014	-0.0051 ± 0.0007	0.2632 ± 0.0040	116 ± 6	-102 ± 6	-542 ± 4
PH120	0.0353 ± 0.0003	-0.0680 ± 0.0015	-0.0454 ± 0.0001	0.2613 ± 0.0039	-67 ± 2	-85 ± 4	361 ± 4
PH150	0.0363 ± 0.0004	-0.0369 ± 0.0014	-0.0738 ± 0.0005	0.2647 ± 0.0040	-192 ± 8	-214 ± 6	1205 ± 2
NQ33TH75PH0	0.0279 ± 0.0002	-0.0017 ± 0.0009	0.1221 ± 0.0017	0.1802 ± 0.0035	-84 ± 2	-46 ± 4	393 ± 2
PH30	0.0275 ± 0.0002	-0.0629 ± 0.0001	0.1045 ± 0.0019	0.1795 ± 0.0036	60 ± 2	-163 ± 2	74 ± 2
PH60	0.0276 ± 0.0002	-0.1070 ± 0.0008	0.0583 ± 0.0016	0.1808 ± 0.0037	87 ± 2	-99 ± 2	203 ± 2
PH90	0.0273 ± 0.0002	-0.1219 ± 0.0015	-0.0038 ± 0.0009	0.1804 ± 0.0037	232 ± 2	7 ± 2	-91 ± 2
PH120	0.0282 ± 0.0002	-0.1056 ± 0.0018	-0.0665 ± 0.0000	0.1833 ± 0.0036	353 ± 2	412 ± 8	-1083 ± 4
PH150	0.0295 ± 0.0002	-0.0599 ± 0.0015	-0.1096 ± 0.0009	0.1870 ± 0.0037	12 ± 4	474 ± 8	-1342 ± 4
NQ33TH100PH0	0.0228 ± 0.0002	0.0401 ± 0.0010	0.1272 ± 0.0013	0.1257 ± 0.0030	-249 ± 2	850 ± 8	871 ± 2
PH30	0.0230 ± 0.0002	-0.0301 ± 0.0003	0.1304 ± 0.0016	0.1268 ± 0.0032	-699 ± 4	604 ± 8	895 ± 2
PH60	0.0229 ± 0.0002	-0.0926 ± 0.0005	0.0980 ± 0.0016	0.1265 ± 0.0033	-876 ± 8	186 ± 6	885 ± 2
PH90	0.0231 ± 0.0002	-0.1300 ± 0.0013	0.0374 ± 0.0012	0.1274 ± 0.0032	-859 ± 10	-333 ± 4	900 ± 4
PH120	0.0226 ± 0.0002	-0.1276 ± 0.0016	-0.0319 ± 0.0004	0.1250 ± 0.0032	-261 ± 8	-626 ± 2	559 ± 2
PH150	0.0216 ± 0.0002	-0.0967 ± 0.0015	-0.0875 ± 0.0005	0.1206 ± 0.0031	263 ± 2	309 ± 4	-458 ± 2
NQ33TH135PH0	0.0159 ± 0.0001	0.0628 ± 0.0007	0.0510 ± 0.0004	0.1182 ± 0.0024	34 ± 2	-351 ± 2	-447 ± 2
PH30	0.0161 ± 0.0001	0.0279 ± 0.0004	0.0767 ± 0.0008	0.1195 ± 0.0024	247 ± 2	-453 ± 2	-453 ± 2
PH60	0.0162 ± 0.0001	-0.0153 ± 0.0000	0.0812 ± 0.0009	0.1200 ± 0.0025	483 ± 2	-315 ± 4	-432 ± 4
PH90	0.0163 ± 0.0001	-0.0554 ± 0.0004	0.0624 ± 0.0008	0.1197 ± 0.0026	636 ± 2	-63 ± 2	-353 ± 4
PH120	0.0161 ± 0.0001	-0.0790 ± 0.0007	0.0265 ± 0.0005	0.1170 ± 0.0026	515 ± 4	171 ± 2	-76 ± 2
PH150	0.0157 ± 0.0001	-0.0805 ± 0.0008	-0.0130 ± 0.0000	0.1159 ± 0.0025	118 ± 2	-8 ± 2	301 ± 2
NQ25TH30PH0	0.0308 ± 0.0004	-0.0001 ± 0.0006	0.0547 ± 0.0010	0.2283 ± 0.0028	-24 ± 6	12 ± 4	80 ± 6
PH30	0.0308 ± 0.0004	-0.0272 ± 0.0001	0.0473 ± 0.0011	0.2288 ± 0.0027	-38 ± 6	72 ± 2	341 ± 4
PH60	0.0309 ± 0.0004	-0.0472 ± 0.0005	0.0274 ± 0.0009	0.2293 ± 0.0028	-114 ± 8	110 ± 2	614 ± 2
PH90	0.0312 ± 0.0005	-0.0548 ± 0.0010	0.0003 ± 0.0004	0.2304 ± 0.0027	-193 ± 10	61 ± 4	756 ± 4
PH120	0.0314 ± 0.0005	-0.0479 ± 0.0012	-0.0271 ± 0.0002	0.2320 ± 0.0029	-212 ± 8	-42 ± 8	791 ± 6
PH150	0.0315 ± 0.0005	-0.0279 ± 0.0010	-0.0477 ± 0.0008	0.2317 ± 0.0028	-153 ± 8	-118 ± 10	663 ± 10
NQ25TH60PH0	0.0246 ± 0.0002	-0.0048 ± 0.0011	0.0952 ± 0.0012	0.1575 ± 0.0018	-77 ± 4	78 ± 2	-97 ± 4
PH30	0.0245 ± 0.0002	-0.0520 ± 0.0005	0.0795 ± 0.0014	0.1578 ± 0.0020	-139 ± 4	75 ± 2	72 ± 4
PH60	0.0245 ± 0.0002	-0.0849 ± 0.0003	0.0425 ± 0.0013	0.1587 ± 0.0021	-131 ± 4	-19 ± 2	-15 ± 4
PH90	0.0245 ± 0.0002	-0.0948 ± 0.0011	-0.0061 ± 0.0008	0.1594 ± 0.0016	-117 ± 2	-84 ± 2	37 ± 4
PH120	0.0250 ± 0.0003	-0.0797 ± 0.0014	-0.0540 ± 0.0000	0.1608 ± 0.0017	-266 ± 6	-239 ± 4	889 ± 2
PH135	0.0259 ± 0.0003	-0.0644 ± 0.0016	-0.0732 ± 0.0004	0.1639 ± 0.0018	-246 ± 10	-310 ± 2	1165 ± 2
PH150	0.0261 ± 0.0003	-0.0442 ± 0.0015	-0.0870 ± 0.0009	0.1640 ± 0.0019	-165 ± 12	-283 ± 2	1106 ± 4
PH165	0.0255 ± 0.0003	-0.0205 ± 0.0014	-0.0943 ± 0.0012	0.1613 ± 0.0017	-85 ± 10	-147 ± 2	733 ± 4
NQ25TH90PH0	0.0185 ± 0.0002	0.0182 ± 0.0012	0.1128 ± 0.0015	0.0847 ± 0.0024	240 ± 2	-1 ± 4	-202 ± 2
PH30	0.0185 ± 0.0002	-0.0417 ± 0.0004	0.1067 ± 0.0019	0.0853 ± 0.0027	225 ± 4	108 ± 4	-236 ± 2
PH60	0.0191 ± 0.0002	-0.0920 ± 0.0007	0.0709 ± 0.0018	0.0883 ± 0.0028	419 ± 8	159 ± 2	-536 ± 2
PH90	0.0190 ± 0.0002	-0.1150 ± 0.0014	0.0146 ± 0.0012	0.0880 ± 0.0028	228 ± 8	329 ± 2	-489 ± 2
PH120	0.0181 ± 0.0002	-0.1074 ± 0.0018	-0.0429 ± 0.0001	0.0835 ± 0.0026	-327 ± 2	-168 ± 2	244 ± 2
PH150	0.0197 ± 0.0002	-0.0736 ± 0.0016	-0.0940 ± 0.0010	0.0892 ± 0.0023	29 ± 2	-743 ± 6	792 ± 2
NQ25TH135PH0	0.0116 ± 0.0001	0.0567 ± 0.0006	0.0314 ± 0.0003	0.0794 ± 0.0014	-163 ± 4	-471 ± 2	-207 ± 2
PH30	0.0117 ± 0.0001	0.0329 ± 0.0004	0.0570 ± 0.0006	0.0792 ± 0.0015	65 ± 4	-548 ± 2	-141 ± 2
PH60	0.0117 ± 0.0001	-0.0002 ± 0.0001	0.0670 ± 0.0007	0.0793 ± 0.0015	333 ± 4	-440 ± 2	-134 ± 2
PH90	0.0118 ± 0.0001	-0.0344 ± 0.0002	0.0583 ± 0.0006	0.0784 ± 0.0017	489 ± 2	-236 ± 2	-57 ± 2
PH120	0.0115 ± 0.0001	-0.0568 ± 0.0005	0.0343 ± 0.0003	0.0761 ± 0.0018	282 ± 2	-70 ± 2	159 ± 2
PH150	0.0112 ± 0.0001	-0.0643 ± 0.0006	0.0030 ± 0.0000	0.0779 ± 0.0016	-122 ± 4	-221 ± 2	258 ± 2
NQ25TH150PH0	0.0112 ± 0.0001	0.0714 ± 0.0016	0.0360 ± 0.0004	0.0983 ± 0.0039	30 ± 2	351 ± 2	152 ± 2
PH30	0.0113 ± 0.0001	0.0435 ± 0.0011	0.0678 ± 0.0012	0.0982 ± 0.0039	-120 ± 2	383 ± 4	78 ± 2
PH60	0.0113 ± 0.0001	0.0033 ± 0.0004	0.0810 ± 0.0016	0.0978 ± 0.0040	-273 ± 2	296 ± 4	13 ± 2
PH90	0.0113 ± 0.0001	-0.0379 ± 0.0005	0.0722 ± 0.0016	0.0967 ± 0.0040	-323 ± 4	150 ± 2	-82 ± 2
PH120	0.0112 ± 0.0001	-0.0678 ± 0.0012	0.0447 ± 0.0012	0.0959 ± 0.0040	-178 ± 4	73 ± 2	-198 ± 2

Continued on next page

TABLE XIX – continued from previous page

CONF	δM_{rad}	δJ_x	δJ_y	δJ_z	V_x	V_y	V_z
PH150	0.0111 ± 0.0001	-0.0798 ± 0.0016	0.0058 ± 0.0004	0.0972 ± 0.0040	25 ± 2	190 ± 2	-224 ± 2
NQ16TH45PH0	0.0192 ± 0.0003	0.0002 ± 0.0010	0.0598 ± 0.0017	0.1320 ± 0.0018	-92 ± 2	-197 ± 14	-363 ± 8
PH30	0.0190 ± 0.0003	-0.0295 ± 0.0014	0.0511 ± 0.0013	0.1312 ± 0.0010	-0 ± 4	-143 ± 10	-189 ± 6
PH60	0.0191 ± 0.0003	-0.0515 ± 0.0004	0.0300 ± 0.0013	0.1324 ± 0.0019	116 ± 12	-162 ± 8	-311 ± 8
PH90	0.0193 ± 0.0003	-0.0598 ± 0.0012	0.0005 ± 0.0008	0.1339 ± 0.0021	232 ± 14	-90 ± 2	-415 ± 10
PH120	0.0186 ± 0.0003	-0.0507 ± 0.0015	-0.0293 ± 0.0003	0.1309 ± 0.0022	-111 ± 2	-47 ± 6	330 ± 4
PH150	0.0193 ± 0.0003	-0.0301 ± 0.0014	-0.0517 ± 0.0013	0.1330 ± 0.0021	-228 ± 6	-199 ± 14	611 ± 6
NQ16TH90PH0	0.0115 ± 0.0001	0.0187 ± 0.0009	0.0735 ± 0.0007	0.0253 ± 0.0012	66 ± 4	-369 ± 2	-153 ± 2
PH30	0.0114 ± 0.0001	-0.0214 ± 0.0004	0.0722 ± 0.0008	0.0256 ± 0.0014	160 ± 4	-251 ± 2	-93 ± 2
PH60	0.0122 ± 0.0001	-0.0581 ± 0.0002	0.0502 ± 0.0009	0.0289 ± 0.0018	-288 ± 2	-125 ± 2	275 ± 4
PH90	0.0123 ± 0.0001	-0.0762 ± 0.0010	0.0136 ± 0.0008	0.0293 ± 0.0015	-239 ± 2	-268 ± 2	312 ± 4
PH120	0.0114 ± 0.0001	-0.0724 ± 0.0014	-0.0234 ± 0.0003	0.0255 ± 0.0009	271 ± 2	234 ± 2	-143 ± 2
PH150	0.0125 ± 0.0001	-0.0515 ± 0.0015	-0.0580 ± 0.0001	0.0291 ± 0.0012	-100 ± 4	429 ± 2	-330 ± 6
NQ16TH115PH0	0.0089 ± 0.0001	0.0539 ± 0.0010	0.0392 ± 0.0005	0.0177 ± 0.0011	-61 ± 4	-481 ± 2	79 ± 2
PH30	0.0089 ± 0.0001	0.0270 ± 0.0007	0.0612 ± 0.0008	0.0172 ± 0.0010	190 ± 4	-441 ± 2	76 ± 2
PH60	0.0085 ± 0.0001	-0.0059 ± 0.0003	0.0651 ± 0.0011	0.0155 ± 0.0011	196 ± 4	-217 ± 2	-50 ± 2
PH90	0.0085 ± 0.0001	-0.0380 ± 0.0004	0.0533 ± 0.0010	0.0148 ± 0.0013	265 ± 2	-90 ± 2	-56 ± 2
PH120	0.0092 ± 0.0001	-0.0629 ± 0.0009	0.0251 ± 0.0006	0.0155 ± 0.0012	445 ± 2	250 ± 2	130 ± 2
PH150	0.0085 ± 0.0001	-0.0636 ± 0.0011	-0.0056 ± 0.0000	0.0159 ± 0.0011	-138 ± 2	-22 ± 2	130 ± 2
NQ16TH135PH0	0.0069 ± 0.0000	0.0425 ± 0.0005	0.0102 ± 0.0001	0.0386 ± 0.0006	134 ± 2	2 ± 2	-162 ± 2
PH30	0.0070 ± 0.0000	0.0324 ± 0.0004	0.0311 ± 0.0002	0.0385 ± 0.0006	118 ± 2	109 ± 2	-166 ± 2
PH60	0.0069 ± 0.0000	0.0128 ± 0.0002	0.0433 ± 0.0004	0.0384 ± 0.0008	61 ± 2	121 ± 2	-167 ± 2
PH90	0.0069 ± 0.0000	-0.0104 ± 0.0001	0.0443 ± 0.0004	0.0384 ± 0.0007	35 ± 2	100 ± 4	-163 ± 2
PH120	0.0068 ± 0.0000	-0.0304 ± 0.0004	0.0329 ± 0.0004	0.0400 ± 0.0006	201 ± 2	39 ± 2	-96 ± 2
PH150	0.0071 ± 0.0000	-0.0443 ± 0.0005	0.0110 ± 0.0002	0.0398 ± 0.0007	342 ± 2	84 ± 2	80 ± 2
NQ16TH150PH0	0.0063 ± 0.0000	0.0326 ± 0.0003	0.0044 ± 0.0001	0.0487 ± 0.0011	226 ± 2	50 ± 2	-64 ± 2
PH30	0.0062 ± 0.0000	0.0265 ± 0.0003	0.0196 ± 0.0003	0.0486 ± 0.0012	175 ± 2	81 ± 2	-85 ± 2
PH60	0.0062 ± 0.0000	0.0135 ± 0.0001	0.0300 ± 0.0004	0.0487 ± 0.0011	133 ± 2	101 ± 2	-94 ± 2
PH90	0.0061 ± 0.0001	-0.0029 ± 0.0001	0.0326 ± 0.0004	0.0491 ± 0.0011	124 ± 2	83 ± 2	-94 ± 2
PH120	0.0061 ± 0.0001	-0.0188 ± 0.0002	0.0259 ± 0.0003	0.0499 ± 0.0011	193 ± 2	35 ± 2	-66 ± 2
PH150	0.0062 ± 0.0000	-0.0303 ± 0.0003	0.0120 ± 0.0001	0.0496 ± 0.0010	261 ± 2	26 ± 2	4 ± 2

TABLE XX: This table corrects errors in the published version. Comparison between remnant horizon properties and radiated quantities. Differences between the two are a much better measurement of the true error than either the (very small) variations in the isolated horizon quantities with time or the extrapolation error in the radiative quantities. Here $\delta\Theta$ is the angle, in degrees, that the total angular momentum \vec{J} precesses from the start of the simulation to the final ringdown. Rows with a bold header differ from the original manuscript.

CONF	$M_{\text{rem}}(\text{IH})$	$M_{\text{rem}}(r)$	$S_{x\text{rem}}(\text{IH})$	$S_{x\text{rem}}(r)$	$S_{y\text{rem}}(\text{IH})$	$S_{y\text{rem}}(r)$	$S_{z\text{rem}}(\text{IH})$	$S_{z\text{rem}}(r)$	$\delta\Theta(\text{IH})$	$\delta\Theta(r)$
NQ200TH30PH0	0.9670	0.9677	-0.0063	0.0011	0.0241	0.0325	0.6210	0.6198	0.9	0.1
	PH30	0.9677		-0.0154		0.0288		0.6200		0.1
	PH60	0.9672	0.9678	-0.0253	-0.0277	0.0260	0.0174	0.6210	0.6203	1.0
	PH90	0.9673	0.9678	-0.0282	-0.0326	0.0060	0.0013	0.6215	0.6204	0.6
	PH120	0.9672	0.9678	-0.0252	-0.0288	-0.0077	-0.0151	0.6215	0.6203	0.8
	PH150	0.9671	0.9677	-0.0280	-0.0172	-0.0367	-0.0275	0.6200	0.6200	1.4
NQ200TH60PH0	0.9687	0.9697	0.0060	0.0046	0.0488	0.0537	0.6091	0.6131	0.8	0.5
	PH30	0.9688	0.9698	-0.0248	-0.0263	0.0449	0.0530	0.6090	0.6157	0.4
	PH60	0.9688	0.9697	-0.0512	-0.0494	0.0428	0.0382	0.6068	0.6166	1.5
	PH90	0.9686	0.9695	-0.0548	-0.0577	0.0008	0.0113	0.6071	0.6161	0.1
	PH120	0.9684	0.9694	-0.0533	-0.0517	-0.0122	-0.0177	0.6066	0.6118	1.5
	PH150	0.9685	0.9695	-0.0247	-0.0322	-0.0490	-0.0408	0.6075	0.6108	0.3

Continued on next page

TABLE XX – continued from previous page

CONF	$M_{\text{rem}}(\text{IH})$	$M_{\text{rem}}(\text{r})$	$S_{x\text{rem}}(\text{IH})$	$S_{x\text{rem}}(\text{r})$	$S_{y\text{rem}}(\text{IH})$	$S_{y\text{rem}}(\text{r})$	$S_{z\text{rem}}(\text{IH})$	$S_{z\text{rem}}(\text{r})$	$\delta\Theta(\text{IH})$	$\delta\Theta(\text{r})$
NQ200TH90PH0	0.9686	0.9692	-0.0040	-0.0053	0.0524	0.0624	0.5869	0.5813	0.8	0.6
	PH30	0.9696		-0.0360		0.0518		0.5833		0.6
	PH60	0.9692	0.9697	-0.0554	-0.0571	0.0342	0.0267	0.5875	0.5831	0.5
	PH90	0.9697		-0.0630		-0.0054		0.5824		0.6
	PH120	0.9689	0.9694	-0.0557	-0.0518	-0.0286	-0.0359	0.5861	0.5812	0.4
	PH150	0.9686	0.9692	-0.0241	-0.0268	-0.0590	-0.0566	0.5851	0.5803	0.9
NQ200TH135PH0		0.9721		-0.0007		0.0464		0.5507		0.4
	PH30	0.9722		-0.0238		0.0398		0.5511		0.4
	PH60	0.9722		-0.0406		0.0226		0.5533		0.4
	PH90	0.9718	0.9722	-0.0500	-0.0466	-0.0019	-0.0008	0.5569	0.5509	0.8
	PH120	0.9721		-0.0400		-0.0239		0.5504		0.5
	PH150	0.9715	0.9720	-0.0124	-0.0227	-0.0357	-0.0405	0.5570	0.5503	0.9
NQ66TH60PH0	0.9534	0.9551	0.0094	0.0050	0.1569	0.1572	0.6985	0.7056	1.6	1.5
	PH30	0.9535	0.9552	-0.0888	-0.0755	0.1411	0.1503	0.6968	0.7056	0.8
	PH60	0.9541	0.9557	-0.1300	-0.1380	0.0897	0.0934	0.7008	0.7081	1.7
	PH90	0.9552	0.9567	-0.1772	-0.1605	0.0012	0.0133	0.6999	0.7126	0.2
	PH120	0.9558	0.9573	-0.1507	-0.1401	-0.0666	-0.0656	0.7054	0.7154	1.7
	PH150	0.9546	0.9562	-0.0789	-0.0841	-0.1414	-0.1274	0.7015	0.7118	1.0
NQ50TH30PH0	0.9501	0.9524	0.0150	0.0009	0.1173	0.1262	0.7567	0.7626	1.2	0.1
	PH30	0.9504	0.9527	-0.0664	-0.0624	0.1124	0.1101	0.7560	0.7640	0.5
	PH60	0.9510	0.9532	-0.0977	-0.1092	0.0537	0.0648	0.7606	0.7655	1.0
	PH90	0.9513	0.9535	-0.1243	-0.1274	-0.0078	0.0018	0.7595	0.7663	0.6
	PH120	0.9510	0.9532	-0.1077	-0.1110	-0.0776	-0.0619	0.7571	0.7652	1.1
	PH150	0.9503	0.9526	-0.0680	-0.0644	-0.1010	-0.1089	0.7567	0.7631	0.7
NQ50TH60PH0	0.9569	0.9589	0.0184	-0.0105	0.1969	0.2152	0.7025	0.7038	2.5	1.0
	PH30	0.9576	0.9595	-0.0915	-0.1040	0.1727	0.1870	0.7058	0.7078	2.3
	PH60	0.9583	0.9601	-0.1864	-0.1903	0.1067	0.1035	0.7022	0.7089	0.6
	PH90	0.9592	0.9610	-0.1997	-0.2115	0.0156	-0.0014	0.7096	0.7132	2.3
	PH120	0.9593	0.9611	-0.1731	-0.1754	-0.1003	-0.1098	0.7098	0.7128	1.9
	PH150	0.9575	0.9594	-0.0949	-0.0980	-0.1853	-0.1857	0.7006	0.7062	1.4
NQ50TH90PH0	0.9657	0.9661	-0.0045	-0.0026	0.2253	0.2270	0.6172	0.6141	2.9	2.7
	PH30	0.9652	0.9657	-0.0992	-0.1155	0.1939	0.1954	0.6174	0.6116	3.7
	PH60	0.9652	0.9657	-0.1968	-0.1973	0.1083	0.1121	0.6139	0.6105	2.9
	PH90	0.9653	0.9657	-0.2197	-0.2278	0.0079	-0.0013	0.6159	0.6103	3.4
	PH120	0.9666	0.9670	-0.1867	-0.1988	-0.1086	-0.1168	0.6245	0.6164	3.9
	PH150	0.9672	0.9676	-0.1132	-0.1127	-0.1989	-0.1997	0.6228	0.6198	2.8
NQ50TH135PH0	0.9760	0.9767	-0.0523	-0.0393	0.1427	0.1543	0.4518	0.4503	7.3	5.3
	PH30	0.9758	0.9765	-0.1188	-0.1158	0.1040	0.1085	0.4481	0.4537	6.8
	PH60	0.9756	0.9763	-0.1611	-0.1646	0.0280	0.0294	0.4443	0.4496	7.2
	PH90	0.9754	0.9761	-0.1461	-0.1701	-0.0518	-0.0533	0.4457	0.4452	7.0
	PH120	0.9754	0.9761	-0.1095	-0.1301	-0.1212	-0.1213	0.4435	0.4435	6.4
	PH150	0.9759	0.9766	-0.0423	-0.0526	-0.1460	-0.1595	0.4512	0.4469	5.4
NQ33TH45PH0	0.9614	0.9630	0.0142	0.0045	0.2549	0.2409	0.7278	0.7354	1.7	0.4
	PH30	0.9617	0.9632	-0.1091	-0.1166	0.2063	0.2110	0.7363	0.7362	0.7
	PH60	0.9621	0.9635	-0.1995	-0.2066	0.1239	0.1249	0.7368	0.7368	0.6
	PH90	0.9628	0.9641	-0.2357	-0.2418	0.0072	0.0051	0.7387	0.7387	0.6
	PH120	0.9634	0.9647	-0.2064	-0.2126	-0.1167	-0.1166	0.7406	0.7406	0.2
	PH150	0.9622	0.9637	-0.1308	-0.1251	-0.2079	-0.2068	0.7336	0.7372	0.9
NQ33TH75PH0	0.9715	0.9721	0.0149	0.0017	0.3120	0.3202	0.6433	0.6392	2.8	1.8
	PH30	0.9718	0.9725	-0.1496	-0.1582	0.2684	0.2785	0.6467	0.6399	3.0
	PH60	0.9718	0.9724	-0.2666	-0.2760	0.1535	0.1628	0.6454	0.6386	2.9
	PH90	0.9720	0.9727	-0.3244	-0.3204	-0.0046	0.0038	0.6374	0.6390	1.4

Continued on next page

TABLE XX – continued from previous page

CONF	$M_{\text{rem}}(\text{IH})$	$M_{\text{rem}}(\text{r})$	$S_{x\text{rem}}(\text{IH})$	$S_{x\text{rem}}(\text{r})$	$S_{y\text{rem}}(\text{IH})$	$S_{y\text{rem}}(\text{r})$	$S_{z\text{rem}}(\text{IH})$	$S_{z\text{rem}}(\text{r})$	$\delta\Theta(\text{IH})$	$\delta\Theta(\text{r})$
PH120	0.9711	0.9718	-0.2752	-0.2774	-0.1623	-0.1546	0.6352	0.6361	1.7	1.9
PH150	0.9698	0.9705	-0.1573	-0.1612	-0.2773	-0.2734	0.6315	0.6324	1.6	1.7
NQ33TH100PH0	0.9768	0.9772	-0.0465	-0.0401	0.3187	0.3233	0.5205	0.5172	5.6	4.8
PH30	0.9766	0.9770	-0.1967	-0.1952	0.2528	0.2598	0.5200	0.5161	5.5	4.8
PH60	0.9767	0.9771	-0.2962	-0.2976	0.1238	0.1273	0.5192	0.5164	5.2	4.8
PH90	0.9765	0.9769	-0.3189	-0.3205	-0.0369	-0.0374	0.5177	0.5155	4.9	4.7
PH120	0.9770	0.9774	-0.2481	-0.2626	-0.1985	-0.1934	0.5244	0.5179	6.1	4.5
PH150	0.9781	0.9784	-0.1321	-0.1286	-0.3045	-0.3027	0.5217	0.5223	4.4	4.8
NQ33TH135PH0	0.9840	0.9841	-0.0587	-0.0628	0.2846	0.2723	0.2912	0.3007	10.6	9.9
PH30	0.9838	0.9839	-0.1928	-0.1896	0.2124	0.2033	0.2922	0.2994	10.5	9.9
PH60	0.9837	0.9838	-0.2731	-0.2647	0.0835	0.0805	0.2917	0.2989	10.8	9.9
PH90	0.9836	0.9837	-0.2750	-0.2679	-0.0667	-0.0624	0.2931	0.2992	10.9	9.8
PH120	0.9837	0.9839	-0.2116	-0.2010	-0.1880	-0.1882	0.2962	0.3019	9.7	9.6
PH150	0.9842	0.9843	-0.0912	-0.0812	-0.2699	-0.2670	0.2991	0.3030	9.5	9.8
NQ25TH30PH0		0.9692		0.0001		0.2055		0.7836		0.3
PH30	0.9673	0.9692	-0.0916	-0.1029	0.1698	0.1781	0.7797	0.7831	0.7	0.3
PH60	0.9671	0.9691	-0.1850	-0.1782	0.1128	0.1027	0.7720	0.7826	1.3	0.3
PH90	0.9668	0.9688	-0.2169	-0.2054	-0.0053	-0.0003	0.7708	0.7815	1.3	0.3
PH120		0.9686		-0.1775		-0.1030		0.7799		0.3
PH150	0.9665	0.9685	-0.0988	-0.1022	-0.1829	-0.1777	0.7735	0.7802	0.7	0.3
NQ25TH60PH0	0.9743	0.9754	0.0035	0.0048	0.3461	0.3553	0.6798	0.6786	1.4	0.8
PH30	0.9745	0.9755	-0.1651	-0.1732	0.3032	0.3106	0.6806	0.6783	1.6	0.8
PH60	0.9744	0.9755	-0.3025	-0.3052	0.1799	0.1827	0.6762	0.6774	0.9	0.7
PH90		0.9755		-0.3557		0.0061		0.6767		0.7
PH120		0.9750		-0.3104		-0.1712		0.6753		0.8
PH135	0.9729	0.9741	-0.2552	-0.2541	-0.2391	-0.2453	0.6707	0.6722	1.2	0.8
PH150	0.9726	0.9739	-0.1832	-0.1810	-0.2952	-0.3031	0.6716	0.6721	1.3	0.7
PH165	0.9733	0.9745	-0.1056	-0.0961	-0.3493	-0.3408	0.6660	0.6748	1.0	0.7
NQ25TH90PH0	0.9810	0.9815	-0.0145	-0.0182	0.4000	0.4065	0.5287	0.5253	3.5	3.1
PH30	0.9810	0.9815	-0.2100	-0.2180	0.3390	0.3430	0.5293	0.5247	3.6	3.1
PH60	0.9804	0.9809	-0.3486	-0.3577	0.1894	0.1888	0.5257	0.5217	3.5	3.0
PH90	0.9805	0.9810	-0.3911	-0.4043	-0.0147	-0.0146	0.5302	0.5220	4.2	2.9
PH120	0.9814	0.9819	-0.3382	-0.3423	-0.2091	-0.2168	0.5308	0.5265	3.7	3.2
PH150	0.9797	0.9803	-0.1661	-0.1861	-0.3537	-0.3557	0.5266	0.5208	4.9	3.2
NQ25TH135PH0	0.9883	0.9884	-0.0557	-0.0567	0.3408	0.3357	0.1754	0.1847	11.8	10.9
PH30	0.9881	0.9883	-0.2207	-0.2164	0.2638	0.2609	0.1760	0.1849	12.1	10.8
PH60	0.9881	0.9883	-0.3204	-0.3177	0.1212	0.1165	0.1774	0.1848	11.5	10.9
PH90	0.9881	0.9882	-0.3362	-0.3327	-0.0503	-0.0583	0.1821	0.1857	10.4	10.9
PH120	0.9884	0.9885	-0.2683	-0.2611	-0.2133	-0.2178	0.1839	0.1880	10.4	10.7
PH150	0.9886	0.9888	-0.1191	-0.1192	-0.3184	-0.3209	0.1912	0.1862	10.2	10.9
NQ25TH150PH0	0.9887	0.9888	-0.0673	-0.0714	0.2247	0.2230	0.1261	0.1226	18.3	19.4
PH30	0.9886	0.9887	-0.1698	-0.1730	0.1558	0.1565	0.1313	0.1227	17.9	19.4
PH60	0.9886	0.9887	-0.2227	-0.2276	0.0522	0.0485	0.1334	0.1231	17.0	19.4
PH90	0.9886	0.9887	-0.2200	-0.2211	-0.0682	-0.0722	0.1324	0.1242	17.6	19.3
PH120	0.9887	0.9888	-0.1570	-0.1565	-0.1714	-0.1742	0.1316	0.1250	18.0	19.3
PH150	0.9888	0.9889	-0.0568	-0.0497	-0.2280	-0.2301	0.1275	0.1237	17.8	19.4
NQ16TH45PH0	0.9793	0.9808	0.0032	-0.0002	0.3503	0.3611	0.7128	0.7179	0.3	0.4
PH30	0.9796	0.9810	-0.1727	-0.1809	0.3059	0.3134	0.7134	0.7187	0.3	0.4
PH60	0.9795	0.9809	-0.2949	-0.3130	0.1795	0.1804	0.7155	0.7175	0.8	0.4
PH90	0.9792	0.9807	-0.3558	-0.3611	-0.0026	-0.0005	0.7111	0.7160	0.3	0.4
PH120	0.9800	0.9814	-0.3085	-0.3138	-0.1684	-0.1811	0.7141	0.7190	0.6	0.4
PH150		0.9807		-0.1803		-0.3128		0.7169		0.4

Continued on next page

TABLE XX – continued from previous page

CONF	$M_{\text{rem}}(\text{IH})$	$M_{\text{rem}}(\text{r})$	$S_{x\text{rem}}(\text{IH})$	$S_{x\text{rem}}(\text{r})$	$S_{y\text{rem}}(\text{IH})$	$S_{y\text{rem}}(\text{r})$	$S_{z\text{rem}}(\text{IH})$	$S_{z\text{rem}}(\text{r})$	$\delta\Theta(\text{IH})$	$\delta\Theta(\text{r})$
NQ16TH90PH0	0.9885		–0.0187		0.5209		0.4351		2.6	
	PH30	0.9886	–0.2758		0.4425		0.4348		2.6	
	PH60	0.9878	–0.4566		0.2470		0.4315		2.3	
	PH90	0.9877	–0.5182		–0.0136		0.4311		2.3	
	PH120	0.9886	–0.4423		–0.2738		0.4349		2.5	
	PH150	0.9875	–0.2457		–0.4567		0.4313		2.4	
NQ16TH115PH0	0.9908	0.9911	–0.0510	–0.0539	0.4954	0.4991	0.2175	0.2097	5.4	5.7
	PH30	0.9909	0.9911	–0.2906	–0.2961	0.4096	0.4050	0.2076	0.2102	5.0
	PH60	0.9913	0.9915	–0.4599	–0.4603	0.2010	0.2040	0.2149	0.2119	5.9
	PH90	0.9913	0.9915	–0.4999	–0.5003	–0.0617	–0.0533	0.2103	0.2126	6.5
	PH120	0.9906	0.9908	–0.4061	–0.4033	–0.2845	–0.2942	0.2184	0.2119	4.7
	PH150	0.9912	0.9915	–0.2187	–0.2055	–0.4518	–0.4606	0.2164	0.2115	3.9
NQ16TH135PH0		0.9931		–0.0425		0.4098		0.0255		7.8
	PH30	0.9929	0.9930	–0.2422	–0.2424	0.3322	0.3326	0.0161	0.0256	8.8
	PH60		0.9931		–0.3765		0.1667		0.0257	7.9
	PH90	0.9929	0.9931	–0.4083	–0.4096	–0.0448	–0.0443	0.0250	0.0257	8.1
	PH120		0.9932		–0.3333		–0.2429		0.0241	8.1
	PH150		0.9929		–0.1657		–0.3747		0.0243	8.1
NQ16TH150PH0	0.9936	0.9937	–0.0293	–0.0326	0.2915	0.2924	–0.0687	–0.0692	10.8	11.2
	PH30	0.9936	0.9938	–0.1682	–0.1749	0.2387	0.2375	–0.0730	–0.0691	11.3
	PH60	0.9937	0.9938	–0.2679	–0.2706	0.1198	0.1184	–0.0704	–0.0692	11.2
	PH90	0.9937	0.9939	–0.2932	–0.2939	–0.0265	–0.0326	–0.0686	–0.0696	10.5
	PH120	0.9937	0.9939	–0.2387	–0.2383	–0.1700	–0.1743	–0.0709	–0.0704	11.0
	PH150	0.9936	0.9938	–0.1192	–0.1181	–0.2668	–0.2691	–0.0705	–0.0701	11.2

TABLE XXI: BH spins during final plunge, recoil velocity, and the angle between $\tilde{\Delta}_\perp$ for PHYYY and $\tilde{\Delta}_\perp$ of the corresponding PH0 configuration; all calculated in a rotated frame where the infall occurs in the xy plane. Note that in this frame, $\tilde{V}_\perp = (V_x, V_y)$ and $V_\parallel = V_z$.

CONF	S_{x1}	S_{y1}	S_{z1}	S_{x2}	S_{y2}	S_{z2}	V_x	V_y	V_z	φ
NQ200TH30PH0	0	0	0	0.0044	0.0426	0.0817	–75	–184	386	0.
	PH30	0	0	–0.0168	0.0412	0.0806	–76	–182	308	28.1
	PH60	0	0	–0.0329	0.0296	0.0807	–73	–182	154	53.8
	PH90	0	0	–0.0410	0.0103	0.0818	–70	–183	–41	81.7
	PH120	0	0	–0.0384	–0.0126	0.0830	–68	–185	–231	114.
	PH150	0	0	–0.0247	–0.0322	0.0829	–71	–185	–358	148.3
NQ200TH60PH0	0	0	0	–0.0680	0.0346	0.0500	–72	–140	142	0.
	PH30	0	0	–0.0742	0.0012	0.0538	–70	–147	–178	26.1
	PH60	0	0	–0.0660	–0.0318	0.0554	–58	–153	–408	52.7
	PH90	0	0	–0.0443	–0.0594	0.0544	–64	–156	–585	80.3
	PH120	0	0	–0.0059	–0.0764	0.0505	–79	–144	–639	112.6
	PH150	0	0	0.0391	–0.0674	0.0479	–83	–129	–461	147.1
NQ200TH90PH0	0	0	0	–0.0291	0.0856	0.0028	–94	–109	585	0.
	PH30	0	0	–0.0774	0.0463	0.0051	–77	–112	190	40.3
	PH60	0	0	–0.0874	0.0214	0.0079	–66	–118	–15	57.4
	PH90	0	0	–0.0887	–0.0139	0.0113	–62	–123	–280	80.1
	PH120	0	0	–0.0680	–0.0591	0.0118	–70	–124	–580	112.2
	PH150	0	0	–0.0282	–0.0858	0.0079	–84	–119	–699	143.
NQ200TH135PH0	0	0	0	0.0239	–0.0614	–0.0643	–107	–45	–369	0.
	PH30	0	0	0.0524	–0.0414	–0.0633	–102	–46	–191	30.4
	PH60	0	0	0.0679	–0.0121	–0.0611	–97	–51	23	58.6
	PH90	0	0	0.0679	0.0176	–0.0593	–93	–52	215	83.2
	PH120	0	0	0.0487	0.0501	–0.0602	–98	–51	399	114.5

Continued on next page

TABLE XXI – continued from previous page

CONF	S_{x1}	S_{y1}	S_{z1}	S_{x2}	S_{y2}	S_{z2}	V_x	V_y	V_z	φ (deg.)
PH150	0	0	0	0.0118	0.0662	-0.0629	-105	-48	453	148.6
NQ66TH60PH0	0	0	0	0.0060	-0.2334	0.1793	-99	-122	1914	0.
	PH30	0	0	0.1136	-0.2187	0.1616	6	-231	1748	26.
	PH60	0	0	0.1813	-0.1745	0.1523	72	-259	1400	44.6
	PH90	0	0	0.2358	-0.0729	0.1593	75	-188	718	71.3
	PH120	0	0	0.2116	0.0695	0.1918	-75	-17	-411	106.7
	PH150	0	0	0.1105	0.1858	0.2000	-153	-1	-1504	147.8
NQ50TH30PH0	0	0	0	0.0960	-0.1438	0.3186	7	-133	1222	0.
	PH30	0	0	0.1719	-0.0797	0.3092	89	-143	890	31.4
	PH60	0	0	0.1765	-0.0051	0.3167	52	-74	415	54.6
	PH90	0	0	0.1377	0.0478	0.3321	-44	-9	-173	75.4
	PH120	0	0	0.0827	0.1019	0.3380	-97	7	-816	107.2
	PH150	0	0	-0.0078	0.1475	0.3309	-72	-62	-1233	149.3
NQ50TH60PH0	0	0	0	-0.0892	0.2794	0.2117	-56	-307	-1785	0.
	PH30	0	0	-0.2302	0.2067	0.1873	124	-402	-1358	30.4
	PH60	0	0	-0.2955	0.1084	0.1777	220	-352	-972	52.2
	PH90	0	0	-0.2939	-0.0026	0.2102	100	-181	-320	72.8
	PH120	0	0	-0.2141	-0.1432	0.2537	-126	-16	838	106.1
	PH150	0	0	-0.0715	-0.2576	0.2433	-182	-117	1778	146.8
NQ50TH90PH0	0	0	0	-0.1806	-0.2965	0.0961	-260	-105	1573	0.
	PH30	0	0	-0.0854	-0.3420	0.0764	-246	-204	1717	17.3
	PH60	0	0	-0.0430	-0.3522	0.0652	-231	-257	1718	24.4
	PH90	0	0	0.0636	-0.3524	0.0452	-179	-364	1600	41.6
	PH120	0	0	0.3266	-0.1464	0.0367	51	-419	709	97.2
	PH150	0	0	0.3170	0.1361	0.1052	-144	-80	-743	144.6
NQ50TH135PH0	0	0	0	0.2971	0.0432	-0.2040	-214	-209	-303	0.
	PH30	0	0	0.2678	0.1409	-0.1990	-249	-170	-584	19.5
	PH60	0	0	0.2191	0.2050	-0.2040	-271	-175	-743	34.8
	PH90	0	0	0.1242	0.2632	-0.2179	-283	-219	-854	56.5
	PH120	0	0	-0.0795	0.2632	-0.2373	-243	-329	-726	98.5
	PH150	0	0	-0.2570	0.1213	-0.2240	-191	-309	-215	146.5
NQ33TH45PH0	0	0	0	-0.1094	0.2619	0.3553	-85	-311	-1348	0.
	PH30	0	0	-0.1865	0.2226	0.3504	-4	-335	-1131	17.3
	PH60	0	0	-0.2165	0.1880	0.3535	29	-304	-938	26.4
	PH90	0	0	-0.2428	0.1124	0.3681	49	-200	-524	42.5
	PH120	0	0	-0.2130	-0.0574	0.3979	-30	-9	375	82.4
	PH150	0	0	-0.0606	-0.2301	0.3868	-153	-97	1226	142.6
NQ33TH75PH0	0	0	0	0.3420	-0.1872	0.2314	-57	-285	280	-12.
	PH30	0	0	0.3610	-0.1086	0.2514	-48	-177	-43	0.
	PH60	0	0	0.3559	-0.1421	0.2418	-49	-221	85	-5.
	PH90	0	0	0.3657	-0.0671	0.2587	-54	-124	-210	6.4
	PH120	0	0	0.2759	0.2318	0.2732	-236	25	-1188	56.8
	PH150	0	0	-0.1161	0.3940	0.1933	-269	-425	-1332	123.2
NQ33TH100PH0	0	0	0	-0.2376	-0.3818	0.0607	-354	-103	1186	-10.
	PH30	0	0	-0.1682	-0.4195	0.0443	-356	-170	1224	0.
	PH60	0	0	-0.2135	-0.3971	0.0526	-356	-127	1201	-6.4
	PH90	0	0	-0.1278	-0.4347	0.0332	-351	-211	1221	5.5
	PH120	0	0	0.3053	-0.3350	-0.0296	-123	-499	713	64.2
	PH150	0	0	0.4296	0.1269	0.0700	-194	-74	-575	128.3
NQ33TH135PH0	0	0	0	0.3938	0.0755	-0.2166	-299	40	-482	0.
	PH30	0	0	0.3416	0.2019	-0.2260	-335	42	-598	19.7
	PH60	0	0	0.2968	0.2574	-0.2367	-355	28	-627	30.1

Continued on next page

TABLE XXI – continued from previous page

CONF	S_{x1}	S_{y1}	S_{z1}	S_{x2}	S_{y2}	S_{z2}	V_x	V_y	V_z	φ (deg.)
PH90	0	0	0	0.1833	0.3336	-0.2546	-384	-18	-621	50.4
PH120	0	0	0	-0.0889	0.3580	-0.2705	-374	-104	-387	93.1
PH150	0	0	0	-0.3555	0.1626	-0.2331	-289	-44	138	144.6
NQ25TH30PH0	0	0	0	-0.1613	-0.0335	0.4889	0	-21	82	0.
PH30	0	0	0	-0.1188	-0.0980	0.4926	-36	-10	348	27.8
PH60	0	0	0	-0.0456	-0.1644	0.4863	-63	-51	629	62.8
PH90	0	0	0	0.0244	-0.1963	0.4759	-56	-113	773	85.4
PH120	0	0	0	0.0600	-0.2020	0.4712	-41	-141	807	94.8
PH150	0	0	0	0.1716	-0.1553	0.4616	37	-173	668	126.1
NQ25TH60PH0	0	0	0	-0.3363	0.0864	0.3807	26	-143	-16	0.
PH30	0	0	0	-0.3336	0.0356	0.3912	7	-89	148	8.3
PH60	0	0	0	-0.3373	0.0635	0.3842	14	-117	63	3.8
PH90	0	0	0	-0.3369	0.0482	0.3872	8	-99	112	6.3
PH120	0	0	0	-0.2147	-0.2412	0.4007	-179	-19	941	62.7
PH135	0	0	0	-0.0495	-0.3605	0.3632	-236	-213	1189	96.6
PH150	0	0	0	0.1527	-0.3687	0.3259	-134	-412	1069	126.9
PH165	0	0	0	0.2858	-0.2694	0.3342	-3	-371	654	151.1
NQ25TH90PH0	0	0	0	-0.3844	0.2992	0.1557	-149	-252	-113	0.
PH30	0	0	0	-0.3768	0.3126	0.1498	-157	-268	-147	-1.8
PH60	0	0	0	-0.2414	0.4375	0.1142	-269	-358	-536	-23.2
PH90	0	0	0	-0.2722	0.4182	0.1178	-246	-351	-464	-19.
PH120	0	0	0	-0.4639	0.0519	0.2088	-128	-15	422	31.5
PH150	0	0	0	-0.0601	-0.4906	0.1336	-401	-225	985	120.9
NQ25TH135PH0	0	0	0	0.4017	0.2132	-0.2489	-293	98	-443	0.
PH30	0	0	0	0.2997	0.3295	-0.2651	-331	67	-458	19.8
PH60	0	0	0	0.2949	0.3324	-0.2665	-332	65	-456	20.5
PH90	0	0	0	0.1756	0.3974	-0.2834	-350	23	-418	38.2
PH120	0	0	0	-0.1931	0.3815	-0.2920	-302	-42	-129	88.9
PH150	0	0	0	-0.4454	0.0807	-0.2482	-236	63	265	141.8
NQ25TH150PH0	0	0	0	-0.2605	-0.1917	-0.4006	-277	-32	264	0.
PH30	0	0	0	-0.1749	-0.2640	-0.4058	-290	-50	284	20.1
PH60	0	0	0	-0.0836	-0.2952	-0.4138	-290	-79	269	37.8
PH90	0	0	0	0.0417	-0.2925	-0.4216	-280	-104	211	61.8
PH120	0	0	0	0.2220	-0.1938	-0.4211	-252	-99	52	102.5
PH150	0	0	0	0.3131	0.0203	-0.4036	-249	-49	-150	147.4
NQ16TH45PH0	0	0	0	-0.2743	0.2196	0.4703	44	-192	-374	0.
PH30	0	0	0	-0.2954	0.1363	0.4889	50	-122	-197	13.9
PH60	0	0	0	-0.2852	0.1979	0.4742	51	-171	-323	3.9
PH90	0	0	0	-0.2634	0.2471	0.4656	42	-211	-433	-4.5
PH120	0	0	0	-0.2149	-0.1343	0.5296	-45	3	349	70.7
PH150	0	0	0	0.0791	-0.3292	0.4791	-68	-196	649	142.2
NQ16TH90PH0	0	0	0	0.5238	-0.0080	0.2691	-116	64	-383	10.4
PH30	0	0	0	0.5208	-0.1038	0.2552	-90	20	-298	0.
PH60	0	0	0	0.2645	-0.5043	0.1550	-201	-263	253	-51.
PH90	0	0	0	0.2135	-0.5293	0.1503	-229	-270	318	-56.8
PH120	0	0	0	0.5253	-0.0314	0.2644	-108	59	-366	7.8
PH150	0	0	0	-0.1442	0.5519	0.1517	-270	-264	-401	115.9
NQ16TH115PH0	0	0	0	0.5279	0.2631	-0.0151	-241	129	-408	1.5
PH30	0	0	0	0.5337	0.2486	-0.0139	-237	131	-403	0.
PH60	0	0	0	0.5667	-0.1470	-0.0317	-141	79	-249	-39.5
PH90	0	0	0	0.5637	-0.1671	-0.0368	-140	72	-238	-41.5
PH120	0	0	0	0.4131	0.4189	-0.0376	-301	82	-425	20.4
PH150	0	0	0	-0.4637	0.3575	-0.0694	-152	-18	114	117.4

Continued on next page

TABLE XXI – continued from previous page

CONF	S_{x1}	S_{y1}	S_{z1}	S_{x2}	S_{y2}	S_{z2}	V_x	V_y	V_z	φ (deg.)	
NQ16TH135PH0	0	0	0	0.3376	-0.3219	-0.3642	-180	-103	37	0.	
	PH30	0	0	0.2854	-0.3673	-0.3650	-192	-108	69	-8.5	
	PH60	0	0	0.3229	-0.3336	-0.3648	-184	-101	45	-2.3	
	PH90	0	0	0.3721	-0.2817	-0.3613	-175	-86	8	6.5	
	PH120	0	0	0.4897	-0.0017	-0.3309	-175	5	-143	43.4	
	PH150	0	0	0.1949	0.4550	-0.3243	-258	-35	-250	110.4	
NQ16TH150PH0	0	0	0	-0.1331	-0.3513	-0.4576	-198	72	116	-20.3	
	PH30	0	0	-0.0032	-0.3672	-0.4639	-190	60	71	0.	
	PH60	0	0	0.0885	-0.3529	-0.4608	-180	56	34	14.6	
	PH90	0	0	0.2120	-0.2984	-0.4643	-164	62	-20	35.9	
	PH120	0	0	0.3638	-0.1072	-0.4526	-152	91	-107	74.1	
	PH150	0	0	0.3305	0.2071	-0.4452	-184	102	-157	122.6	
KTH45PH0	-0.1815	-0.0207	0.0933	-0.0487	0.1872	-0.0674	233	-379	-1794	0	
	PH30	-0.1429	-0.1005	0.1079	-0.1384	0.1353	-0.0637	331	-434	-2029	28.6
	PH60	-0.1211	-0.1249	0.1099	-0.1619	0.1083	-0.0590	362	-421	-2048	39.4
	PH90	-0.0720	-0.1559	0.1132	-0.1905	0.0554	-0.0447	354	-373	-2007	58.7
	PH105	-0.0252	-0.1722	0.1101	-0.2015	0.0088	-0.0292	288	-316	-1833	75.1
	PH120	0.0383	-0.1761	0.0998	-0.1966	-0.0540	-0.0165	201	-229	-1390	95.8
	PH135	0.0954	-0.1604	0.0870	-0.1722	-0.1112	-0.0182	123	-166	-597	114.2
	PH150	0.1499	-0.1161	0.0793	-0.1166	-0.1662	-0.0344	98	-177	419	135.7
	PH165	0.1792	-0.0546	0.0833	-0.0413	-0.1939	-0.0553	133	-273	1304	156.5
	KTH22.5PH0	-0.0319	-0.0997	0.1773	-0.1181	0.0640	-0.1535	183	-412	-1601	0
PH30	0.0234	-0.1086	0.1736	-0.1453	0.0117	-0.1429	157	-366	-1304	29.9	
	PH60	0.0671	-0.0983	0.1680	-0.1454	-0.0353	-0.1396	125	-321	-807	52.1
	PH90	0.1000	-0.0737	0.1641	-0.1246	-0.0757	-0.1423	75	-304	-58	71.4
	PH120	0.1216	-0.0141	0.1656	-0.0575	-0.1199	-0.1558	80	-339	895	101.6
	PH150	0.0905	0.0627	0.1748	0.0521	-0.1121	-0.1631	158	-411	1534	142.5

- [1] M. C. Miller and E. Colbert, Int.J.Mod.Phys. **D13**, 1 (2004), arXiv:astro-ph/0308402 [astro-ph].
- [2] F. Pretorius, Phys. Rev. Lett. **95**, 121101 (2005), gr-qc/0507014.
- [3] M. Campanelli, C. O. Lousto, P. Marronetti, and Y. Zlochower, Phys. Rev. Lett. **96**, 111101 (2006), gr-qc/0511048.
- [4] J. G. Baker, J. Centrella, D.-I. Choi, M. Koppitz, and J. van Meter, Phys. Rev. Lett. **96**, 111102 (2006), gr-qc/0511103.
- [5] M. Campanelli, Class. Quant. Grav. **22**, S387 (2005), astro-ph/0411744.
- [6] J. G. Baker, J. Centrella, D.-I. Choi, M. Koppitz, J. R. van Meter, and M. C. Miller, Astrophys. J. **653**, L93 (2006), arXiv:astro-ph/0603204 [astro-ph].
- [7] J. G. Baker, W. D. Boggs, J. Centrella, B. J. Kelly, S. T. McWilliams, M. C. Miller, and J. R. van Meter, Astrophys. J. **668**, 1140 (2007), arXiv:astro-ph/0702390 [ASTRO-PH].
- [8] J. G. Baker, W. D. Boggs, J. Centrella, B. J. Kelly, S. T. McWilliams, M. C. Miller, and J. R. van Meter, Astrophys. J. **682**, L29 (2008), arXiv:0802.0416 [astro-ph].
- [9] B. Brugmann, J. A. Gonzalez, M. Hannam, S. Husa, and U. Sperhake, Phys. Rev. **D77**, 124047 (2008), arXiv:0707.0135 [gr-qc].
- [10] M. Campanelli, C. O. Lousto, Y. Zlochower, and D. Merritt, Phys. Rev. Lett. **98**, 231102 (2007), gr-qc/0702133.
- [11] M. Campanelli, C. O. Lousto, Y. Zlochower, and D. Merritt, Astrophys. J. **659**, L5 (2007), gr-qc/0701164.
- [12] D.-I. Choi, B. J. Kelly, W. D. Boggs, J. G. Baker, J. Centrella, and J. van Meter, Phys. Rev. **D76**, 104026 (2007), arXiv:gr-qc/0702016 [GR-QC].
- [13] S. Dain, C. O. Lousto, and Y. Zlochower, Phys. Rev. **D78**, 024039 (2008), arXiv:0803.0351 [gr-qc].
- [14] J. A. González, U. Sperhake, B. Brugmann, M. Hannam, and S. Husa, Phys. Rev. Lett. **98**, 091101 (2007), gr-qc/0610154.
- [15] J. A. González, M. D. Hannam, U. Sperhake, B. Brugmann, and S. Husa, Phys. Rev. Lett. **98**, 231101 (2007), gr-qc/0702052.
- [16] J. Healy, F. Herrmann, I. Hinder, D. M. Shoemaker, P. Laguna, and R. A. Matzner, Phys. Rev. Lett. **102**, 041101 (2009), arXiv:0807.3292 [gr-qc].
- [17] F. Herrmann, I. Hinder, D. Shoemaker, and P. Laguna, AIP Conf. Proc. **873**, 89 (2006).
- [18] C. O. Lousto and Y. Zlochower, Phys. Rev. **D77**, 044028 (2008), arXiv:0708.4048 [gr-qc].
- [19] F. Herrmann, I. Hinder, D. Shoemaker, P. Laguna, and R. A. Matzner, Astrophys. J. **661**, 430 (2007), gr-qc/0701143.

- [20] F. Herrmann, I. Hinder, D. M. Shoemaker, P. Laguna, and R. A. Matzner, Phys. Rev. **D76**, 084032 (2007), arXiv:0706.2541 [gr-qc].
- [21] F. Herrmann, I. Hinder, D. Shoemaker, and P. Laguna, Class. Quant. Grav. **24**, S33 (2007).
- [22] K. Holley-Bockelmann, K. Gultekin, D. Shoemaker, and N. Yunes, Astrophys. J. **686**, 829 (2008), arXiv:0707.1334.
- [23] J. L. Jaramillo, R. P. Macedo, P. Moesta, and L. Rezzolla, Phys. Rev. **D85**, 084030 (2012), arXiv:1108.0060 [gr-qc].
- [24] M. Koppitz, D. Pollney, C. Reisswig, L. Rezzolla, J. Thornburg, P. Diener, and E. Schnetter, Phys. Rev. Lett. **99**, 041102 (2007), arXiv:gr-qc/0701163 [GR-QC].
- [25] P. Laguna, Matters Grav. **34**, 5 (2009).
- [26] C. O. Lousto and Y. Zlochower, Phys. Rev. **D79**, 064018 (2009), arXiv:0805.0159 [gr-qc].
- [27] C. O. Lousto and Y. Zlochower, Phys. Rev. **D83**, 024003 (2011), arXiv:1011.0593 [gr-qc].
- [28] H. Nakano, M. Campanelli, C. O. Lousto, and Y. Zlochower, Class. Quant. Grav. **28**, 134005 (2011), arXiv:1011.2767 [gr-qc].
- [29] C. O. Lousto and Y. Zlochower, Phys. Rev. Lett. **107**, 231102 (2011), arXiv:1108.2009 [gr-qc].
- [30] C. O. Lousto and Y. Zlochower, Phys. Rev. **D87**, 084027 (2013), arXiv:1211.7099 [gr-qc].
- [31] C. O. Lousto, Y. Zlochower, M. Dotti, and M. Volonteri, Phys. Rev. **D85**, 084015 (2012), arXiv:1201.1923 [gr-qc].
- [32] S. H. Miller and R. A. Matzner, Gen. Rel. Grav. **41**, 525 (2009), arXiv:0807.3028 [gr-qc].
- [33] D. Pollney, C. Reisswig, L. Rezzolla, B. Szilágyi, M. Ansorg, B. Deris, P. Diener, E. N. Dorband, M. Koppitz, A. Nagar, and E. Schnetter, Phys. Rev. **D76**, 124002 (2007), arXiv:0707.2559 [gr-qc].
- [34] L. Rezzolla, R. P. Macedo, and J. L. Jaramillo, Phys. Rev. Lett. **104**, 221101 (2010), arXiv:1003.0873 [gr-qc].
- [35] J. D. Schnittman, A. Buonanno, J. R. van Meter, J. G. Baker, W. D. Boggs, J. Centrella, B. J. Kelly, and S. T. McWilliams, Phys. Rev. **D77**, 044031 (2008), arXiv:0707.0301 [gr-qc].
- [36] C. F. Sopuerta, N. Yunes, and P. Laguna, Astrophys. J. **656**, L9 (2007), astro-ph/0611110.
- [37] C. F. Sopuerta, N. Yunes, and P. Laguna, Phys. Rev. D **74**, 124010 (2006), astro-ph/0608600.
- [38] W. Tichy and P. Marronetti, Phys. Rev. **D76**, 061502 (2007), gr-qc/0703075.
- [39] J. R. van Meter, M. C. Miller, J. G. Baker, W. D. Boggs, and B. J. Kelly, apj **719**, 1427 (2010), arXiv:1003.3865 [astro-ph.HE].
- [40] Y. Zlochower, M. Campanelli, and C. O. Lousto, Class. Quant. Grav. **28**, 114015 (2011), arXiv:1011.2210 [gr-qc].
- [41] J. Healy, C. O. Lousto, and Y. Zlochower, Phys. Rev. **D90**, 104004 (2014), arXiv:1406.7295 [gr-qc].
- [42] M. Campanelli, C. O. Lousto, and Y. Zlochower, Phys. Rev. **D74**, 041501(R) (2006), gr-qc/0604012.
- [43] L. Boyle, M. Kesden, and S. Nissanke, Phys. Rev. Lett. **100**, 151101 (2008), arXiv:0709.0299 [gr-qc].
- [44] L. Boyle and M. Kesden, Phys. Rev. **D78**, 024017 (2008), arXiv:0712.2819 [astro-ph].
- [45] A. Buonanno, L. E. Kidder, and L. Lehner, Phys. Rev. **D77**, 026004 (2008), arXiv:0709.3839 [astro-ph].
- [46] W. Tichy and P. Marronetti, Phys. Rev. **D78**, 081501 (2008), arXiv:0807.2985 [gr-qc].
- [47] M. Kesden, Phys. Rev. **D78**, 084030 (2008), arXiv:0807.3043 [astro-ph].
- [48] E. Barausse and L. Rezzolla, Astrophys. J. Lett. **704**, L40 (2009), arXiv:0904.2577 [gr-qc].
- [49] L. Rezzolla, Class. Quant. Grav. **26**, 094023 (2009), arXiv:0812.2325 [gr-qc].
- [50] C. O. Lousto, M. Campanelli, Y. Zlochower, and H. Nakano, Class. Quant. Grav. **27**, 114006 (2010), arXiv:0904.3541 [gr-qc].
- [51] C. O. Lousto and Y. Zlochower, Phys. Rev. **D89**, 104052 (2014), arXiv:1312.5775 [gr-qc].
- [52] C. M. Hirata, Phys. Rev. **D83**, 104024 (2011), arXiv:1011.4987 [gr-qc].
- [53] M. van de Meent, Phys. Rev. **D90**, 044027 (2014), arXiv:1406.2594 [gr-qc].
- [54] J. D. Schnittman, Phys. Rev. Lett. **113**, 261102 (2014), arXiv:1410.6446 [astro-ph.HE].
- [55] E. Berti, R. Brito, and V. Cardoso, Phys. Rev. Lett. **114**, 251103 (2015), arXiv:1410.8534 [gr-qc].
- [56] H. Yang, A. Zimmerman, and L. Lehner, Phys. Rev. Lett. **114**, 081101 (2015), arXiv:1402.4859 [gr-qc].
- [57] Y. Zlochower, J. G. Baker, M. Campanelli, and C. O. Lousto, Phys. Rev. **D72**, 024021 (2005), arXiv:gr-qc/0505055.
- [58] P. Marronetti, W. Tichy, B. Brügmann, J. González, and U. Sperhake, Phys. Rev. **D77**, 064010 (2008), arXiv:0709.2160 [gr-qc].
- [59] C. O. Lousto and Y. Zlochower, Phys. Rev. **D77**, 024034 (2008), arXiv:0711.1165 [gr-qc].
- [60] F. Löffler, J. Faber, E. Bentivegna, T. Bode, P. Diener, R. Haas, I. Hinder, B. C. Mundim, C. D. Ott, E. Schnetter, G. Allen, M. Campanelli, and P. Laguna, Class. Quant. Grav. **29**, 115001 (2012), arXiv:1111.3344 [gr-qc].
- [61] Einstein Toolkit home page: <http://einstein toolkit.org>.
- [62] Cactus Computational Toolkit home page: <http://cactuscode.org>.
- [63] E. Schnetter, S. H. Hawley, and I. Hawke, Class. Quant. Grav. **21**, 1465 (2004), gr-qc/0310042.
- [64] J. Thornburg, Class. Quant. Grav. **21**, 743 (2004), gr-qc/0306056.
- [65] O. Dreyer, B. Krishnan, D. Shoemaker, and E. Schnetter, Phys. Rev. **D67**, 024018 (2003), gr-qc/0206008.
- [66] M. Campanelli and C. O. Lousto, Phys. Rev. **D59**, 124022 (1999), arXiv:gr-qc/9811019 [gr-qc].
- [67] C. O. Lousto and Y. Zlochower, Phys. Rev. **D76**, 041502(R) (2007), gr-qc/0703061.
- [68] At least in the similar mass regime, we found that the $\ell \geq 5$ modes contributes a smaller amount to the recoil than the extrapolation error to infinite radius, while, at the same time, these modes are poorly resolved using our choice of gridspacing. We therefore suppress these modes in our calculation.
- [69] M. Ansorg, B. Brügmann, and W. Tichy, Phys. Rev. **D70**, 064011 (2004), gr-qc/0404056.
- [70] S. Brandt and B. Brügmann, Phys. Rev. Lett. **78**, 3606 (1997), gr-qc/9703066.
- [71] E. Racine, Phys. Rev. **D78**, 044021 (2008), arXiv:0803.1820 [gr-qc].
- [72] C. O. Lousto and Y. Zlochower, Phys. Rev. **D89**, 021501 (2014), arXiv:1307.6237 [gr-qc].
- [73] G. B. Arfken and H. J. Weber, *Mathematical methods for physicists 6th ed.* (Elsevier Academic Press, 2005).

- [74] D. A. Hemberger, G. Lovelace, T. J. Loredo, L. E. Kidder, M. A. Scheel, B. Szilágyi, N. W. Taylor, and S. A. Teukolsky, Phys. Rev. **D88**, 064014 (2013), arXiv:1305.5991 [gr-qc].
- [75] J. D. Schnittman, Phys. Rev. **D70**, 124020 (2004), arXiv:astro-ph/0409174.
- [76] M. Kesden, U. Sperhake, and E. Berti, Astrophys. J. **715**, 1006 (2010), arXiv:1003.4993 [astro-ph.CO].
- [77] E. Berti, M. Kesden, and U. Sperhake, Phys. Rev. **D85**, 124049 (2012), arXiv:1203.2920 [astro-ph.HE].
- [78] C. O. Lousto, H. Nakano, Y. Zlochower, and M. Campanelli, Phys. Rev. **D81**, 084023 (2010), arXiv:0910.3197 [gr-qc].
- [79] Q. Yu, Y. Lu, R. Mohayaee, and J. Colin, Astrophys. J. **738**, 92 (2011), arXiv:1105.1963 [astro-ph.CO].
- [80] K. R. Stewart, J. S. Bullock, E. J. Barton, and R. H. Wechsler, Astrophys. J. **702**, 1005 (2009), arXiv:0811.1218 [astro-ph].
- [81] P. F. Hopkins, K. Bundy, D. Croton, L. Hernquist, D. Keres, S. Khochfar, K. Stewart, A. Wetzel, and J. D. Younger, Astrophys. J. **715**, 202 (2010), arXiv:0906.5357 [astro-ph.CO].
- [82] B. Aylott *et al.*, Class. Quant. Grav. **26**, 165008 (2009), arXiv:0901.4399 [gr-qc].
- [83] B. Aylott *et al.*, Class. Quant. Grav. **26**, 114008 (2009), arXiv:0905.4227 [gr-qc].
- [84] P. Ajith *et al.*, Class. Quant. Grav. **29**, 124001 (2012), arXiv:1201.5319 [gr-qc].
- [85] J. Aasi *et al.* (LIGO Scientific Collaboration, Virgo Collaboration, NINJA-2 Collaboration), Class. Quant. Grav. **31**, 115004 (2014), arXiv:1401.0939 [gr-qc].
- [86] S. Komossa, Adv. Astron. **2012**, 364973 (2012), arXiv:1202.1977 [astro-ph.CO].
- [87] T. Bogdanović, Astrophys. Space Sci. Proc. **40**, 103 (2015), arXiv:1406.5193 [astro-ph.HE].
- [88] L. Blecha, T. J. Cox, A. Loeb, and L. Hernquist, Mon.Not.Roy.Astron.Soc. **412**, 2154 (2011), arXiv:1009.4940 [astro-ph.CO].
- [89] L. Blecha and A. Loeb, mnras **390**, 1311 (2008), arXiv:0805.1420.
- [90] C. R. Galley, F. Herrmann, J. Silberholz, M. Tiglio, and G. Guerberoff, Class. Quant. Grav. **27**, 245007 (2010), arXiv:1005.5560 [gr-qc].
- [91] M. Kesden, D. Gerosa, R. O'Shaughnessy, E. Berti, and U. Sperhake, Phys. Rev. Lett. **114**, 081103 (2015), arXiv:1411.0674 [gr-qc].